

1 **Response to anonymous referee #1:**

2 We thank the referee for their comprehensive and detailed review of our manuscript and provide responses to  
3 the questions and suggestions below:

4 Major comments:

5 There is too much similarity between the abstract and the conclusions. The conclusion section should benefit  
6 from including an outlook paragraph (which, e.g., should not be in the abstract). Now that a study has been  
7 done on modifying the chemistry and the resolution, and improvements in the model performance are  
8 moderate, what could be the next points of focus for further development of TM5. What would be the way  
9 forward to further improve CTMs? Another aspect which could be discussed in the conclusion : as the  
10 differences between 1x1 and 2x3 are moderate, is it an option to still use the 3x2 version profiles as a priori for  
11 retrievals?

12 We have now limited our abstract to focus on chemical trace species that will be retrieved by TM5-MP. We  
13 modify the abstract accordingly:

14 *We provide a comprehensive description of the high-resolution version of the TM5-MP global Chemistry-*  
15 *Transport Model, which is to be employed for deriving highly resolved vertical profiles of nitrogen dioxide*  
16 *(NO<sub>2</sub>), formaldehyde (CH<sub>2</sub>O), and sulphur dioxide (SO<sub>2</sub>) for use in satellite retrievals from platforms such as*  
17 *the Ozone Monitoring Instrument (OMI) and the Sentinel-5 Precursor, the TROPOspheric Monitoring*  
18 *Instrument (tropOMI). Comparing simulations conducted at horizontal resolutions of 3° x 2° and 1° x 1°*  
19 *reveals differences of ±20% exist in the global seasonal distribution of <sup>222</sup>Rn, being larger near specific coastal*  
20 *locations and tropical oceans. For tropospheric ozone (O<sub>3</sub>), analysis of the chemical budget terms shows that*  
21 *the impact on globally integrated photolysis rates is rather low, in spite of the higher spatial variability of*  
22 *meteorological data fields from ERA-Interim at 1° x 1°. Surface concentrations of O<sub>3</sub> in high-NO<sub>x</sub> regions*  
23 *decrease between 5-10% at 1° x 1° due to a reduction in NO<sub>x</sub> recycling terms and an increase in the associated*  
24 *titration term of O<sub>3</sub> by NO. At 1° x 1°, the net global stratosphere-troposphere exchange of O<sub>3</sub> decreases by*  
25 *~7%, with an associated shift in the hemispheric gradient. By comparing NO, NO<sub>2</sub>, HNO<sub>3</sub> and PAN profiles*  
26 *against measurement composites, we show that TM5-MP captures the vertical distribution of NO<sub>x</sub> and long-*  
27 *lived NO<sub>x</sub> reservoirs at background locations, again with modest changes at 1° x 1°. We show that surface*  
28 *mixing ratios in both NO and NO<sub>2</sub> are generally underestimated in both low and high NO<sub>x</sub> scenarios. For*  
29 *Europe, a negative bias exists for [NO] at the surface across the whole domain, with lower biases at 1° x 1° at*  
30 *only ~20% of sites. For NO<sub>2</sub>, biases are more variable, with lower (higher) biases at 1° x 1° occurring at*  
31 *~35% (~20%) of sites, with the remainder showing little change. For CH<sub>2</sub>O, the impact of higher resolution on*  
32 *the chemical budget terms is rather modest, with changes less than 5%. The simulated vertical distribution of*  
33 *CH<sub>2</sub>O agrees reasonably well with measurements in pristine locations, although column-integrated values are*  
34 *generally underestimated relative to satellite measurements in polluted regions. For SO<sub>2</sub>, the performance at*  
35 *1° x 1° is principally governed by the quality of the emission inventory, with limited improvements in the site*

36 *specific biases with most showing no significant improvement. For the vertical column, improvements near*  
37 *strong source regions occur which reduce the biases in the integrated column.*

38 Previous studies have quantified retrieval errors with respect to horizontal resolution (e.g. Boersma et al., 2007;  
39 Heckel et al., ACP, 2011) and considering the small footprint of the new tropOMI instrument, it seems  
40 disingenuous to use a  $3^\circ \times 2^\circ$  model grid to perform such retrievals considering the progress made in the  
41 instrument resolution.

42 *I have the impression that the manuscript is too strong in its argumentation that emissions are an important*  
43 *reason for discrepancies with observations. I would suggest that the authors make this claim more solid, e.g.,*  
44 *by doing sensitivity experiments.*

45 Performing such sensitivity studies would then turn our manuscript into a scientific paper rather than a model  
46 description and validation paper, whereas the purpose of our submission to GMD is to provide a peer-reviewed  
47 benchmarking reference. It is envisaged that studies related to emission estimates and retrievals from tropOMI  
48 will occur once the satellite is launched (spring 2017). Other independent studies have placed discrepancies  
49 between models and measurements almost entirely on missing emission terms, therefore allowing inversion  
50 studies to be performed (e.g. Elburn et al., ACP, 2007; Kim et al., ACP, 2011; Manning et al., JGR, 2011).  
51 Moreover, the basis of emission trend studies from Earth-orbiting satellites relies on the missing component  
52 being almost entirely due to emission fluxes (e.g. Schneider et al., 2015). Given the large discrepancy between  
53 e.g. lower tropospheric  $\text{NO}_x$  in Texas, an area subject to high Anthropogenic emissions, the first-order impact  
54 is also thought to be from under-estimates in emissions (e.g. de Gouw et al., Env. Sci. Tech., 2011).

55 *The analysis of the differences between the two resolutions should be improved. What about the difference in*  
56 *turbulent vertical transport between both model simulations? What about dry deposition parameterisations*  
57 *affected by the different resolutions? What about lightning  $\text{NO}_x$  parameterisations? In the current manuscript,*  
58 *there is a lot of focus on convection, whereas other parameterizations might also play a role.*

59 We focus on the convective aspect as the source of the convective mass-fluxes has changed in this version of  
60 the model compared to previous versions, rather than the e.g. turbulent mixing scheme, which is identical.  
61 Resolution effects on turbulent mixing would require a separate study and, again, we consider this a model  
62 validation paper with a focus on retrievable trace gases, and therefore present the cumulative result of all  
63 resolution induced changes. Additional tuning was performed between simulations so that the lightning  $\text{NO}_x$  is  
64 constrained to an annual global total of  $6 \text{ Tg N yr}^{-1}$  throughout, as described in the text, thus:

65 *For lightning  $\text{NO}_x$  we use the parameterization which uses convective precipitation fields (Meijer et al., 2001)*  
66 *and constrain the annual global emission term at  $\sim 6 \text{ Tg N yr}^{-1}$ . This uses the convective flux values meaning*  
67 *that re-scaling of the nudging term was necessary in order to achieve similar total lightning  $\text{NO}_x$  across*  
68 *simulations.*

69 This ensures that the  $\text{NO}_x$  emission total is the same between runs allowing a valid comparison.

70 The vertical grid is identical between  $3^\circ \times 2^\circ$  and  $1^\circ \times 1^\circ$  simulations. For the dry deposition, although regional  
71 terms may exhibit larger differences, the small change in the  $O_3$  deposition term in the Northern Hemisphere  
72 given in Table 4 implies this is not a dominating source of the modest differences found.

73 It is also not made clear how large the differences are in the meteorological fields seen by the different  
74 resolutions. E.g., is the total precipitation equal in  $3 \times 2$  and  $1 \times 1$ ? Are the convective mass fluxes, when globally  
75 averaged, equal in both versions? Is the cloud cover equal when globally averaged? And the albedo? If not, it  
76 would be informative to quantify that.

77 For details on the use of meteorological fields in TM5-MP the referee is pointed to Bregman et al., ACP, 2003  
78 and Huijnen et al., GMD, 2010. The similarity in both the regional photolysis frequencies (where clouds  
79 dominate the total Optical Depth; Figure S4) and the wet and dry deposition fluxes shows that there are no  
80 significant changes in the global and zonal mean terms for such quantities. Transport will be better defined  
81 using higher resolution wind fields, but this is one of the benefits of increasing horizontal resolution evident in  
82 the March INTEX-B comparisons of e.g.  $O_3$ . We feel that a comparison of such meteorological fields would  
83 detract from the real focus of our paper, which is whether the integrated effect of the change in resolution alters  
84 the chemical composition of the troposphere significantly.

85 As one of the aims of the model is to use it for generating instantaneous a-priori profiles and columns, it is not  
86 sufficient in this study to look at biases only. One should also look at the high frequency behaviour and thus,  
87 e.g., at correlations. E.g., Table 9 gives seasonal biases, but I think it is necessary to also show correlations. In  
88 addition, as the satellite retrievals will be used globally, it is not sufficient to quantify the difference between  
89 the  $3^\circ \times 2^\circ$  and  $1^\circ \times 1^\circ$  versions only for the observation locations of the manuscript. As the (tropospheric)  
90 columns of  $NO_2$ ,  $SO_2$  and  $CH_2O$  from TM5 will be important for the retrieval, one could, e.g., estimate how  
91 well the  $3^\circ \times 2^\circ$  and  $1^\circ \times 1^\circ$  distributions are correlated spatially. This could also allow to better quantify  
92 whether using  $3^\circ \times 2^\circ$  instead of  $1^\circ \times 1^\circ$  still makes sense.

93 As well as presenting the biases at EMEP surface sites in Europe, we also present comparisons of vertical  
94 profiles across a wide area from the INTEX-B and Texas-AQSII campaigns (Singh et al., ACP, 2009; Parrish  
95 et al., JGR, 2009). The locations chosen for validation are significantly restricted by data availability during  
96 2006. However, the main findings are consistent across all selected regions, therefore we feel confident that as  
97 we have compared surface values and vertical profiles in both remote and urban scenarios (i.e. over different  
98 chemical regimes) the main biases in any a-priori fields have been sufficiently quantified.

99 At the request of the referee, we have examined the Pearson correlation co-efficients for the seasonal biases  
100 given between observations and instantaneous values at 13:00hrs in Tables 7 and 8. For  $NO_2$ , only a few sites  
101 exhibit significant correlations with  $r > 0.65$  (i.e.) with many more exhibiting anti-correlations i.e. negative  $r$   
102 values, especially during DJF, or  $r$  values between -0.3-0.3 indicating no meaningful correlation between  
103 model and measurements at all. There is typically a marked difference in  $r$  between seasons at sites for both  
104 simulations, with JJA generally exhibiting higher correlations. Looking across sites reveals increasing  
105 resolution does not necessarily increase correlation though, with 1/3 of the sites exhibiting less correlation at  $1^\circ$   
106  $\times 1^\circ$  and  $1/4$  being relatively unaffected. Comparing  $r$  values at  $1^\circ \times 1^\circ$  using the Tiedke convective scheme

107 shows that although there is some impact, there is not a consistent increase in correlation when using the ERA-  
 108 interim archived mass-fluxes, with many sites exhibiting significant decreases. Therefore, similar to the  
 109 conclusions regarding seasonal biases, the use of  $1^\circ \times 1^\circ$  does not lead to a systematic improvement in  
 110 correlation showing the constraints of using monthly mean estimates for emissions towards capturing  
 111 variability.

112 We include the following text to summarise this:

113 *Analyzing the corresponding seasonal correlation co-efficients (not shown) shows in ~25% of the cases there*  
 114 *is little seasonal correlation between the weekly [NO<sub>2</sub>] in TM5-MP and the measurements regardless of*  
 115 *resolution for both seasons (Pearson's r in the range -0.3-0.3). In ~30% of cases there is actually a*  
 116 *degradation in r between resolutions, the changes somewhat reflect those seen in the seasonal biases i.e.*  
 117 *simultaneous changes to both the meteorology and local emission fluxes do not necessarily improve the*  
 118 *performance of the model. Comparing  $1^\circ \times 1^\circ$  values both with and without the Tiedtke convection scheme*  
 119 *shows that for the most convective regions (e.g. south of  $45^\circ\text{N}$ ) increases in r generally occur during JJA when*  
 120 *employing the ERA-interim mass-fluxes. Conversely for e.g. Finland the correlation becomes worse.*

121 Finally, it is not clear what selection criterium is used for putting some figures and tables in the main document  
 122 and others in the supplementary material? If a reader decides not to read the supplementary material, he should  
 123 at least have an idea of what he will miss.

124 The authors selected which Figures they find most revealing i.e. that show the most interesting findings typical  
 125 of most manuscripts. We reference the Supplementary Material many times in the text of the manuscript, so  
 126 assume that the reader has the opportunity to look at all Figures shown if he/she is interested in any particular  
 127 trace gas.

128 **Specific comments:**

129 page 1, line 15-17 differences ... differences

130 page 1, line 15-17 increases/decreases : it is not clear which resolution is the reference.

131 We modify the sentence thus: *Differences of  $\pm 20\%$  exist in the global seasonal distribution of  $^{222}\text{Rn}$  between*  
 132 *simulations conducted at  $3^\circ \times 2^\circ$  and  $1^\circ \times 1^\circ$ , being larger near specific coastal locations and tropical oceans.*

133 page 1, line 18 "strength" of convective activity is rather vague. Is CAPE meant, updraft velocity, updraft mass  
 134 flux?

135 The archived convective mass-fluxes and detrainment rates are the new meteorological fields employed in  
 136 TM5-MP from the ECMWF meteorological dataset as described in Sect. 2.1 of the manuscript. We refer to the  
 137 cumulative changes in convection determined using the  $^{222}\text{Rn}$  tracer, which come from a combination of  
 138 parameters in the meteorological dataset, now summarized as the term "convective transport".

139 page 1, line 19 NH is not yet defined. What is meant by "NH (tropics)"?

140 We remove this abbreviation from the abstract and change the text accordingly: *Analyzing vertical profiles of*  
141 *<sup>222</sup>Rn above source regions, differences in the strength of the convective transport of between 2 and 10% (~10*  
142 *and 20%) occur below 700hPa (200hPa) in the Northern Hemisphere around the tropics.*

143 *page 1, line 20-21 from simulations at 1x1 horizontal resolution. Isn't it also done for 3x2?*

144 To determine any difference in J values requires the comparison of two different runs. We clarify this in the  
145 abstract thus: *For tropospheric ozone (O<sub>3</sub>) analysis of the chemical budget terms between simulations shows*  
146 *that the impact on globally integrated photolysis rates is rather low, in spite of the higher spatial variability of*  
147 *meteorological data fields from ERA-Interim at 1° x 1°.*

148 *page 1, line 31-32 not clear whether for both resolutions.*

149 We change the text accordingly: *“By comparing NO, NO<sub>2</sub>, HNO<sub>3</sub> and PAN profiles from both simulations*  
150 *against a host of measurements ... “*

151 *page 1, line 34 shouldn't 20 and 35 sum up to 100? At this stage, the reader is not yet aware of the fact that*  
152 *changes of less than 5% are not accounted for.*

153 We imply that at 45% of the sites there is no significant change in the bias. We change the text accordingly:  
154 *For NO<sub>2</sub>, biases are more variable, with lower (higher) biases at 1° x 1° occurring at ~35% (~20%) of sites,*  
155 *with the remainder showing little change.*

156 *page 1, line 35 in TM5-PP : only the high resolution version.*

157 Figure 8 shows that there is a seasonal cycle in [HNO<sub>3</sub>] for both simulations, where there is a strong correlation  
158 for between simulations.

159 *page 2, line 55 The text mentions current resolutions of 2–4° in latitude and 2–6° in longitude. There are*  
160 *however currently models with higher resolutions, see, e.g., Yu et al. [2013.]*

161 We thank the referee for this information and update the text accordingly.

162 *page 3, line 113 which replaces the parameterization of Tiedtke (1989). Be clearer about what sub-grid scale*  
163 *parameterizations are still calculated in TM5. E.g., are turbulent diffusion coefficients calculated, or have they*  
164 *been archived too?*

165 We now include the following text: *“The vertical diffusion in the free troposphere is calculated according to*  
166 *Louis (1979), and in the BL by the approach of Holtslag and Boville (1993). Diurnal variability in the BL*  
167 *height is determined using the parameterization of Voegelezang and Holtslag (1996).”*

168 *page 3, line 117-119 Concerning large scale transport, one mentions the CFL criterium. In addition, maybe it is*  
169 *interesting for the reader to mention which transport scheme is used.*

170 We change the text accordingly: “*We use the first-order moments scheme with an iterative time-step to prevent*  
 171 *too much mass being transported out of any particular grid-cell...*”

172 page 6, line 231 The Schery et al. (2004) reference for the  $^{222}\text{Rn}$  emissions is difficult to find, as it is part of a  
 173 book. It would therefore be useful to describe shortly some aspects of the  $^{222}\text{Rn}$  emission map: is it only from  
 174 continents, is there a latitudinal gradient, are there emissions at high latitudes, is it very patchy or rather  
 175 homogeneous? Is it dependent on soil moisture or precipitation?

176 The distribution of global  $^{222}\text{Rn}$  emissions is shown in Zhang et al, ACP, 2011. We now reference this  
 177 publication for readers interested in the specifics of the  $^{222}\text{Rn}$  distribution. We feel that an in-depth discussion  
 178 of the emission inventories used detracts from the main focus of our manuscript.

179 page 8, line 290-293 Differences are attributed to the resolution of the emission data set, and the convection. It  
 180 is not clear why the temporal resolution of the emissions should play a large role. Isn't it mainly the horizontal  
 181 resolution which plays a role in explaining the difference between  $3^\circ \times 2^\circ$  and  $1^\circ \times 1^\circ$ ? In addition is written  
 182 earlier in the text (page 8, line 283) that  $^{222}\text{Rn}$  is emitted at a steady rate.

183 The emissions, which are typically provided at  $0.5\text{-}1^\circ$  resolution, are distributed onto the working model grid.  
 184 Therefore more heterogeneity occurs on a higher resolution as urban and rural centers are differentiated more  
 185 acutely. Emission at a steady rate means there is no variability in the monthly mean emission flux representing  
 186 meteorological factor or diurnal variability.

187 page 8, line 301-303 are the globally averaged  $^{222}\text{Rn}$  emissions equal in  $3^\circ \times 2^\circ$  and  $1^\circ \times 1^\circ$ ? Are the globally  
 188 average convective mass fluxes equal in  $3^\circ \times 2^\circ$  and  $1^\circ \times 1^\circ$ ?

189 page 8, line 304-306 I would expect that, if archived mass fluxes are used, the global total mass flux is equal,  
 190 independent of the resolution ( $1^\circ \times 1^\circ$  or  $3^\circ \times 2^\circ$ ). Secondly, if mass fluxes were stronger in  $1^\circ \times 1^\circ$ , I would  
 191 expect for  $1^\circ \times 1^\circ$  (compared to  $3^\circ \times 2^\circ$ ) lower  $^{222}\text{Rn}$  concentrations at the surface and higher concentrations  
 192 between 900 and 700 hPa. But for DJF in Paris and London one sees the inverse

193 All globally integrated emission fluxes of  $^{222}\text{Rn}$  are identical between simulations allowing a valid comparison  
 194 of results, similar to the other emissions introduced into TM5-MP. The values at specific locations do change  
 195 though due to the degree of coarsening of the  $0.5^\circ \times 0.5^\circ$  ECMWF data needed for the different resolutions  
 196 (although the area-weighted total is equal to the original ECMWF data in both cases). For comprehensive  
 197 details on the use of meteorological datasets in TM5 the referee is referred to Huijnen et al. (2010), which for  
 198 the sake of brevity we do not include in our manuscript. As would be expected, the global mean of the  
 199 convective mass fluxes calculated using  $3^\circ \times 2^\circ$  and  $1^\circ \times 1^\circ$  values can be slightly different due to potentially  
 200 wider spread in the  $1^\circ \times 1^\circ$  values (more members of the data array), although the summed total will be equal.  
 201 This holds for other tropospheric parameters such as temperature and surface albedo. Here we are more  
 202 interested in regional differences. To remove the variability in emission fluxes above point locations averaging  
 203 of the  $1^\circ \times 1^\circ$  profiles is necessary (where decomposition of the  $3^\circ \times 2^\circ$  profile at sub-grid scale is not  
 204 possible), thus being able to differentiate the impact of the meteorology. Under instances of weak convective

205 activity (DJF), our results show that indeed the coarsened 3 x 2 convective mass-flux can result in more uplift  
 206 than at 1° x 1°, due to the variability in the averaged 1° x 1° values being high.

207 page 9, line 341 and around Iceland for JJA. This difference is hard to distinguish.

208 We remove this from the text and will provide a higher resolution version of the diagram to improve clarity.

209 page 9, line 344-346 Here no averaging is performed towards an identical hor ... : does it mean that the value of  
 210 a 1° x 1° grid box is compared with the value of a 3° x 2° grid box? Is there a spatial interpolation between 3° x  
 211 2° grid points, and 1° x 1° grid points?

212 We use the geographical location of the cities to perform interpolation in both cases, as for all the profile  
 213 comparisons for trace gases shown in the manuscript.

214 page 10, line 368-369 Is this relevant as only 90°S-30°S, 30°S-30°N, and 30°N-90°N are shown?

215 Yes, because these three zones are comprised of cumulative sums from the 10° bands, therefore we inform the  
 216 reader as to the resolution of the budget terms.

217 page 10, line 372-373 The abbreviations O3S (tagged O3 tracer which undergoes only ...) and BO3S  
 218 (stratospheric burden of O<sub>3</sub>) are confusing. If O3S is a tracer as defined above, it would be logical that BO3S  
 219 would be just the total burden of that tracer, whereas here that is not the case.

220 BO3S is the burden of O3S, thus : *“The stratospheric burden of O<sub>3</sub> (BO<sub>3</sub>S) exhibits a strong hemispheric*  
 221 *gradient ... “*

222 page 10, line 390-391 ”At 1°x1° the largest increase in STE occurs in the SH during JJA.” : This cannot be  
 223 seen from the numbers in the tables. Isn't the aim explaining the 7% reduction?

224 Figure 2 is introduced at the start of this paragraph (line 387) and we refer to this when discussing the change  
 225 in the latitudinal gradient in Stratospheric O<sub>3</sub> with respect to the downwelling.

226 page 11, line 414-417 Differences are attributed to only 4 causes. Might there not be an impact of the  
 227 resolution on the dry deposition, the turbulent mixing, the large scale transport, or the mass conservation of the  
 228 transport?

229 The fact that the cumulative deposition velocities for e.g. O<sub>3</sub> (Table 3) are essentially the same between the 3°  
 230 x 2° and 1° x 1° simulations shows that dry deposition effects are minimal. We implicitly examine the  
 231 differences in the turbulent mixing with the Rn<sup>222</sup> comparisons, which hold for O<sub>3</sub> considering the  
 232 tropospheric lifetime is typically > 20 days. We modify the text accordingly. The large scale transport does  
 233 change as shown in the INTEXB comparison and we comment on it there. Without performing tagged O<sub>3</sub>  
 234 experiments we cannot fully quantify changes in the long-range transport component.

235 page 12, line 428 shows that differences are small : across resolutions?

236 Between the different simulations thus resolutions. We change the text thus:” ... *shows that differences are*  
237 *small between simulations, and typically mimic those which occur at the surface.*”

238 *page 11-12, line 436-438 this does not seem to hold on a regional scale.*

239 All budget terms we show are for the global or a zonal domain. There is no 3D budget file output during a run  
240 due to computational constraints. We realise that providing analyzing results in this way will not provide exact  
241 changes in clean/polluted regions. However, the comparison of O<sub>3</sub> mixing ratios in Europe again EMEP  
242 measurements shows that differences between resolutions are small, therefore changes are no so large as to  
243 lead to first-order reductions in resident [O<sub>3</sub>] due to much higher [NO].

244 *page 13, l 501 What is ORGNTR?*

245 This is the tracer name for lumped alkyl nitrates. We now include a definition at the end of the introduction  
246 along with HNO<sub>3</sub> and PAN.

247 *page 13, line 482-483 In the lower troposphere (<900 hPa) : as it is written here, one interpretes it as if (<900*  
248 *hPa) is the definition of the lower troposphere. It is however meant to be an extra condition.*

249 Rather than referring to a designated definition, we only use the terms to describe our conclusions on what is  
250 shown in Fig.6.

251 *page 13, line 490-493 And what about October?*

252 This is now corrected.

253 *page 13, line 504 to quantify the effect on higher spatial resolution.*

254 Now changed.

255 *page 13, line 515 decrease marginally by 2-3% : looking at Table S1, shouldn't it be 1-3%?*

256 Now corrected.

257 *page 15, line 581 splitting the atmosphere in 3 regions (NH extra-tropics, tropics, SH extra-tropics) is much*  
258 *rougher than ”zonally integrated”*

259 Zonally integrated refers to the cumulative values across all longitudes.

260 *page 16, line 603 Fig. S13 : is this the correct figure to be referred to?*

261 We have now corrected to text referencing the correct Figure.

262 *page 16, line 616-617 Isn't it the increase in spatial resolution which helps?*

263 Any improvement in the temporal distribution comes from an using a higher horizontal resolution on which  
 264 gridded emission estimates are applied. We now change the text to: “ *At 1° x 1° significant improvements occur*  
 265 *as a result of the better temporal resolution of the emission sources as a result of increasing horizontal*  
 266 *resolution.*”

267 page 16, line 619 aggregated on a weekly basis does not matter if one looks at seasonal biases; it would have  
 268 played a role if one also shows correlations.

269 The value presented is a mean seasonal bias as derived using the bias values from weekly points rather than a  
 270 single seasonal value.

271 page 24, Table 4 Whereas most terms in this table are in units of TgO<sub>3</sub> yr<sup>-1</sup>, it is unclear in what units BO<sub>3</sub>  
 272 and Strat. BO<sub>3</sub> are. If these are burdens, one would expect Strat. BO<sub>3</sub> to be a larger fraction of BO<sub>3</sub>, than the  
 273 values shown here (e.g., on the global scale 80 and 378).

274 We now include in the Table heading : “ .. with all quantities being given in Tg O<sub>3</sub> yr<sup>-1</sup>.” We take our number  
 275 from the individual budget files in order to quantify our Strat. BO<sub>3</sub>. Figure 2 shows that the zonal mean ratio is  
 276 between 0.05-0.7 in the troposphere, with the higher ratio correlating with lower air pressure thus less mass.  
 277 Given that through most of the troposphere the ratio changes between 0.05-0.3, 80 Tg seems a reasonable total.

278 page 24, Table 4 It is not clear where one can find “The fraction of the tropospheric burden originating from  
 279 the stratosphere is also given.” Does one mean Strat BO<sub>3</sub>? Are these absolute values Tg, or is it %?

280 We now remove this from the Table legend.

281 page 24, Table 4 Why no % for the NH/SH/tropical STE changes? As these values are not given, the sentence  
 282 on page 10, line 379 is rather unclear : “The increase in STE in the SH, with an associated decrease in the NH  
 283 ...”

284 We now add the percentage differences for each chosen zone.

285 page 25, line 744-745 Those with differences <5% are considered to exhibit no discernible change in the bias.  
 286 An interpretation should not be written in the caption of a figure.

287 The final print version of this Table will include coloring such that the number of positive and negative biases  
 288 >5% can be discerned quickly. The policy of GMD is not to include colour in the text in the first instance. The  
 289 <5% comment relates to the fact that the (black) entries in the table represent stations that are essentially  
 290 unchanged. Therefore, rather than a definition is pertains to entries in the Table.

291 page 31-32, Figs. 4-5 Are the observations also just the 13:00 values?

292 Yes, please see Sect. 2.3.

293 page 35, line 823 during September 2006 : but October 2006 is apparently also shown.

294 Figure legend now corrected.

295 **Response to anonymous referee #2:**

296 We thank the referee for their review of our manuscript and provide responses to the questions and suggestions  
297 below:

298 *A much more rigorous description of the two model setups and their differences is required. There is currently  
299 no mention of the vertical resolution although this is later reported as being important for e.g. STE fluxes. In its  
300 current format the model description in Section 2 is lacking information and is written in a way that makes it  
301 unclear which modifications are applied to the new TM5 model version and which to the higher resolution.*

302 We now add more details regarding the vertical resolution employed which is identical to that described in  
303 Huijnen et al. (2010). In the interests of brevity we did not include these specific details but will address this  
304 point by adding the following sentence:

305 *Although TM5-MP can adopt all 60 vertical levels provided by the ECMWF ERA-Interim analysis, we employ  
306 34 vertical levels for this study with higher resolution in the troposphere and the upper-troposphere-lower  
307 stratosphere (UTLS).*

308 An identical model version is compared in our study, with the only change between simulations being the  
309 horizontal resolution that is employed. This allows us to attribute the changes shown to the use of increased  
310 resolution. We now add the following sentence to the end of the first paragraph in Sect. 2.

311 *The following model description pertains to both  $3^\circ \times 2^\circ$  and  $1^\circ \times 1^\circ$  simulations discussed in this manuscript.*

312 *A paragraph should be added in Section 2 to clearly describe all details for the two model integrations used for  
313 this work. In particular, the authors should specify:*

314 *- start date of integrations and run length*

315 *- chemical initial conditions and spin up periods*

316 *- details of the analysis used (horizontal, vertical and temporal resolution).*

317 *Are these the same for both model resolutions or are they different? Are the simulated model years the same  
318 used for the emissions and observational datasets?*

319 We now provide extra details regarding the simulations as requested by the referee. Again the only model  
320 parameter changed between the simulations is the horizontal resolution, increasing from  $3^\circ \times 2^\circ$  to  $1^\circ \times 1^\circ$ . We  
321 only use 2006 observational data and clarify this in Sect. 2.3:

322 *We choose a range of ground-based and airborne measurements taken at diverse locations during the year  
323 2006 representing different chemical regimes.*

324 The use of EMEP observations in it's current state is confusing. In line 242-243 the authors state that sites in  
325 “Norway, Finland, The Netherlands, Belgium, Poland, Germany, Spain, Italy and Portugal” are used for  
326 comparison. Why just use EMEP stations from the above and not the ones in other countries? Or is this a  
327 mistake (see later)?

328 This was an oversight and has now been corrected in the text, thus:

329 ... where we exploit measurements taken at various background sites in Norway, Finland, The Netherlands,  
330 Belgium, Poland, the Czech republic, Germany, Great Britain, Spain, Slovakia, Italy and Portugal. The  
331 number of sites used for comparisons of trace species other than  $O_3$  is smaller due to data availability.

332 In Fig 3, EMEP sites from “ Finland, The Netherlands, Belgium, Poland, Slovakia and Italy” are used,  
333 aggregated by nation. The authors should explain why just these six countries? Why aggregate the sites?  
334 Poland and Slovakia should be mentioned in the list of sites in Section 2!

335 For the sake of brevity, we choose not to show individual stations but rather aggregates as has been presented  
336 in other studies (e.g. Williams et al., 2013), since we feel a station by station decomposition is not the ideal  
337 presentational form. The aggregates shown cover a significant range of latitudes throughout Europe and we  
338 wish to show comparisons for the entire European domain to provide confidence in the model performance.  
339 We now change the text to:

340 *Figure 3 shows comparisons of simulated and observed mass mixing ratios of surface  $O_3$  at EMEP sites across*  
341 *Europe ([www.emep.int](http://www.emep.int); Aas et al. 2001), with countries chosen so to cover a range of latitudes.*

342 In Fig 4, four EMEP sites are selected for comparison. Why these 4 sites? Again the sites in the Czech  
343 Republic and Great Britain used in this figure are not listed in Section 2.

344 These sites were chosen to show the diverse changes that can occur for different locations. Again the range in  
345 latitudes and longitudes shown for the European domain is broad, where only a limited number of EMEP  
346 stations measure NO and  $NO_2$  therefore identical composites as those for  $O_3$  cannot be presented. The biases  
347 for all stations are shown in Table 6.

348 In Fig 5, two sites are selected for comparison and again no explanation as to why those specific sites are used.

349 For brevity we choose to show a high and low  $NO_x$  rather than an extended set. Table 7 does provide the  
350 seasonal biases across all stations if the reader is curious as to the behavior at other sites.

351 Similarly, Table 6 and 7 use yet two different subsets of EMEP stations for comparison without explaining the  
352 reason for their choice.

353 Tables 6 and 7 present seasonal biases for all EMEP stations which measure NO and  $NO_2$ . Therefore the  
354 selection is dictated by data availability rather than by the authors. We modify the table heading accordingly:  
355 *Values are shown for both the  $3^\circ \times 2^\circ$  and  $1^\circ \times 1^\circ$  simulations for all stations with available data.*

356 In Fig 8, four selected EMEP sites are shown (from Norway, Germany, Austria and Slovakia). Same issues as  
357 above.

358 See explanations given for previous referee comments related to EMEP sites above. The number of stations  
359 measuring HNO<sub>3</sub> is a small subset of the total number of stations in the EMEP network.

360 If the purpose of the comparison with EMEP is to evaluate the model performance in the new configuration, as  
361 well as addressing the differences in model resolution, the current analysis is not convincing. Comparison of  
362 model data with tropospheric ozone column from satellite would help better evaluate model performance on  
363 the global scale. This could also lead to better evaluate the model ozone profiles which currently show  
364 significant discrepancies with MOZAIC data. Further comparison with EMEP surface sites (and other  
365 campaign data) would then add to the analysis, so far as the comparison is done across all suitable sites and a  
366 clear explanation is given if only a subset of sites is selected.

367 Due to the lack of stratospheric chemistry and microphysics in TM5MP we actually employ tropospheric  
368 ozone columns from the Multi-Sensor Re-analysis (van der A et al., 2010) for constraining the overhead ozone  
369 column (i.e.) the total column is nudged towards the observed value. Details of this method are given in Sect  
370 2.1. This means an independent comparison against satellite data is not feasible as a large fraction of O<sub>3</sub> exists  
371 above the tropopause, which is the threshold where the nudging constraint is applied. The tropospheric  
372 component of any total column value is notoriously difficult to retrieve (e.g. de Laat et al., ACP, 2009) with a  
373 high uncertainty in the value, further compounded by sampling (totally cloudy skies). EMEP comparisons are  
374 regularly used to assess the accuracy of air quality models and have high temporal coverage throughout the day  
375 for all seasons therefore act as an excellent dataset for evaluating near surface O<sub>3</sub> as long as interpolation is  
376 done well. We also provide comparisons against two independent campaigns which cover multiple days and  
377 locations, allowing an assessment of the vertical profile in the tropopause which the referee fails to mention.  
378 We feel that our conclusions are robust as to the effect of higher horizontal resolution of tropospheric O<sub>3</sub>, with  
379 similar behavior seen across independent comparisons.

380 In Section 5 the authors provide an analysis of budget terms for tropospheric ozone and compare these at the  
381 two different model resolutions. They state: “the chemical tropopause calculated for 3x2 is applied for the  
382 analysis of 1x1 budget terms to ensure that a valid comparison is performed”. However, if convection and  
383 convective transport is significantly different in the two model resolutions (as the authors suggest) the position  
384 of the chemical tropopause at 1x1 should be at a higher altitude in the tropics compared to 3x2. Using the 3x2  
385 chemical tropopause to analyse 1x1 budget terms is in my view inconsistent and the reduction in STE term  
386 with increasing resolution is likely to change if the 1x1 chemical tropopause is used.

387 Initially we did not impose the 3° x 2° tropopause definition onto the 1° x 1° budget analysis using the 150ppb  
388 gradient to diagnose the chemical tropopause for both simulations. The resulting burdens are entirely different  
389 as a different total mass of air is compared, making the STE component unrealistically large and the analysis  
390 incompatible with the profile comparisons shown throughout the manuscript. Many CTM studies adopt a  
391 climatological tropopause such as that provided by e.g. Lawrence et al., ACP, 2001 for their analysis in order  
392 to address this total mass issue.

393 **The high-resolution version of TM5-MP for optimised satellite retrievals: Description and Validation.**

394

395 **J. E. Williams<sup>1</sup>, K. F. Boersma<sup>1,2</sup>, P. Le Sager<sup>1</sup>, W. W. Verstraeten<sup>1,2,\*</sup>**

396

397 [1] {KNMI, De Bilt, The Netherlands}

398 [2] {Meteorology and Air Quality Group, Wageningen University, Wageningen, The Netherlands}

399 [\*] now at: KMI, Ukkel, Brussels, Belgium

400

401 **Abstract**

402 We provide a comprehensive description of the high-resolution version of the TM5-MP global Chemistry-  
 403 Transport Model, which is to be employed for deriving highly resolved vertical profiles of nitrogen dioxide  
 404 (NO<sub>2</sub>), formaldehyde (CH<sub>2</sub>O), and sulphur dioxide (SO<sub>2</sub>) for use in satellite retrievals from platforms such as  
 405 the Ozone Monitoring Instrument (OMI) and the Sentinel-5 Precursor, the TROPOspheric Monitoring  
 406 Instrument (tropOMI). Comparing simulations conducted at horizontal resolutions of 3° x 2° and 1° x 1° reveals  
 407 differences of ±20% exist in the global seasonal distribution of <sup>222</sup>Rn, being larger near specific coastal  
 408 locations and tropical oceans. For tropospheric ozone (O<sub>3</sub>), analysis of the chemical budget terms shows that  
 409 the impact on globally integrated photolysis rates is rather low, in spite of the higher spatial variability of  
 410 meteorological data fields from ERA-Interim at 1° x 1°. Surface concentrations of O<sub>3</sub> in high-NO<sub>x</sub> regions  
 411 decrease between 5-10% at 1° x 1° due to a reduction in NO<sub>x</sub> recycling terms and an increase in the associated  
 412 titration term of O<sub>3</sub> by NO. At 1° x 1°, the net global stratosphere-troposphere exchange of O<sub>3</sub> decreases by  
 413 ~7%, with an associated shift in the hemispheric gradient. By comparing NO, NO<sub>2</sub>, HNO<sub>3</sub> and PAN profiles  
 414 against measurement composites, we show that TM5-MP captures the vertical distribution of NO<sub>x</sub> and long-  
 415 lived NO<sub>x</sub> reservoirs at background locations, again with modest changes at 1° x 1°. We show that surface  
 416 mixing ratios in both NO and NO<sub>2</sub> are generally underestimated in both low and high NO<sub>x</sub> scenarios. For  
 417 Europe, a negative bias exists for [NO] at the surface across the whole domain, with lower biases at 1° x 1° at  
 418 only ~20% of sites. For NO<sub>2</sub>, biases are more variable, with lower (higher) biases at 1° x 1° occurring at ~35%  
 419 (~20%) of sites, with the remainder showing little change. For CH<sub>2</sub>O, the impact of higher resolution on the  
 420 chemical budget terms is rather modest, with changes less than 5%. The simulated vertical distribution of  
 421 CH<sub>2</sub>O agrees reasonably well with measurements in pristine locations, although column-integrated values are  
 422 generally underestimated relative to satellite measurements in polluted regions. For SO<sub>2</sub>, the performance at 1°  
 423 x 1° is principally governed by the quality of the emission inventory, with limited improvements in the site  
 424 specific biases with most showing no significant improvement. For the vertical column, improvements near  
 425 strong source regions occur which reduce the biases in the integrated column.

426

427 **1. Introduction**

428

429 One application of Chemistry Transport Models (CTM) is to provide accurate vertical and horizontal global  
 430 distributions of trace gases such as ozone (O<sub>3</sub>), nitrogen dioxide (NO<sub>2</sub>), sulphur dioxide (SO<sub>2</sub>) and  
 431 formaldehyde (CH<sub>2</sub>O) that are used as *a-priori* best-guesses in the retrievals of tropospheric abundances from  
 432 instruments mounted on Earth-orbiting satellites such as the Tropospheric Emission Sounder (TES; Worden et  
 433 al., 2007) Global Ozone Monitoring Experiment (GOME), SCanning Imaging Absorption spectroMeter for  
 434 Atmospheric CHartography (SCIAMACHY; De Smedt et al., 2008), the Ozone Monitoring Instrument (OMI;  
 435 Boersma et al., 2011), and GOME-2 (Valks et al., 2011). To date, although high-resolution regional models

436 have been employed for selected regions such as the US and Europe (e.g. Russell et al., 2011; Zhou et al.,  
437 2012; Vinken et al., 2014), at global scale the CTMs resolutions employed are still rather coarse (between 1.1-  
438 4.0° latitude and 1.1-6° longitude), resulting in ‘footprints’ which aggregate hundreds of kilometers in area.  
439 This has limitations as the resulting total columns are sensitive to topography, surface albedo and the shape of  
440 the *a-priori* vertical profiles themselves. Using rather coarse resolution leads to substantial errors in the  
441 retrievals (e.g. Boersma et al., 2007; Heckel et al., 2011; Russell et al., 2011) and imposes limitations towards  
442 capturing the regional scale variability in short-lived trace gas abundances observed from high-resolution  
443 satellite instruments such as OMI.

444 This lack of spatial detail is particularly relevant for situations where strong spatio-temporal variability in the  
445 vertical distribution of NO<sub>2</sub>, SO<sub>2</sub>, and CH<sub>2</sub>O can be expected. Examples include shipping lanes in the relatively  
446 unpolluted marine boundary layer (e.g. Vinken et al., 2014) and coal-fired power plant SO<sub>2</sub> pollution (e.g.  
447 Fioletov et al., 2015). Moreover, during the day the local lifetime and mixing ratios of trace gases such as nitric  
448 oxide (NO) and NO<sub>2</sub> are critically dependent on a host of variables e.g. temperature, surface albedo, cloud  
449 cover (via photolysis), chemical conversion (i.e. NO/NO<sub>2</sub> ratio) and the extent of mixing by convective  
450 upwelling (i.e. land type) and advective transport. Thus, the information provided for the retrievals is affected  
451 by the coarsening of the high-resolution meteorological data used to drive the CTM. Recently, Heckel et al.  
452 (2011) demonstrated that there is an associated uncertainty of ~2 using a-priori data from a global CTM rather  
453 than a regional CTM, principally due to loss of spatial information. Two other studies focusing on the impact  
454 of horizontal resolution on the retrieval of vertical column densities of NO<sub>2</sub> suggested that errors of up to ~50%  
455 exist (Yamaji et al., 2014; Lin et al., 2014). This problem becomes accentuated for the next generation of  
456 Earth-orbiting satellites such as the Tropospheric Monitoring Instrument (tropOMI), which has a smaller  
457 footprint compared to its predecessors (Veefkind et al., 2012). Applications of TM5 include the retrieval of  
458 NO<sub>2</sub>, CH<sub>2</sub>O, and SO<sub>2</sub> column densities from OMI and tropOMI (e.g. van Geffen et al., 2016), where studies  
459 related to the influence of horizontal resolution have been limited principally to NO<sub>2</sub>.

460 The dominant tropospheric loss terms for CH<sub>2</sub>O are photolysis and scavenging into cloud droplets (wet  
461 deposition; Jacob, 2000). Thus the atmospheric lifetime of CH<sub>2</sub>O is highly sensitive to the extent of cloud  
462 cover and the vertical profiles of the photolysis rates. A dominant application of CH<sub>2</sub>O retrievals is to provide  
463 constraints on tropical and sub-tropical isoprene emission fluxes (e.g. Palmer et al., 2006; Stavrou et al.,  
464 2009; Marais et al., 2012). The resulting emission estimates are highly sensitive to the stoichiometric yield of  
465 CH<sub>2</sub>O from isoprene oxidation, the chemical lifetime of CH<sub>2</sub>O and spatial differences in land cover. Other  
466 applications include estimating emissions released during Biomass Burning (BB) episodes (Gonzi et al., 2011),  
467 whose spatial location is also smeared via coarsening in TM5-MP. For SO<sub>2</sub>, which predominantly originates  
468 from point sources, an adequate spatial distribution of such sources is crucial for estimating accurate biases in  
469 existing emission inventories.

470 In this paper we provide a comprehensive description of the global, high-resolution 1° x 1° version of the TM5  
471 CTM tailored for the application of satellite retrievals (hereafter referred to as TM5-MP). In Sect. 2 we give  
472 details related to the modifications which have been made to the TM5 model compared to previous versions,  
473 the emission inventories employed, updates that have been made to the modified CB05 chemical mechanism,  
474 the stratospheric boundary conditions, the photolysis scheme, the heterogeneous conversion and the overall

475 model structure. In Sect. 3 we analyse the impact on convective and advective transport of trace species from  
476 the BL as derived using radon ( $^{222}\text{Rn}$ ) distributions. In Sect. 4 we investigate the effects on regional photolysis  
477 frequencies and in Sect. 5 we examine the differences introduced for both tropospheric  $\text{O}_3$ ,  $\text{NO}_x$  and N-  
478 containing species (i.e. nitric acid ( $\text{HNO}_3$ ), peroxy-acetyl-nitrate (PAN) and lumped organic nitrates  
479 (ORGNTR)) at higher resolution and make comparisons against both surface and aircraft measurements to  
480 investigate effects. In Sect. 6 we examine impact on the global  $\text{CH}_2\text{O}$  budget and integrated columns, and in  
481 Sect. 7 we show the subsequent improvement in the distribution of  $\text{SO}_2$  at  $1^\circ \times 1^\circ$ . In Sect. 8, we present our  
482 conclusions.

483

## 484 **2 Description of TM5-MP**

485

486 Previous versions of TM5 (TM5-chem-v3.0, Huijnen et al., 2010) included a two-way nested zooming option  
487 as described by Krol et al. (2005). This option allowed high-resolution simulations to be performed over any  
488 pre-defined regional, with boundary conditions being determined by the global simulation at coarser resolution.  
489 Typically, global simulations at  $3^\circ \times 2^\circ$  with zoom regions at  $1^\circ \times 1^\circ$  were performed to alleviate the long  
490 runtime of a global  $1^\circ \times 1^\circ$  run. In the new version of TM5 (hereafter referred to as TM5-MP; the massively  
491 parallel version), the usage of MPI has been totally rewritten. Zoom regions are no longer available, but data  
492 sets are distributed along longitudes and latitudes, instead of model levels and tracers. The advantages of that  
493 overhaul towards domain decomposition are a smaller memory requirement and the possibility to use more  
494 processors making global  $1^\circ \times 1^\circ$  simulations feasible in terms of runtime and affordable in terms of computing  
495 resources. A TM5-MP global  $3^\circ \times 2^\circ$  ( $1^\circ \times 1^\circ$ ) run is  $\sim 6$  ( $\sim 20$ ) times faster than the previous version of TM5  
496 (Huijnen et al., 2010) for similar resources. The following model description pertains to both  $3^\circ \times 2^\circ$  and  $1^\circ \times 1^\circ$   
497 simulations discussed in this manuscript.

498 Here we provide a comprehensive description of the modifications and updates introduced into TM5-MP  
499 compared to TM5 v3.0 (Huijnen et al., 2010). The model is driven using the ERA-interim meteorological re-  
500 analysis (Dee et al., 2011) and updated every 3 hours, with interpolation of fields for the intermediate time  
501 periods. Although TM5-MP can adopt all 60 vertical levels provided by the ECMWF ERA-Interim reanalysis,  
502 we employ 34 vertical levels for this study with higher resolution in the troposphere and Upper Troposphere-  
503 Lower Stratosphere (UTLS). Convective mass-fluxes and detrainment rates are taken from ERA-interim  
504 dataset to describe the updraft velocities from the BL into the free troposphere, which replaces the  
505 parameterization of Tiedtke (1989) used in previous versions. The vertical diffusion in the free troposphere is  
506 calculated according to Louis (1979), and in the BL by the approach of Holtslag and Boville (1993). Diurnal  
507 variability in the BL height is determined using the parameterization of Voegelezang and Holtslag (1996). We  
508 use the first-order moments scheme with an iterative time-step to prevent too much mass being transported out  
509 of any particular grid-cell during the time-step according to the preservation of the Courant-Friedrichs-Lewy  
510 (CFL) criterium (Bregman et al., 2003), which is especially relevant when reducing the size of grid-cells as  
511 done here.

512 The gas-phase chemistry in TM5-MP is described by an expanded version of the modified CB05 chemical  
513 mechanism (hereafter mCB05; Williams et al., 2013). We have placed emphasis on updating and expanding

514 the fast NO<sub>x</sub> chemistry to account for an accurate partitioning of nitrogen for higher NO<sub>x</sub> regimes than those  
515 occurring at coarser horizontal resolutions. All reaction rate data is now taken from the latest IUPAC  
516 recommendations (sited at <http://iupac.pole-ether.fr/>; last access June 2016) using updated formulations for  
517 third-body collisions, where the rate data for fast NO<sub>x</sub> and CH<sub>2</sub>O chemistry is given in Table 1. This includes  
518 the recent update to the formation rate of HNO<sub>3</sub> determined by Möllner et al. (2010). The most relevant  
519 modifications are: (i) The yield of CH<sub>2</sub>O, methanol (CH<sub>3</sub>OH) and the hydro-peroxy radical (HO<sub>2</sub>) from the  
520 self-termination of the methyl-peroxy radical (CH<sub>3</sub>O<sub>2</sub>) is increased according to Yarwood et al. (2005), (ii) the  
521 direct formation of CH<sub>2</sub>O from the reaction of CH<sub>3</sub>O<sub>2</sub> + HO<sub>2</sub> is added using the temperature dependent  
522 branching ratio defined in Atkinson et al. (2004), (iii) the production of HNO<sub>3</sub> during the oxidation of di-  
523 methyl sulphide (DMS) by the NO<sub>3</sub> is now included, (iv) explicit organic peroxy radicals have been introduced  
524 as products from the oxidation of propene (C<sub>3</sub>H<sub>6</sub>) and propane (C<sub>3</sub>H<sub>8</sub>) by OH, which are lost by either the  
525 reaction with nitric oxide (NO) or HO<sub>2</sub> allowing the in-situ chemical formation of acetone (CH<sub>3</sub>COCH<sub>3</sub>) and  
526 higher aldehydes (ALD2), respectively, following the stoichiometry given in Emmons et al. (2010), (v) a  
527 second product channel for N<sub>2</sub>O<sub>5</sub> photolysis is added producing NO, (vi) the formation and photo-dissociation  
528 of HONO has been included, (vi) the formation and transport of methyl peroxy nitrate (CH<sub>3</sub>O<sub>2</sub>NO<sub>2</sub>) is also  
529 included (Browne et al., 2011), and (vii) modifications to the gas-phase chemistry involving NH<sub>3</sub> have been  
530 introduced following the stoichiometry given in Hauglestaïne et al. (2014). This version of the modified CB05  
531 chemical mechanism is hereafter referred to as mCB05v2.

532 The calculation of height resolved photolysis rates (*J* values) is performed using a tailored version of the  
533 Modified Band Approach (MBA). The implementation and performance of this parameterization in TM5 has  
534 been fully described in Williams et al. (2012). For the calculation of the height-resolved actinic fluxes at the  
535 seven specific wavelengths used for calculating the *J* values (these being 205.1nm, 287.9nm, 302.0nm,  
536 311.0nm, 326.5nm, 385.0nm and 610.0nm), the 2-stream radiative transfer solver of Zdunkowski et al. (1980)  
537 is embedded into TM5-MP. Details regarding the parameterizations used to account for the scattering and  
538 absorption introduced by gaseous molecules, aerosols and clouds the reader is referred to Williams et al.  
539 (2012). For aerosols, the climatology of Shettle and Fenn (1979) is included. The calculation of the effective  
540 radius (*r<sub>eff</sub>*) of cloud droplets is now performed using the approach of Martin et al. (1994), where different  
541 parameter values are used for over the land and ocean using cloud condensation nuclei concentrations of 40  
542 and 900, respectively. Due to potentially erroneous values at low horizontal resolution, we weight the final *r<sub>eff</sub>*  
543 value using the land fraction in each grid-cell. We apply limits between 4-16µm on the resulting *r<sub>eff</sub>* values.  
544 This improves the representation of the scattering component due to cloud droplets used for the calculation of  
545 the actinic flux in the lower troposphere (LT; not shown). For the scattering effects from cloud droplets, we  
546 subsequently downsize the physical *r<sub>eff</sub>* by ~0.5-2µm to account for the relationship between the optical and  
547 physical *r<sub>eff</sub>* values.

548 For aerosols, an aerosol scheme is available for use within TM5-MP (aan den Brugh et al., 2010), but we  
549 choose not to use it for the purpose of satellite retrievals due to the extra computational expense needed when  
550 performing high resolution simulations that would potentially hinder operational use. We acknowledge that the  
551 description of aerosols in this study is rather crude and increasing scattering could have an impact under  
552 instances of low cloud coverage. For the application of TM5-MP towards satellite retrieval, it is preferable to  
553 use any advancements in computational performance on further increases in the horizontal resolution

554 employed. Therefore it is not currently envisaged that a full description of aerosol processes will be included  
555 during operational satellite retrievals.

556 However, heterogeneous conversion processes still need the description of the total reactive Surface Area  
557 Density (SAD) from aerosols. In TM5-MP this is assumed as the cumulative value of contributions from  
558 sulphate, nitrate, ammonium and methane sulphonic acid as calculated by the EQUilibrium Simplified Aerosol  
559 Model (EQSAM) approach (Metzer et al., 2002), thus the secondary organic aerosol component is not  
560 included. The distribution of these aerosol species is calculated online and coupled to the respective gaseous  
561 precursors. The density of each aerosol type ( $1.7 \text{ g/cm}^3$ ) and  $r_{eff}$  (of between  $0.18\text{-}0.2\mu\text{m}$ ) is prescribed as in  
562 Huijnen et al. (2014). Swelling at higher relative humidities ( $> 70\%$ ) is crudely accounted for by increasing  $r_{eff}$   
563 between  $0.25\text{-}0.27\mu\text{m}$ . The contributions due to sea-salt, black carbon and organic carbon towards  
564 heterogeneous loss are not accounted for. Temperature dependent gas-phase diffusion co-efficients ( $D_g$ ) are  
565 used in the derivation of the pseudo first-order heterogeneous rate constants based on the theory of Schwartz  
566 (1986).

567 For  $\text{N}_2\text{O}_5$ , the uptake coefficient ( $\gamma$ ) is calculated using the parameterization of Evans and Jacob (2005),  
568 therefore dependent on both temperature and relative humidity. Once a surface reaction with  $\text{H}_2\text{O}$  occurs two  
569 molecules of  $\text{HNO}_3$  are formed. No uptake on cirrus particles is included for  $\text{HNO}_3$ , which can lead to de-  
570 nitrification of the upper troposphere (Lawrence and Crutzen, 1998; von Kuhlmann and Lawrence, 2006). For  
571  $\text{HO}_2$  we adopt a fixed  $\gamma_{\text{HO}_2} = 0.06$  across all aerosol types as taken from Abbatt et al. (2012) and for  $\text{NO}_3$  we  
572 adopt a fixed  $\gamma_{\text{NO}_3} = 10^{-3}$  as recommended by Jacob (2000). For  $\text{HO}_2$ , heterogeneous conversion forms 0.5  
573 molecules of Hydrogen Peroxide ( $\text{H}_2\text{O}_2$ ), whereas for  $\text{NO}_3$  it forms one molecule of  $\text{HNO}_3$  is formed,  
574 following Emmons et al. (2010). For the SAD associated with cloud droplets we use the  $r_{eff}$  values that are  
575 calculated by Martin et al. (1994) thus maintaining consistency between the size of the cloud droplets used for  
576 the scattering component in the calculation of  $J$  values and heterogeneous loss rates on the clouds. By using the  
577 ECMWF cloud fraction for each respective grid-cell, we assume that instantaneous mixing throughout the grid-  
578 cell does not occur in order to avoid exaggerated conversion rates on cloud surfaces.

579 As TM5-MP contains no explicit stratospheric chemistry, we apply constraints above the tropopause to ensure  
580 realistic Stratosphere-Troposphere Exchange (STE) of  $\text{O}_3$  and for constraining the incoming radiation reaching  
581 the troposphere needed for the MBA (Williams et al., 2012). For stratospheric  $\text{O}_3$ , we use total column values  
582 derived from the assimilation of satellite observations as provided in the improved version of the Multi-Sensor  
583 Re-analysis (MSR, van der A., 2010), which is vertically distributed according to the climatology of Fortuin  
584 and Kelder (1998). Three distinct zonal bands are used for nudging the stratospheric  $\text{O}_3$  fields, these being  
585  $30^\circ\text{S}\text{-}30^\circ\text{N}$ ,  $30\text{-}66^\circ\text{S/N}$  and  $> 66^\circ\text{S/N}$ , where nudging occurs at pressure levels  $<45\text{hPa}$ ,  $<95\text{hPa}$  and  $<120\text{hPa}$ ,  
586 with relaxation times of 2.5 days, 3 days and 4 days, respectively.

587 For stratospheric  $\text{CH}_4$  we use the monthly 2D climatological fields provided by Grooß and Russell (2005), with  
588 the nudging heights and relaxation times being identical to those used for stratospheric  $\text{O}_3$ . For stratospheric  
589  $\text{CO}$  and  $\text{HNO}_3$  we constrain mixing ratios by using monthly mean ratios of  $\text{CO}/\text{O}_3$  (Dupuy et al., 2004) and  
590  $\text{HNO}_3/\text{O}_3$  (Jégou et al., 2008; Urban et al., 2009) based on the latitudinal climatologies derived from ODIN  
591 observations using data for 2003/2004 ( $\text{CO}$ ) and 2001-2009 ( $\text{HNO}_3$ ). In order to avoid jumps in the nudging  
592 constraints between months, we gradually change between ratios using the total monthly difference/number of

593 days in the month. These ratios are applied using the monthly mean stratospheric O<sub>3</sub> distribution in TM5-MP,  
594 which is constrained by the MSR dataset (van der A et al., 2010). For both species, model fields are nudged at  
595 5.5hPa, 10hPa and 28hPa using relaxation times of 5, 10 and 60 days, respectively. Previous versions of TM5  
596 used a HNO<sub>3</sub> climatology from the UARS MLS instrument and applied nudging constraints at 10hPa only  
597 (Huijnen et al., 2010).

598 For our study concerned with the impact of horizontal resolution on the performance of TM5-MP present 12  
599 month simulations for the year 2006, which has been used for previous benchmarking studies (Huijnen et al.,  
600 2010; Williams et al., 2012). We use a one year spin-up from the same initial conditions, where the initial  
601 conditions are representative of the state-of-the-atmosphere for January 2005 taken from a previous simulation  
602 (see Zeng et al., 2015). The model is run using 34 levels, as it will be used operationally for satellite retrievals,  
603 where details of the pressure levels being given in Huijnen et al., 2010.

604

## 605 **2.2 Emission inventories**

606

607 All emission inventories applied in TM5-MP are yearly specific meaning that the year-to-year variability in  
608 emission fluxes due to changes in anthropogenic activity, biogenic activity and burning extent are taken into  
609 account. For the anthropogenic emission of NO<sub>x</sub>, CO, SO<sub>2</sub>, NH<sub>3</sub> and Non-Methane Volatile Organic  
610 Compounds (NMVOC), we adopt the MACCity emission estimates described in Granier et al. (2011). The lack  
611 of sector-specific information complicates the use of daily cycles for e.g. the road transport component. For  
612 volcanic SO<sub>2</sub> emissions, the estimated emission flux has been scaled up to 10 Tg S yr<sup>-1</sup> based on Halmer et al.  
613 (2002). For the biogenic component, where available we use the CLM-MEGANv2.1 emission inventories  
614 produced for the Southern Hemispheric Multi-model Intercomparison Project (SHMIP) as described in Zeng et  
615 al. (2015), with the missing trace species (e.g. ethane, propane, higher organics) coming from alternative  
616 MEGAN simulations as outlined in Sindelarova et al. (2014). A diurnal cycle is imposed on the isoprene  
617 emissions and introduced into the first ~50m between 20°S-20°N. The BB emissions are taken from the  
618 monthly estimates provided by the GFEDv3 inventory (van der Werf et al., 2010) and latitude dependent  
619 injection heights and a tropical burning cycle are implemented following Huijnen et al. (2010). All emission  
620 inventories are provided on a 0.5° x 0.5° resolution and subsequently coarsened onto the horizontal resolution  
621 employed in any simulation. For lightning NO<sub>x</sub> we use the parameterization which uses convective  
622 precipitation fields (Meijer et al., 2001) and constrain the annual global emission term at ~6 Tg N yr<sup>-1</sup>. This  
623 uses the convective flux values meaning that re-scaling of the nudging term was necessary in order to achieve  
624 similar total lightning NO<sub>x</sub> across simulations. In TM5-MP all NO<sub>x</sub> emissions are introduced as NO, rather  
625 than speciating a fraction which is emitted directly as NO<sub>2</sub> (Carslaw and Beevers, 2005). Global NO<sub>x</sub> emissions  
626 for the year 2006 total 49 Tg N yr<sup>-1</sup> (including lightning). Other notable species include CO (1081 Tg CO yr<sup>-1</sup>),  
627 SO<sub>2</sub> (117 Tg S yr<sup>-1</sup>), CH<sub>2</sub>O (13.5 Tg C yr<sup>-1</sup>) and isoprene (510 Tg C yr<sup>-1</sup>). An overview of the global and zonal  
628 emissions terms used in the simulations analysed here are given in Table 3.

629 Latitudinal constraints on CH<sub>4</sub> global distributions are applied using the methodology given in Banda et al.  
630 (2015) with a 3-day relaxation time. We also introduce similar constraints based on the appropriate surface  
631 measurements for H<sub>2</sub> in order to account for the latitudinal gradient and variability across seasons, which

632 replaces the fixed global value of 550ppb used in previous versions. Finally, for Radon ( $Rn^{222}$ ) emissions we  
633 apply the estimates of Schery (2004), whose global distribution is given in Zhang et al. (2011).

634

### 635 **2.3 Observations**

636

637 Although the performance of mCB05 in TM5 v3.0 has been validated for selected NMVOC,  $O_3$ ,  $CH_2O$ , CO  
638 and  $NO_y$  in both hemispheres (Williams et al., 2013; 2014; Fisher et al., 2015; Zeng et al., 2015), the  
639 significant changes made to both the chemical scheme and the rate parameters in mCB05v2 necessitate  
640 independent validation at both  $3^\circ \times 2^\circ$  and  $1^\circ \times 1^\circ$ . We choose a range of ground-based and airborne  
641 measurements taken at diverse locations during the year 2006 representing different chemical regimes. Here  
642 we briefly describe the observations utilised for this purpose.

643 For validation of simulated surface concentrations we use measurements of gaseous  $O_3$ , NO,  $NO_2$ ,  $HNO_3$  and  
644  $SO_2$  available from the European Monitoring and Evaluation program (EMEP, [www.emep.int](http://www.emep.int)), where we  
645 exploit measurements taken at various background sites in Norway, Finland, The Netherlands, Belgium,  
646 Poland, the Czech republic, Germany, Great Britain, Spain, Slovakia, Italy and Portugal. The number of sites  
647 used for comparisons of trace species other than  $O_3$  is smaller due to data availability. For the model  
648 composites we extract data from 3 hourly instantaneous output in order to assemble both the weekly and  
649 monthly mean values from the simulations. For the weekly comparisons of  $NO_2$  and  $SO_2$  we use values  
650 extracted at 13:00 local time, close to the overpass time of the OMI instrument (e.g. Boersma et al, 2008). The  
651 selected stations allow validation of the seasonality for both rural regions (FI37) and urban regions (NL09),  
652 where we include identical stations where possible for both species. For  $HNO_3$  we assemble the weekly values  
653 from the daily averages.

654 Measured [ $O_3$ ] in the EMEP network are obtained using UV monitors (Aas et al. 2001). For all species, spatial  
655 interpolation of model data is performed accounting for the height of the measurement station and by  
656 weighting using the distance of the station from the surrounding grid-cells. The wide range of measurement  
657 sites chosen ensures that both background and polluted cases are assessed.

658 For validating the vertical distribution of relevant trace species such as  $O_3$ ,  $SO_2$  and  $CH_2O$ , we use  
659 measurements by the DC-8 aircraft during the Intercontinental Chemical Transport Experiment B (INTEX-B;  
660 Singh et al., 2009) that took place between March and May 2006. Observations of a host of co-located  
661 nitrogen-containing species are available (namely NO,  $NO_2$ , PAN and  $HNO_3$ ). These flights were conducted  
662 over a wide region, and we use all three months of measurements. Each month sampled a different region  
663 representing different meteorological conditions and local emission sources, namely: the Gulf of Mexico ( $90-$   
664  $100^\circ W$ ,  $15-30^\circ N$ ), the remote Pacific ( $176-140^\circ W$ ,  $20-45^\circ N$ ) and to the south and west of Alaska over the  
665 ocean ( $160-135^\circ W$ ,  $20-60^\circ N$ ). Measurements cover altitudes up to 10.5km, and we bin the values with respect  
666 to pressure using 50 hPa bins or less in the LT. We interpolated three-hourly output against measurements for  
667 each respective day, similar to the comparisons performed in previous evaluations of TM5 (e.g. Huijnen et al.,  
668 2010), but we segregate our comparisons into the three distinct regions. For details relating to the location of  
669 each flight the reader is referred to the campaign overview of Singh et al. (2009).

670 For tropospheric  $O_3$ , we supplement the INTEX-B comparisons with measurements taken over more polluted  
671 regions as part of the Measurement of Ozone, water vapour, carbon monoxide and nitrogen oxides by Airbus

672 In-service aircraft initiative (MOZAIC; Thouret et al., 1998). We aggregate the measurements as seasonal  
673 means for December-January-February (DJF) and June-July-August (JJA) in order to provide a robust number  
674 of samples for each location. Here we choose to use profiles representative of the Northern mid-latitudes,  
675 namely: London (0.2°W, 51.2°N), Vienna (16.5°E, 48.1°N), Washington (77.5°W, 38.9°N), Portland (122.6°W,  
676 45.6°N), Shanghai (121.8°E, 31.2°N) and Tokyo (140.4°E, 35.8°N).

677 We also make comparisons of O<sub>3</sub>, NO, NO<sub>2</sub>, selected N-reservoir species, SO<sub>2</sub> and CH<sub>2</sub>O profiles using  
678 measurements made aboard the NOAA WP-3D aircraft as part of the Second Texas Air Quality Study  
679 (TexAQS II; Parrish et al, 2009), which was conducted over the Texas sea-board during September and  
680 October 2006. This allows the assessment of TM5-MP over a region with higher NMVOC emissions and  
681 industrial activity. These measurements were typically sampled at altitudes below 500hPa, therefore no  
682 measurements in the UTLS are available from this campaign.

683

### 684 **3 The Effect on Atmospheric Transport**

685

686 Here we analyse the differences in convective transport out of the BL by analysing the vertical and horizontal  
687 distribution of <sup>222</sup>Rn, which is a diagnostic typically used for assessing the differences in transport in CTMs  
688 (e.g. Jacob et al., 1997). <sup>222</sup>Rn is emitted at a steady rate and exhibits a half-life of ~3.8 days, which is long  
689 enough to be transported from the BL into the FT due to chemical passivity, with loss via wet scavenging and  
690 dry deposition being negligible. Therefore, it acts as an ideal tracer to assess differences in convective transport  
691 from the surface out of the BL.

692 Figure 1 shows seasonal mean horizontal global distributions of <sup>222</sup>Rn for DJF and JJA in the 1° x 1° simulation  
693 averaged between 800 and 900hPa (i.e. sampling the LT). Also shown are the associated percentage  
694 differences against the re-binned 3° x 2° <sup>222</sup>Rn distribution, allowing a direct comparison. Resolution dependent  
695 differences result from the cumulative effects of the use of higher resolution mass-fluxes from the ERA-interim  
696 meteorological data for describing convective activity and the more accurate temporal distribution of regional  
697 <sup>222</sup>Rn emissions at 1° x 1°. In general it can be seen that seasonal differences of ±20% exist, typically with  
698 increases over continents and decreases over oceans in the 1° x 1° simulations. Maximal differences of >60%  
699 occur near selected coastal regions (California, West Africa, Madagascar) or in outflow regions such as off  
700 South America and Africa, where differences exhibit a strong seasonal dependency. This is due to the large  
701 differences in convective strength due to the variability in heating rates, and thus temperatures, between land  
702 and ocean (e.g. Sutton et al., 2007).

703 A comparison of the ratio of the monthly mean <sup>222</sup>Rn profiles (1° x 1° / 3° x 2°) extracted above selected  
704 European cities for January (black) and July (blue) 2006 are shown in Fig. S1 in the Supplementary Material.  
705 The typical tropospheric profile of <sup>222</sup>Rn exhibits an exponential decay from the LT to the FT (not shown). In  
706 order to homogenise the emission flux in the comparison, we coarsen the 1° x 1° data onto the 3° x 2° grid by  
707 averaging the six individual values into a representative mean column. The extent of the changes in the vertical  
708 distribution of <sup>222</sup>Rn is somewhat site specific meaning an in depth analysis is beyond the scope of this paper.  
709 In summary, the 1° x 1° simulation generally provides stronger convective activity for January, with the main  
710 impact occurring below 700hpa (e.g. London and Paris). The changes in <sup>222</sup>Rn in the LT range between 2 and  
711 10% (i.e. ratios of 0.9 to 1.1), implying both weaker and stronger convective transport depending on changes in

712 location (e.g. orography and land type). In that the impact at Berlin is larger than at e.g. Barcelona also shows  
713 that, surprisingly, the inclusion of a large ocean fraction (with weaker convective mixing) in the  $3^\circ \times 2^\circ$  cell  
714 does not seem to introduce dominating effects. For July the changes in the vertical distribution extend into the  
715 FT up to 500hPa, although changes in the upper FT have a significant component due to changes in long-range  
716 transport. The magnitude of the changes are similar to those exhibited during January, although maybe of the  
717 opposite sign (e.g. Rome). Thus the influence on e.g.  $\text{NO}_2$ ,  $\text{CH}_2\text{O}$  and  $\text{SO}_2$  *a-priori* vertical profiles will be  
718 non-negligible and diverse.

719 For the tropical cities located in regions where convective mixing is stronger, the corresponding differences  
720 can reach  $\pm 20\%$ , especially near the surface (e.g. Caracas and Karachi). There is a site-specific seasonal  
721 dependency in the magnitude of the changes related to the regional land characteristics (e.g. Lagos versus  
722 Kuala Lumpur). Thus, differences in *a-priori* vertical profiles of trace gases for  $1^\circ \times 1^\circ$  can be considerable  
723 compared to those provided at a  $3^\circ \times 2^\circ$  resolution.

724 We also show comparisons of profiles from  $1^\circ \times 1^\circ$  simulations using the convective scheme of Tiedke (1989)  
725 against those using the convective mass-fluxes from the ERA-interim meteorological dataset for Europe (Fig.  
726 S3). For this comparison no daily averaging is employed with  $^{222}\text{Rn}$  profiles extracted from 3 hourly  
727 instantaneous sampling, with the profiles shown being interpolated directly above urban conurbations (with  
728 high trace gas emissions). The residuals show that the significant differences exist, with the convective mass-  
729 fluxes from ERA-interim being somewhat weaker than those calculated online using Tiedke (1989) (i.e) the  
730 ratio is typically less than 1, especially during July.

731

#### 732 **4 The Impact on tropospheric photolysis frequencies**

733

734 The changes in the spatio-temporal distribution of cloud cover and surface albedo have the potential to alter the  
735 penetration depth and upwelling of photolysing light, and thus photochemical production and destruction  
736 terms. The similarity in the monthly mean photolysis frequencies for  $\text{O}_3$  and  $\text{NO}_2$  across resolutions (hereafter  
737 denoted  $J_{\text{O}_3}$  and  $J_{\text{NO}_2}$ , respectively) are shown in Fig. S4 of the Supplementary Material. Comparisons of the  
738 monthly mean  $J_{\text{O}_3}$  and  $J_{\text{NO}_2}$  values are shown at five different locations identical to those shown in Williams et  
739 al. (2012). For  $J_{\text{O}_3}$  the impact of increasing resolution is limited to a few percent in the monthly mean values.  
740 At global scale this leads to a reduction of  $\sim 2\%$  in the total mass of  $\text{O}_3$  photolysed (not shown). For  $J_{\text{NO}_2}$ , the  
741 corresponding differences become more appreciable, with  $1^\circ \times 1^\circ$  exhibiting  $\sim 5\text{-}10\%$  higher values at high  
742 Northern latitudes (associated with the high- $\text{NO}_x$  scenario).

743 Focusing on  $J_{\text{NO}_2}$  and comparing seasonal mean values near the surface shows that very similar spatial patterns  
744 occur for both simulations at global scale (c.f. Fig. S5). The highest  $J_{\text{NO}_2}$  values occur over the tropical oceans  
745 and high altitude regions (e.g. Nepal). Although more regional fine-structure can be seen at  $1^\circ \times 1^\circ$  (e.g. South-  
746 Western US for DJF), these seasonal averages show that the small perturbations shown in Fig. S3 extend to the  
747 global scale leading to a reduction of  $\sim 5\%$  at  $1^\circ \times 1^\circ$ .

748 Comparisons of monthly mean profiles of  $J_{\text{O}_3}$  and  $J_{\text{NO}_2}$  extracted over the location of selected tropical cities are  
749 shown in the Figs. S6a and b, respectively, in the Supplementary Material. Here no averaging is performed  
750 towards an identical horizontal resolution, therefore values are representative of the  $J$  values directly above the  
751 selected urban centres. The  $J_{\text{O}_3}$  profiles are affected to a larger extent than the  $J_{\text{NO}_2}$  profiles due to the

752 characteristic absorption spectra of each species, which makes  $J_{O_3}$  more sensitive to the additional scattering  
753 introduced due to clouds. Profiles over Dubai act as a proxy for clear-sky conditions, where values of unity  
754 exist in the residual of  $J_{O_3}$  and  $J_{NO_2}$  calculated through most of the column. The small difference at the surface  
755 is due to changes in the surface albedo between resolutions, with Dubai being situated on the coast meaning  
756 that a sharp horizontal gradient exists in surface albedo. For other cities, the largest perturbations occur away  
757 from the surface (e.g. Jakarta, Nairobi and Lagos) around the altitude where tropospheric clouds are most  
758 abundant. There are typically changes of between  $\pm 5$ -10% in the monthly mean profiles. The changes in  $J_{NO_2}$   
759 reflect those simulated for  $J_{O_3}$ , with somewhat smaller perturbations.

760

## 761 **5 Implications for oxidative capacity and tropospheric O<sub>3</sub>**

762

763 The partitioning of reactive N between the short- and long-lived chemical N-reservoirs included in TM5-MP  
764 depends on the oxidative capacity simulated for the troposphere via competition between the various different  
765 radicals (i.e. OH, CH<sub>3</sub>C(O)O<sub>2</sub>, NO<sub>3</sub> and CH<sub>3</sub>O<sub>2</sub>). Therefore, changes to the distribution and resident mixing  
766 ratios of tropospheric O<sub>3</sub> subsequently impose changes on the fractional composition of the NO<sub>y</sub> budget (e.g.  
767 Olszyna et al., 1994) and the also the efficiency of the NO<sub>x</sub> recycling terms by altering the chain length  
768 (Lelieveld et al., 2004). In this section we analyse the global and zonal chemical budget terms for tropospheric  
769 O<sub>3</sub> to highlight the inter-hemispheric differences which occur (i.e. under low and high-NO<sub>x</sub> environments).

770 Table 4 provides the zonally segregated chemical budget terms for tropospheric O<sub>3</sub>, from which the global  
771 component due to STE can be determined by closing the budget terms following the methodology given in  
772 Stevenson et al. (2006). The chemical tropopause calculated for 3° x 2° is applied for the analysis of 1° x 1°  
773 budget terms to ensure that a valid comparison is performed, (i.e. the same mass of air is accounted for). For  
774 computational efficiency the budget terms are aggregated in 10° latitudinal bins and summed across all  
775 longitudes providing the cumulative terms.

776 The most significant change with resolution concerns STE. By using a dedicated tagged stratospheric O<sub>3</sub> tracer  
777 (which only undergoes photo-chemical destruction and deposition in the troposphere; hereafter denoted as  
778 O<sub>3</sub>S) changes in the zonal mean STE can be determined. The stratospheric burden of O<sub>3</sub> (BO<sub>3</sub>S) exhibits a  
779 strong hemispheric gradient with much more downwelling occurring in the NH peaking during boreal  
780 springtime. At global scale the STE exchange is 579 Tg O<sub>3</sub> yr<sup>-1</sup>, which agrees well with the multi-model mean  
781 for STE of 556±154 Tg O<sub>3</sub> yr<sup>-1</sup> in Stevenson et al. (2006), with observational estimates being ~550±140 Tg O<sub>3</sub>  
782 yr<sup>-1</sup> (Olsen et al., 2001). The ~7% reduction of STE at 1° x 1° is encouraging considering that previous studies  
783 using TM5 have concluded that STE in TM5 at 3° x 2° was biased high compared to STE inferred from TES  
784 and MLS satellite observations (Verstraeten et al. (2015)). The increase in STE in the SH, with an associated  
785 decrease in the NH (see below), implies that there is a shift in circulation patterns at 1° x 1° even though BO<sub>3</sub>S  
786 remains essentially unchanged. Previous studies have shown that in order to resolve the correct spatial and  
787 temporal Stratosphere-Troposphere flux, high resolution is required both in the horizontal and the vertical  
788 gridding (e.g. Meloen et al., 2002). The NH STE diagnosed with TM5-MP is an order of magnitude smaller  
789 than estimates derived in a CTM study also conducted at a 1° x 1° resolution (Tang et al, 2011; ~200 TgO<sub>3</sub> yr<sup>-1</sup>),  
790 which identified deep convection as important for STE. Here we use a different vertical grid and

791 meteorological dataset to drive TM5-MP, both of which affect the ability towards capturing an accurate STE  
792 flux (Meloan et al., 2002).

793 The zonal seasonal means of the fraction of O<sub>3</sub>S to O<sub>3</sub> (O<sub>3</sub>S/O<sub>3</sub>) for both simulations are shown in Fig. 2 for  
794 DJF and JJA. There is a clear seasonal zonal shift in the fractional contribution due to the O<sub>3</sub> transported  
795 downwards from the Stratosphere exhibiting a longer lifetime in the winter hemisphere reflecting a lower  
796 photochemical destruction rate. At 1° x 1° the largest increase in STE occurs in the Southern Hemisphere (SH)  
797 during JJA. Here ~20-25% of tropospheric O<sub>3</sub> is transported down from the Stratosphere. Comparing the 0.2  
798 contour for the NH mid-troposphere shows significant changes, extending further down towards the surface  
799 during boreal wintertime leading to the higher total mass of O<sub>3</sub>S in the troposphere. The extent of nudging  
800 towards the MSR climatology is essentially constant across simulations (c.f. Table 4). Interestingly, less O<sub>3</sub>S  
801 reaches the surface in the tropics at 1° x 1° due to the enhanced chemical destruction term in the Free  
802 Troposphere. Approximately 10% of the global deposition term for O<sub>3</sub> is associated with O<sub>3</sub> that originates  
803 from the Stratospheric at 1° x 1° (c.f. ~5% at 3° x 2°). For the NH, this contributes to the simulated increase in  
804 deposition of ~9%.

805 For tropospheric O<sub>3</sub> there are similarities that occur between the NH, tropics and SH (i.e.) high and low-NO<sub>x</sub>  
806 scenarios, resulting in a cumulative decrease in O<sub>3</sub> production of ~2-4% across zones. For the chemical loss  
807 terms there is a decrease of ~3% (~1%) in the NH (SH) reflective of the changes discussed for J<sub>O<sub>3</sub></sub>, which acts  
808 as the primary destruction term. There is a zonal gradient in the tropospheric burden of O<sub>3</sub> (BO<sub>3</sub>) following the  
809 zonal gradient in NO<sub>x</sub> emissions. Comparing terms shows that BO<sub>3</sub> decreases at 1° x 1° by a few percent at  
810 global scale (~7 Tg O<sub>3</sub>) making a rather small impact on oxidative capacity. This is of the same order of  
811 magnitude as that found in previous studies concerned with horizontal resolution (e.g. Wild and Prather, 2006).  
812 Interestingly, changes in the deposition flux of O<sub>3</sub> are rather small, even though there is a larger amount of  
813 variability in the land surfaces and better-resolved land-sea contrast at 1° x 1°, although differences in regional  
814 deposition fluxes can be more significant. Multi-model inter-comparisons of surface deposition terms across  
815 models have shown previous versions of TM5 to be at the low end of the model spread in terms of O<sub>3</sub> (Hardacre  
816 et al., 2015), suggesting that the surface deposition flux to e.g. should be increased by ~10% in TM5-MP  
817 towards the multi-model mean value. This can be partly attributed to the large uncertainty which exists related  
818 to the loss of O<sub>3</sub> to the ocean (Hardacre et al., 2015).

819 Figure 3 shows comparisons of simulated and observed mass mixing ratios of surface O<sub>3</sub> at EMEP sites across  
820 Europe ([www.emep.int](http://www.emep.int); Aas et al. 2001), with countries chosen so to cover a range of latitudes. Previous  
821 comparisons using mCB05 have revealed high biases in surface O<sub>3</sub>, especially during boreal summertime  
822 (Williams et al., 2013). These high biases originate from cumulative effects associated with the accuracy of the  
823 emission inventories, the convective and turbulent mixing component, the underestimation of the scattering  
824 and absorption of photolysing light due to aerosols and the chemical mechanism that is employed. For the  
825 emission component it should be noted that even at 1° x 1° coarsening is performed, where emission  
826 inventories are typically supplied at 0.5° x 0.5° resolution. The seasonal cycle in surface O<sub>3</sub> is captured to a  
827 large degree, and the high bias exhibited by the model is generally reduced by ~2-5 ppb (or ~20%) at 1° x 1°.  
828 This is associated with perturbations in the NO<sub>x</sub> recycling terms, chemical titration by NO, changes to the  
829 turbulent diffusion and convective mixing out of the BL. In that the improvement in biases is largest during  
830 boreal summertime is associated with the shorter chain length of the NO<sub>x</sub> recycling term during boreal

831 wintertime (c.f. Fig 2). However, there is still a significant monthly mean bias in both simulations when  
832 compared against observations throughout the year, especially for locations impacted by a large anthropogenic  
833 NO<sub>x</sub> source. This is partly due to the low NO/NO<sub>2</sub> ratio as discussed in Sect. 4 below.

834 Comparing vertical profiles from composites assembled from the MOZAIC measurements for DJF and JJA  
835 (Figs. S7a and S7b, respectively), INTEX-B (Singh et al, 2009; Fig. S8) and TexAQS II (Parrish et al, 2009;  
836 Fig. S9) shows that differences are small between simulations, and typically mimic those which occur at the  
837 surface. There is a general positive bias of 20-40% in mixing ratios exhibited across all comparisons, although  
838 the variability in the vertical gradients across regions is captured rather well. Such positive biases have  
839 consequences for both the NO<sub>x</sub> recycling terms and HNO<sub>3</sub> formation discussed in the sections below.

840

#### 841 **4 Implications for the distribution of NO and NO<sub>2</sub>**

842

843 Table 5 provides the zonally segregated annual NO<sub>x</sub> recycling terms involving the main peroxy-radicals and  
844 the direct titration term involving NO for the 1° x 1° simulation. The conversion rate of NO back into NO<sub>2</sub>  
845 decreases by ~2-3% across zones as a consequence of an associated increase in the titration term and re-  
846 partitioning of N into long-lived reservoir species (see below). For the titration term involving NO, although  
847 the globally integrated flux remains relatively constant, there is contrasting behaviour for the two most  
848 important zones (TR, NH), which exhibit a lower and higher titration term, respectively. It has been shown that  
849 for regions such as Europe the increased titration results in lower surface O<sub>3</sub> mixing ratios (c.f. Fig. 3),  
850 improving the boreal summertime high bias at the surface.

851 Important model uncertainties include the quality of the MACCity NO<sub>x</sub> emission inventory, the lifetime of NO<sub>2</sub>  
852 simulated in TM5 and the recycling term via the chemical titration of O<sub>3</sub>. Figures 4 and 5 shows comparisons  
853 of weekly [NO] and [NO<sub>2</sub>] surface measurements against the corresponding composites from both of the  
854 simulations, sampled at 13:00 local time which is close to the time of overpass for OMI and tropOMI.  
855 Although the number of EMEP sites conducting NO<sub>x</sub> measurements is smaller than those measuring O<sub>3</sub>, we  
856 choose stations located throughout Europe in both high and low NO<sub>x</sub> regimes. To supplement these  
857 comparisons we provide the seasonal mean biases for DJF and JJA from both simulations in Tables 6 and 7,  
858 respectively, calculated using weekly binned data from all EMEP sites, which measure hourly [NO] and [NO<sub>2</sub>]  
859 levels. Here we perform an analysis across sites rather than focusing on the behaviour at selected individual  
860 locations.

861 For the determination of [NO<sub>2</sub>], the reduction of NO on a Molybdenum convertor takes place with subsequent  
862 detection by chemi-luminescence, with an associated detection limit of ~0.4ppb. Previous studies have shown  
863 that some bias can result due to the oxidation of nitrogen reservoirs such as PAN (Dunlea et al., 2007;  
864 Steinbacher et al., 2007). In TM5-MP all NO<sub>x</sub> emissions are introduced as NO, although a fraction for road  
865 transport is known to be emitted directly as NO<sub>2</sub> (e.g. Carslaw and Beevers, 2005). Many studies have been  
866 performed comparing satellite NO<sub>2</sub> columns with model values, implying that inadequacies in emission  
867 inventories are somewhat region specific (e.g. Zyrichidou et al., 2015; Pope et al., 2015).

868 Table 6 shows a negative bias of a few µg m<sup>-3</sup> in TM5-MP in seasonal surface [NO] in Europe. This is a  
869 cumulative effect of the accuracy of the MACC NO<sub>x</sub> emission estimates and, to a lesser extent, too high  
870 surface [O<sub>3</sub>] (enhancing the oxidation rate of NO to NO<sub>2</sub>). As anthropogenic emissions are the principle source

871 of NO, there is no significant seasonal cycle in the monthly emission estimates. Seasonal differences in  
872 convective mixing do cause somewhat higher surface [NO] during DJF, which is often captured in TM5-MP.  
873 For ~80% of the EMEP sites we do not observe any significant change in the quality of the comparisons. For  
874 ~20% of sites, simulations of [NO] at 1° x 1° introduce significant improvements over those at 3° x 2° and there  
875 is an improvement regarding the extent of seasonal variability (Fig. 4).

876 Table 7 shows that for [NO<sub>2</sub>] the biases are more variable being typically in the range of ±0-6 μg m<sup>-3</sup>, with both  
877 positive and negative biases occurring across sites. Both the conversion efficiency from NO, loss to reservoir  
878 compounds (e.g. HNO<sub>3</sub>), photo-dissociation rate and emission estimates contribute to these biases. The  
879 seasonal biases show improvements at 1° x 1° for ~35% of the EMEP sites, accompanied with degradations at  
880 ~20% of the sites. The maximal biases in [NO<sub>2</sub>] at 1° x 1° can be approximately double those for [NO]. For the  
881 corresponding NO/NO<sub>2</sub> ratio, there will generally be an under prediction in the model due to the negative  
882 biases shown for the [NO] comparisons. Analyzing the corresponding seasonal correlation co-efficients (not  
883 shown) shows in ~25% of the cases there is little seasonal correlation between the weekly [NO<sub>2</sub>] in TM5-MP  
884 and the measurements regardless of resolution for both seasons (Pearson's *r* in the range -0.3-0.3). In ~30% of  
885 cases there is actually a degradation in *r* between resolutions, the changes somewhat reflect those seen in the  
886 seasonal biases i.e. simultaneous changes to both the meteorology and local emission fluxes do not necessarily  
887 improve the performance of the model. Comparing 1° x 1° values both with and without the Tiedtke convection  
888 scheme shows that for the most convective regions (e.g. south of 45°N) increases in *r* generally occur during  
889 JJA when employing the ERA-interim mass-fluxes. Conversely for e.g. Finland the correlation becomes worse.  
890 Beyond Europe, we compared monthly mean TM5-MP vertical distributions of NO and NO<sub>2</sub> between March  
891 and May 2006 against measurements taken during the INTEX-B campaign in Fig. 6. In general differences  
892 between 1° x 1° and 3° x 2° simulations are the order of a few percent, with NO<sub>2</sub> biased low in the LT by ~70-  
893 80%. This is partially associated with the take-off and landing of the aircraft from polluted airfields, where  
894 point sources of high anthropogenic emissions cannot be resolved at 1° x 1°. For the FT, TM5-MP captures the  
895 observed gradient to reasonable degree. In the UT there is a consistent high bias for NO and an associated low  
896 bias for NO<sub>2</sub> suggesting that the conversion term is too low and the NO<sub>x</sub> cycle is out of synch at these cold  
897 temperatures despite the addition of new reservoir species (i.e. CH<sub>3</sub>O<sub>2</sub>NO<sub>2</sub>).

898 One important gauge as to whether the chemical mechanism can capture the correct recycling efficiency of NO  
899 into NO<sub>2</sub> is to examine their ratio, which is presented in the third column of Fig. 6. In the LT (< 900 hPa)  
900 NO/NO<sub>2</sub> ratios of 0.1-0.2 exist which TM5-MP represents quite well, with negligible differences between 3° x  
901 2° and 1° x 1° simulations. For the FT, TM5-MP consistently overestimates the ratio in spite of a high bias in  
902 O<sub>3</sub> (c.f. Fig. 3) suggesting an exaggerated photo-dissociation rate or low bias in HO<sub>2</sub>.

903 Finally in Fig. 7 we show the corresponding comparisons against measurements taken during the TexAQS II  
904 campaign (Parrish et al, 2009) for both September and October 2006. There is a significant underestimation in  
905 NO and NO<sub>2</sub>, mixing ratios, with both model profiles outside the 1-σ variability in the observational mean of  
906 the measured mixing ratios. This is clearly related to the emission estimates for this region being  
907 underestimated in the emission inventories (e.g. Kim et al., 2011). For the resulting NO/NO<sub>2</sub> ratio TM5-MP  
908 captures the correct ratio in the lowest few hundred meters of the BL, but overestimates the ratio at higher  
909 altitudes. In this case, the high NO and NO<sub>2</sub> mixing ratios at the top of the BL imply that TM5-MP under-

910 represents the  $\text{NO}_2$  fraction, regardless of the increased recycling term related to the titration of  $\text{O}_3$  (c.f. Table  
911 2).

912

## 913 **5 Changes in the $\text{NO}_y$ budget**

914

### 915 **5.1 Long-lived reservoirs**

916

917 The resolution dependent changes in the temporal distribution of  $[\text{NO}_2]$ , and associated differences in NMVOC  
918 chemical pre-cursor emissions have the potential to alter the partitioning of reactive  $\text{NO}_x$  between the three  
919 main chemical reservoirs included in mCB05v2 (i.e.  $\text{HNO}_3$ , PAN and ORGNTR). The differences in both the  
920 deposition efficiency and tropospheric lifetimes between trace species at  $1^\circ \times 1^\circ$  suggests that the fraction of  
921  $\text{NO}_x$  that can be transported out of source regions could change significantly. Here we briefly examine the  
922 zonally integrated nitrogen budget terms between simulations to quantify the effect of higher spatial resolution.  
923 The seasonal distribution of these three dominant reservoir species at  $1^\circ \times 1^\circ$  and their individual contributions  
924 to total  $\text{NO}_y$  are shown in Figures S10 to S13 for DJF and JJA, respectively. Here we define  $\text{NO}_y$  as the  
925 cumulative total of  $\text{NO}$ ,  $\text{NO}_2$ ,  $\text{NO}_3$ ,  $\text{HNO}_3$ , PAN,  $\text{CH}_3\text{O}_2\text{NO}_2$ , HONO,  $2^*\text{N}_2\text{O}_5$ , lumped organic nitrates and  
926  $\text{HNO}_4$ . These are provided as reference for the reader to aid understanding of the discussion below.

927 Table S1 in the Supplementary Material provides a zonal decomposition of the tropospheric chemical budget  
928 terms for  $\text{HNO}_3$ , PAN and ORGNTR. For  $\text{HNO}_3$ , even though the recent kinetic rate parameters increase  
929 (decrease) the chemical production term at the surface (UTLS) compared to older rate data (e.g. Seltzer et al.,  
930 2015), changes in the integrated column term are small. The changes at  $1^\circ \times 1^\circ$  are somewhat latitude  
931 dependant (low and high  $\text{NO}_x$  regimes), with only small increases occurring in the NH and associated  
932 decreases in the tropics related to lower  $[\text{OH}]$  (i.e. chemical production).

933 For PAN, both the production and destruction terms decrease marginally by  $\sim 1\text{-}3\%$  across all zones, meaning  
934 the transport of  $\text{NO}_x$  out of the main source regions remains relatively robust. The total mass of N cycled  
935 through PAN is  $\sim$ four times that of  $\text{HNO}_3$ . The changes in the production term due to temporal increases in  
936  $\text{NO}_2$  near high  $\text{NO}_x$  source regions (c.f. Fig. 5) are partially offset by a reduction in the mixing ratios of the  
937 acetyl-peroxy radical ( $\text{C}_2\text{O}_3$  in Table 1) due to e.g. increased dry deposition of organic precursors at  $1^\circ \times 1^\circ$ .  
938 Although the chemical budget terms only exhibit small changes, it can be expected that the global distribution  
939 of PAN is somewhat different due the changes in the convective and advective mixing due to the application of  
940 higher resolution meteorological data.

941 For ORGNTR, there is a 5% reduction in the production term at  $1^\circ \times 1^\circ$ , with an associated decrease in the loss  
942 by deposition. Both the largest production term and decrease occur in the tropics related to the strongest source  
943 being biogenic pre-cursors. Thus at  $1^\circ \times 1^\circ$ , this intermediate trace species becomes less important as a  $\text{NO}_x$   
944 reservoir.

945 Finally, the one additional intermediate not shown is  $\text{CH}_3\text{O}_2\text{NO}_2$ , which is primary a stable vehicle for  
946 transporting  $\text{NO}_x$  from the surface up to the UTLS, where at cold temperatures it accounts for a significant  
947 fraction of  $\text{NO}_2$  speciation along with  $\text{HNO}_4$  (Browne et al., 2011). At global scale three times as much  
948 nitrogen cycles through  $\text{CH}_3\text{O}_2\text{NO}_2$  compared to PAN, although the thermal stability is low at temperatures  $>$   
949  $255^\circ\text{K}$  thus resident mixing ratios are typically small. This results in maximal mixing ratios occurring in the

950 cold upper troposphere (up to  $\sim 0.2$  ppb) and subsequently dissociates primarily by thermal decomposition  
951 (photolytic destruction accounting for  $<0.1\%$  of all destruction). At  $1^\circ \times 1^\circ$  there is a few percent decrease in  
952 the chemical production term as a result of lower  $\text{CH}_3\text{O}_2$  mixing ratios and more variability in the temporal  
953 temperature distribution.

954 Comparisons of weekly  $[\text{HNO}_3]$  at the surface in Europe are shown in Figure 8 against measurements from the  
955 EMEP network. It has recently been determined that  $\text{HNO}_3$  measurements are also sensitive to ambient night-  
956 time  $[\text{N}_2\text{O}_5]$ , which could result in a positive bias in the observations (Phillips et al., 2013). In general, the  
957 modelled seasonal cycle is not evident in the measurements, which exhibit a rather homogeneous variation in  
958 mixing ratios throughout the year typically leading to an underestimation in TM5-MP during March and an  
959 overestimation during JJA. No such seasonal pattern is observed for  $[\text{NO}_2]$  (c.f. Fig. 5), thus seasonal  $[\text{OH}]$   
960 variability due to variations in photo-chemical activity and  $[\text{H}_2\text{O}_{(\text{g})}]$  is a likely cause. The impact of resolution  
961 on  $[\text{HNO}_3]$  is rather muted for most weeks resulting in no significant changes to the seasonal biases (not  
962 given), as constrained by the improvements in surface  $[\text{NO}_2]$  (c.f. Fig. 5). The heterogeneous scavenging of  
963  $\text{HNO}_3$  into ammonium nitrate can act as a moderator toward gaseous  $\text{HNO}_3$  and, although included in TM5-  
964 MP, generally produces low concentrations of e.g. ammonium nitrate (not shown). Thus, gaseous  $[\text{HNO}_3]$   
965 remains too high due to too little conversion into particles.

966 For other regions, we make comparisons of vertical profiles of  $\text{HNO}_3$  and PAN between March and October  
967 2006 against those measured during INTEX-B (Figure 9) and Texas (Figure S14). PAN is a good marker for  
968 transport in the free-troposphere due to the relatively long-lifetime at colder temperatures. For all regions the  
969 vertical gradients for both species are captured quite well, although some fine-structure is lost due to the  
970 vertical resolution of TM5-MP. This implies that the underestimation in  $\text{NO}_2$  (Fig. 6) is not due to lack of  
971 transport away from source regions and therefore should be more attributed to local underestimations in  
972 emission fluxes.

973 Finally, we present the corresponding comparisons for September 2006 for  $\text{HNO}_3$  and PAN measured during  
974 the TexAQS II campaign (Parrish et al., 2009) as Figure S14 in the Supplementary Material. For  $\text{HNO}_3$ ,  
975 although the vertical gradient is captured quite well, there is a significant low bias related to the low bias in  
976  $\text{NO}_2$  shown in Fig. 7, with the  $1^\circ \times 1^\circ$  showing a marginal improvement in the LT for  $\text{HNO}_3$ . For PAN the  
977 vertical profile in TM5-MP is somewhat anti-correlated around 900hPa in both simulations, with the rapid  
978 decrease at the surface not being captured by either simulation and the bias being larger for  $1^\circ \times 1^\circ$ .

979

## 980 **5.2 Short-lived reservoirs**

981

982 Here we briefly discuss the perturbations introduced for the short-lived N-reservoirs, namely HONO,  $\text{HNO}_4$   
983 and  $\text{N}_2\text{O}_5$ , where the chemical budget terms for all three species are provided in Table S2 in the Supplementary  
984 Material. For HONO it should be noted that many tropospheric CTMs have difficulty in simulating observed  
985 mixing ratios (e.g. Goncalves et al, 2012) suggesting missing (heterogeneous) source terms. The global  
986 production for HONO is an order of magnitude less than that for the other short-lived N-reservoirs. At  $1^\circ \times 1^\circ$   
987 there is  $\sim 10\%$  more chemical production of HONO in high  $\text{NO}_x$  regions and no appreciable effect in the low  
988  $\text{NO}_x$  regions. Thus the impact of increased resolution on HONO production is rather small, which is surprising  
989 considering the higher  $\text{NO}$  mixing ratios that occur in high  $\text{NO}_x$  regions (c.f. Fig 4). The muted response is due

990 to competing oxidative processes which effectively lower the OH available for forming HONO. For HNO<sub>4</sub>,  
 991 approximately the same mass of N cycles through this species as for PAN, although the shorter lifetime means  
 992 that it is more important at regional scale. Again, the impact of resolution on this species is small, where  
 993 decreases in [HO<sub>2</sub>] result in no significant net change in production for the NH. The most significant changes  
 994 occur for the global production and heterogeneous conversion of N<sub>2</sub>O<sub>5</sub>, with enhanced chemical production of  
 995 ~12% at global scale, increasing the heterogeneous sink term by ~6%, although the changes in the total mass of  
 996 N converted are small. In general, this is due to an increase in the production of the NO<sub>3</sub> radical by ~10% at 1°  
 997 x 1° (not shown) resulting in enhanced N<sub>2</sub>O<sub>5</sub> mixing ratios.

998

## 999 **6 Implications for tropospheric CH<sub>2</sub>O retrieval**

1000

1001 The implications of higher resolution for the global distribution of CH<sub>2</sub>O are rather modest. In Table 8, we  
 1002 show zonally integrated chemical production and destruction terms for CH<sub>2</sub>O, which suggests changes of the  
 1003 order of a few percent at global scale. The most notable difference is the increase in the cumulative deposition  
 1004 term of ~4% at 1° x 1°, thus reducing the atmospheric lifetime of CH<sub>2</sub>O in TM5-MP. Again this low impact  
 1005 shows that the increase in the temporal variability of the meteorological data at 1° x 1°, and thus the local  
 1006 variability of cloud SAD, only changes the net deposition term by a few percent. Even though the temporal  
 1007 distribution of the surface mixing ratios shows more variability at 1° x 1° due to the better representation of  
 1008 regional pre-cursor sources terms (e.g.) isoprene and terpene, only moderate improvements occur to the  
 1009 simulated profiles and total columns due to changes in transport. For instance, when analysing individual  
 1010 production terms (not given) for the tropics, decreases are related to small changes in the dominating chemical  
 1011 source terms (e.g. oxidation of CH<sub>3</sub>OOH; a reduction of ~3-5 Tg CH<sub>2</sub>O yr<sup>-1</sup>). For the chemical destruction  
 1012 term, the relative insensitivity of the photolysis of CH<sub>2</sub>O towards resolution (similar to J<sub>O3</sub>; c.f. Fig S4) results  
 1013 in small net decreases in line with changes in the chemical production term.

1014 Figure 10 compares monthly mean tropospheric profiles of CH<sub>2</sub>O measured during INTEX-B (Singh et al.,  
 1015 2009) with those from both TM5-MP simulations for March to May 2006. In general, there is a fair  
 1016 representation of the vertical gradient of CH<sub>2</sub>O by TM5-MP for all months shown, although surface mixing  
 1017 ratios are typically too high suggesting loss by deposition is underestimated or that the chemical production  
 1018 term is too. Moreover, there appears to be a missing (chemical) source term in the UTLS in TM5-MP leading  
 1019 to a ~ 30-50% (~0.05 ppb) low bias above 600hPa, therefore no significant improvement to the  
 1020 underestimation in the SH CH<sub>2</sub>O column in TM5-MP occurs compared to previous versions (Zeng et al, 2015)  
 1021 . Comparing profiles shows that the changes in the vertical distribution of CH<sub>2</sub>O at 1° x 1° are minimal in the  
 1022 chemical background compared to 3° x 2°, with the main differences originating from more efficient transport  
 1023 out of source regions (c.f. March). These findings are further confirmed by the comparisons of TM5-MP  
 1024 against TexAQS II measurements for September and October 2006 (Figure S15).

1025

## 1026 **7 Implications for tropospheric SO<sub>2</sub> retrieval**

1027

1028 In Figure 11, we compare weekly [SO<sub>2</sub>] for 2006 at a number of EMEP sites in Austria (AT02, forested), The  
 1029 Netherlands (NL09, rural), Great Britain (GB43, rural) and Spain (ES10, rural), with most sites being

1030 positioned away from strong point sources. For SO<sub>2</sub> in Europe, the main emission source is anthropogenic (e.g.  
1031 from the energy sector) and subsequently oxidised to sulphate predominantly in the aqueous phase, with the  
1032 tropospheric lifetime varying between ~2 days during winter and ~19 hours during summer (Lee et al, 2011).  
1033 High [SO<sub>2</sub>] has been observed throughout the EMEP network in e.g. The Netherlands and Spain, which is  
1034 significantly higher than that measured in Central Europe (Tørseth et al., 2012). Although the measurement  
1035 uncertainty is somewhat site specific due to the different methodology employed, it is typically around ~1.3  
1036 ug/m<sup>3</sup> (e.g. Hamad et al., 2010). Comparing weekly averages shows that for most sites shown there is a  
1037 significant low bias at 3° x 2°, indicating inaccuracies in the MACC emission inventory and the effect of  
1038 coarsening to the model resolution. At 1° x 1° significant improvements occur as a result of the better temporal  
1039 resolution of the emission sources as a result of increasing horizontal resolution.

1040 Table 9 provides an overview of the seasonal biases for all of the EMEP sites that measure hourly [SO<sub>2</sub>], with  
1041 the biases calculated for the overpass time of tropOMI aggregated on a weekly basis. Improvements occur at 1°  
1042 x 1° for ~20% of the sites during both seasons, with the majority (~50%) of sites showing no significant  
1043 improvement (< 5%). In such instances the local [SO<sub>2</sub>] is determined more by long-range transport (thus  
1044 sensitive to wash-out) rather than a local emission source, where strong mitigation practises have been  
1045 implemented in Europe over the last few decades reducing resident [SO<sub>2</sub>] significantly (Tørseth et al., 2012).  
1046 For some sites there is a notable increase in biases at 1° x 1° (20% DJF, 25% JJA) indicating that too strong  
1047 local emission sources occur in the MACC inventories (e.g. ES13 and GR01). For others (e.g. ES08 and NL07)  
1048 significantly low biases occur suggesting the opposite problem.

1049 Finally, for the vertical profiles we make comparisons against monthly mean composites assembled from  
1050 measurements taken during INTEX-B (Fig. S14) and TexAQS II (Fig. 12) as for the other trace species. For  
1051 the more pristine locations there are typically low biases at 3° x 2° for all months, especially at the surface  
1052 during March indicating a significant underestimation in the emission fluxes of SO<sub>2</sub>. Increasing to 1° x 1° only  
1053 provides an improved correlation for March, due to the transport in the FT being described better as shown for  
1054 NO<sub>2</sub> in Fig. 6. For April, the comparison shows a significant underestimation in the column for both  
1055 simulations, where corresponding comparisons of the vertical profiles of di-methyl sulphide, which acts as a  
1056 key source of SO<sub>2</sub> in the Equatorial Pacific (Alonza Gray et al., 2011), also show significant low biases (not  
1057 shown). For May again no significant improvement occurs, although both simulations capture the peak in SO<sub>2</sub>  
1058 mixing ratios at the top of the BL. More relevant for satellite based retrievals is the observed column near  
1059 strong anthropogenic source regions as shown in Fig. 13 over Texas during September and October 2006.  
1060 Here a clear improvement occurs at 1° x 1°, with the low bias in the BL being reduced significantly although  
1061 the integrated column is still too low. Again this is due to the underestimation in the source emission fluxes in  
1062 the anthropogenic emission inventory employed.

1063

## 1064 **8 Conclusions**

1065

1066 In this paper we have provided a comprehensive description of the high-resolution 1° x 1° version of TM5,  
1067 which is to be used for the purpose of providing *a-priori* columns for the satellite retrieval of trace gas columns  
1068 of NO<sub>2</sub>, CH<sub>2</sub>O and SO<sub>2</sub>. By performing identical simulations at a horizontal resolution of 3° x 2° and 1° x 1°,  
1069 and comparing the resulting global distributions of trace gas species, photolysis frequencies and chemical

1070 budget terms, we quantify and validate both the near-surface and vertical distributions for the evaluation year  
1071 of 2006.

1072 Comparing the seasonal distribution in  $^{222}\text{Rn}$  we show that differences of  $\pm 20\%$  exist at global scale, with  
1073 significantly larger differences for specific coastal regions and tropical oceans. In order to assess the changes in  
1074 convective activity above strong  $\text{NO}_x$  sources, we show that differences of between  $\sim 2\text{-}10\%$  ( $\sim 10\text{-}20\%$ ) exist  
1075 for the Northern mid-latitudes (tropics) at higher resolution, with both weaker and stronger upwelling  
1076 occurring depending on the region and the season. The differences are site specific being somewhat affected by  
1077 local orography.

1078 The impact of resolution on global monthly mean  $J_{\text{O}_3}$  and  $J_{\text{NO}_2}$  surface values over a range of conditions is  
1079 limited to  $\sim 2\%$  and  $\sim 5\text{-}10\%$ , respectively. This is surprising considering the larger variability in cloud cover  
1080 and surface albedo that occurs at  $1^\circ \times 1^\circ$ . Examining changes in  $J_{\text{O}_3}$  and  $J_{\text{NO}_2}$  which occur throughout the  
1081 tropospheric column reveals that significant differences of  $>10\%$  can occur at the top of the BL at tropical  
1082 locations. Such modest changes associated with this dominant loss term result in the change in the integrated  
1083 chemical budget terms to be rather low.

1084 Analysing the chemical budget terms for tropospheric  $\text{O}_3$  shows (i) a reduction in the stratosphere-troposphere  
1085 exchange flux of  $\sim 7\%$  to  $597 \text{ Tg O}_3 \text{ yr}^{-1}$ , (ii) a repartitioning of the contribution from stratospheric  
1086 downwelling in both the Northern and Southern hemispheres, (iii) no significant change in the tropospheric  
1087 burden of  $\text{O}_3$  and (iv) modest changes in the integrated chemical production and destruction terms. Comparing  
1088 simulated mixing ratios against surface measurements in Europe shows that the positive bias present in TM5  
1089 decreases by  $\sim 20\%$  at  $1^\circ \times 1^\circ$  between 2-5 ppb/month. This positive bias persists throughout the vertical  
1090 column across diverse global regions regardless of the local  $\text{NO}_x$  emissions, although the vertical gradient in  
1091 tropospheric  $\text{O}_3$  through the tropospheric column is captured quite well.

1092 For  $\text{NO}$  and  $\text{NO}_2$  increasing horizontal resolution results in only modest differences in the zonal mean  
1093 recycling terms and the loss of  $\text{O}_3$  by chemical titration. Comparisons against surface measurements in Europe  
1094 shows that there is a consistent negative bias in weekly  $[\text{NO}]$  of a few  $\mu\text{g m}^{-3}$  associated with both too high  
1095 surface  $\text{O}_3$  (enhanced  $\text{NO}$  titration) and the inaccuracy of the  $\text{NO}_x$  emission inventories. For  $\text{NO}_2$ , the biases in  
1096 the weekly concentrations are larger and can be both positive and negative. Increasing horizontal resolution has  
1097 little effect on reducing the  $\text{NO}$  biases, but results in improvements for  $\text{NO}_2$  at  $\sim 35\%$  of the available sites, with  
1098  $\sim 45\%$  of sites showing limited changes. Examining correlation co-efficients shows that although there is  
1099 typically a higher correlation at  $1^\circ \times 1^\circ$ , many sites still exhibit very low correlation or anti-correlation for  
1100 some seasons. For the tropospheric column the improvement in the comparisons is only by a few percent, with  
1101 a significant underestimation in both  $\text{NO}$  and  $\text{NO}_2$  throughout the tropospheric column. Analysing the  $\text{NO}/\text{NO}_2$   
1102 ratio and comparing against observations shows that although partitioning is captured in the BL there is a  
1103 significant overestimation in the upper troposphere.

1104 Finally for  $\text{CH}_2\text{O}$  and  $\text{SO}_2$ , which can also be retrieved from satellite measurements, the effect of increased  
1105 resolution is rather modest due to compensating changes towards the chemical budget terms. When compared  
1106 against observations there is a persistent low bias for tropospheric  $\text{CH}_2\text{O}$  due to missing production terms  
1107 especially on the Free Troposphere. For  $\text{SO}_2$  comparison with surface observations in Europe shows lower  
1108 biases at 20% of sites due to more accurate local emission fluxes, whereas for the majority of cases ( $\sim 50\%$ )  
1109 there is no significant change. Comparing vertical profiles shows a significant underestimation in the

1110 tropospheric column likely associated with either missing precursors or an underestimation in the direct  
1111 emission terms.

1112 Future updates will most likely focus on developing an online Secondary Organic Aerosol scheme,  
1113 tropospheric halogen chemistry and incorporating an updated isoprene oxidation scheme, which will be built  
1114 using TM5-MP as the core.

1115

#### 1116 **Code Availability**

1117 The TM5-MP code can be downloaded from the SVN server hosted at KNMI, The Netherlands. A request to  
1118 generate a new user account for access can be made by e-mailing [sager@knmi.nl](mailto:sager@knmi.nl). Any new user groups need to  
1119 agree to the protocol set out for use, where it is expected that any developments are accessible to all users after  
1120 publication of results. Attendance at 9-monthly TM5 international meetings is encouraged to avoid duplicity  
1121 and conflict of interests.

1122

#### 1123 **Acknowledgements**

1124 We thank M. van Weele for processing the MSR2 stratospheric ozone data record used for constraining the  
1125 overhead O<sub>3</sub> field and T. P. C. van Noije for updating the SO<sub>x</sub> emission estimates. We thank V. Huijnen for  
1126 providing estimates on the heterogeneous uptake co-efficients.

1127

1128 Table 1: Details of the reaction rate data applied for NO<sub>x</sub> and nitrogen reservoirs. The k<sub>0</sub> terms are multiplied by  
 1129 the relevant air density to calculate the correct forward and backward rate constants. The reaction data and  
 1130 stoichiometry are taken from Atkinson et al. (2004) accommodating the latest evaluation at [http://iupac.pole-](http://iupac.pole-ether.fr)  
 1131 [ether.fr](http://iupac.pole-ether.fr).

Reactants	Products	Rate parameters
NO + O <sub>3</sub>	NO <sub>2</sub>	$3.0 \times 10^{-12} \cdot \exp(-1500/T)$
NO <sub>2</sub> + O <sub>3</sub>	NO <sub>3</sub>	$1.4 \times 10^{-13} \cdot \exp(-2470/T)$
NO + HO <sub>2</sub>	NO <sub>2</sub> + OH	$3.3 \times 10^{-12} \cdot \exp(270/T)$
NO + CH <sub>3</sub> O <sub>2</sub>	CH <sub>2</sub> O + HO <sub>2</sub> + NO <sub>2</sub>	$2.8 \times 10^{-12} \cdot \exp(300/T)$
OH + NO <sub>2</sub>	HNO <sub>3</sub>	$k_0 = 3.2 \times 10^{-30} \cdot (300/T)^{4.5}$ $k_\infty = 3.0 \times 10^{-11}$
NO + NO <sub>3</sub>	NO <sub>2</sub> + NO <sub>2</sub>	$1.8 \times 10^{-11} \cdot \exp(110/T)$
NO <sub>2</sub> + NO <sub>3</sub>	N <sub>2</sub> O <sub>5</sub>	$k_0 = 8.0 \times 10^{-27} \cdot (300/T)^{3.5}$ $k_\infty = 3.0 \times 10^{-11} \cdot (300/T)^{1.0}$
N <sub>2</sub> O <sub>5</sub> + M	NO <sub>2</sub> + NO <sub>3</sub>	$k_0 = 1.3 \times 10^{-3} \cdot (300/T)^{3.5} \cdot \exp(-11000/T)$ $k_\infty = 9.7 \times 10^{14} \cdot (300/T)^{-0.1} \cdot \exp(-11080/T)$
HO <sub>2</sub> + NO <sub>2</sub>	HNO <sub>4</sub>	$k_0 = 1.4 \times 10^{-31} \cdot (300/T)^{3.1}$ $k_\infty = 4.0 \times 10^{-12}$
HNO <sub>4</sub> + M	HO <sub>2</sub> + NO <sub>2</sub>	$k_0 = 4.1 \times 10^{-5} \cdot \exp(-10650/T)$ $k_\infty = 6.0 \times 10^{15} \cdot \exp(-11170/T)$
OH + HNO <sub>4</sub>	NO <sub>2</sub>	$1.3 \times 10^{-12} \cdot \exp(380/T)$
OH + NO + M	HONO	$k_0 = 7.0 \times 10^{-31} \cdot (300/T)^{4.4}$ $k_\infty = 3.6 \times 10^{-11} \cdot (300/T)^{0.1}$
HONO + hν	OH + NO	
OH + HONO	NO <sub>2</sub>	$2.5 \times 10^{-12} \cdot \exp(260/T)$
NO <sub>2</sub> + CH <sub>3</sub> C(O)O <sub>2</sub>	PAN	$k_0 = 3.28 \times 10^{-28} \cdot (300/T)^{6.87}$ $k_\infty = 1.125 \times 10^{-11} \cdot (300/T)^{1.105}$
PAN	NO <sub>2</sub> + CH <sub>3</sub> C(O)O <sub>2</sub>	$k_0 = 1.1 \times 10^{-5} \cdot \exp(-10100/T)$ $k_\infty = 1.9 \times 10^{17} \cdot \exp(-14100/T)$

PAN + hv	CH <sub>3</sub> C(O)O <sub>2</sub> + NO <sub>2</sub>	
	CH <sub>3</sub> O <sub>2</sub> + NO <sub>3</sub>	
CH <sub>3</sub> O <sub>2</sub> + NO <sub>2</sub>	CH <sub>3</sub> O <sub>2</sub> NO <sub>2</sub>	$k_0 = 2.5 \times 10^{-30} * (300/T)$
CH <sub>3</sub> O <sub>2</sub> NO <sub>2</sub>	CH <sub>3</sub> O <sub>2</sub> + NO <sub>2</sub>	$k_{\infty} = 1.8 \times 10^{-11}$
		$k_0 = 9.0 \times 10^{-5} * \exp(-9690/T)$
NO <sub>3</sub> + HO <sub>2</sub>	HNO <sub>3</sub>	$k_{\infty} = 1.1 \times 10^{16} * \exp(-10560/T)$
		$4.0 \times 10^{-12}$

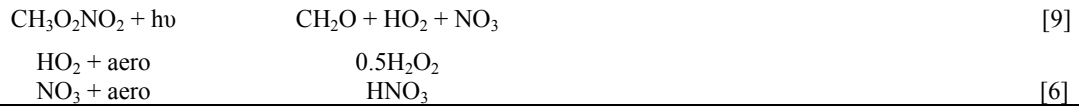
---

1132

1133

1134 Table 2: Details of updates made to the reaction data and stoichiometry of the modified CB05 chemical  
 1135 mechanism for other reactions. Data is taken from the following: [1] Atkinson et al. (2004) accommodating the  
 1136 latest evaluation at <http://iupac.pole-ether.fr>, [2] branching ratio (R) equal to  $1/(1+498 \cdot \exp(-1160./T))$ , [3]  
 1137 Yarwood et al. (2005), [4] Sander et al. (2011), [5], Atkinson et al. (2006), [6] Emmons et al. (2010), [7]  
 1138 Hauglustaine et al. (2014), [8] rate assumed equal to  $\text{NH}_2$  analogue, [9] assumed to be equal to  $\text{HNO}_4$  after  
 1139 Browne et al. (2011) and E is an estimated value.  
 1140

Reactants	Products	Rate expression	Ref.
$\text{CH}_3\text{O}_2 + \text{HO}_2$	$\text{CH}_3\text{OOH}$	$3.8 \times 10^{-13} \cdot \exp(750/T) \cdot R$	[1],[2]
$\text{CH}_3\text{O}_2 + \text{HO}_2$	$\text{CH}_2\text{O}$	$3.8 \times 10^{-13} \cdot \exp(750/T) \cdot (1-R)$	[1],[2]
$\text{CH}_3\text{O}_2 + \text{CH}_3\text{O}_2$	$1.37\text{CH}_2\text{O} + 0.74\text{HO}_2 + 0.63\text{CH}_3\text{OH}$	$9.5 \times 10^{-14} \cdot \exp(390/T)$	[3],[4]
$\text{OH} + \text{C}_3\text{H}_8$	$i\text{-C}_3\text{H}_7\text{O}_2$	$7.6 \times 10^{-12} \cdot \exp(-585/T)$	[5],[6]
$\text{NO} + \text{IC}_3\text{H}_7\text{O}_2$	$0.82\text{CH}_3\text{COCH}_3 + \text{HO}_2 + 0.27\text{ALD2} + \text{NO}_2$	$4.2 \times 10^{-12} \cdot \exp(180/T)$	[6]
$\text{HO}_2 + \text{IC}_3\text{H}_7\text{O}_2$	$\text{ROOH}$	$7.5 \times 10^{-13} \cdot \exp(700/T)$	[6]
$\text{OH} + \text{C}_3\text{H}_6$	$\text{C}_3\text{H}_6\text{O}_2$	$k_0 = 8.0 \times 10^{-27} \cdot (-300/T)^{3.5}$ $k_\infty = 3.0 \times 10^{-11} \cdot (-300/T)^{1.0}$	[5],[6]
$\text{NO}_3 + \text{C}_5\text{H}_8$	$0.2\text{ISPD} + \text{XO}_2 + 0.8\text{HO}_2 + 0.8\text{ORGNTR} + 0.8\text{ALD2} + 2.4\text{PAR} + 0.2\text{NO}_2$	$2.95 \times 10^{-12} \cdot \exp(465/T)$	[5]
$\text{NO} + \text{C}_3\text{H}_6\text{O}_2$	$\text{ALD2} + \text{CH}_2\text{O} + \text{HO}_2 + \text{NO}_2$	$4.2 \times 10^{-12} \cdot \exp(180/T)$	[6]
$\text{HO}_2 + \text{C}_3\text{H}_6\text{O}_2$	$\text{ROOH}$	$7.5 \times 10^{-13} \cdot \exp(700/T)$	[6]
$\text{NO}_3 + \text{DMS}$	$\text{SO}_2 + \text{HNO}_3$	$1.9 \times 10^{-13} \cdot \exp(520/T)$	[1]
$\text{NH}_2 + \text{OH}$		$3.4 \times 10^{-11}$	[E]
$\text{NH}_2 + \text{HO}_2$	$\text{NH}_3$	$3.4 \times 10^{-11}$	[4],[7]
$\text{NH}_2 + \text{O}_3$	$\text{NH}_2\text{O}_2$	$4.3 \times 10^{-12} \cdot \exp(-930/T)$	[4],[7]
$\text{NH}_2 + \text{O}_2$	$\text{NO}$	$6.0 \times 10^{-21}$	[1],[7]
$\text{NH}_2\text{O}_2 + \text{NO}$	$\text{NH}_2 + \text{NO}_2$	$4.0 \times 10^{-12} \cdot \exp(450/T)$	[7],[8]
$\text{NH}_2\text{O}_2 + \text{O}_3$	$\text{NH}_2$	$4.3 \times 10^{-12} \cdot \exp(-930/T)$	[7],[8]
$\text{NH}_2\text{O}_2 + \text{HO}_2$	$\text{NH}_2$	$3.4 \times 10^{-11}$	[8]
$\text{CH}_3\text{O}_2\text{NO}_2 + h\nu$	$\text{CH}_3\text{O}_2 + \text{NO}_2$		[9]

1141  
1142

1143 Table 3: The zonally segregated emission totals introduced into TM5-MP for the year 2006. All  
 1144 organic hydrocarbons are given in Tg C yr<sup>-1</sup>, except for CO, CH<sub>2</sub>O and CH<sub>3</sub>OH and all NO<sub>x</sub> emissions  
 1145 are introduced as NO. No direct emissions occur for HNO<sub>3</sub>, PAN, ORGNTR, HONO, N<sub>2</sub>O<sub>5</sub>, NO<sub>2</sub>,  
 1146 CH<sub>3</sub>O<sub>2</sub>NO<sub>2</sub> or O<sub>3</sub>.  
 1147

Species Tg Yr <sup>-1</sup>	Global	30-90°S	30S-30°N	30-90°N
CO	1081.0	24.4	755.1	301.27
NO <sub>x</sub> (as N)	49.0	1.5	24.0	23.6
SO <sub>2</sub>	117.0	3.0	49.2	64.3
DMS (as S)	19.2	6.7	9.3	3.2
NH <sub>3</sub>	56.6	3.1	27.9	25.6
CH <sub>2</sub> O	13.5	0.3	10.5	2.7
PAR	34.1	0.7	18.5	14.9
OLE	22.4	0.9	16.6	4.9
ALD2	13.4	0.4	11.2	1.8
CH <sub>3</sub> CHCHO	2.2	0.0	1.2	1.0
CH <sub>3</sub> OH	100.7	3.3	82.5	14.9
CH <sub>3</sub> CH <sub>2</sub> OH	70.4	2.8	52.6	15.1
C <sub>2</sub> H <sub>4</sub>	25.9	1.0	19.0	5.9
C <sub>2</sub> H <sub>6</sub>	6.1	0.3	5.3	1.5
C <sub>3</sub> H <sub>8</sub>	5.6	0.4	3.6	1.6
C <sub>3</sub> H <sub>6</sub>	19.6	0.9	14.8	3.9
CH <sub>3</sub> COCH <sub>3</sub>	27.4	0.8	22.0	4.6
HCOOH	1.8	0.0	1.5	0.3
CH <sub>3</sub> COOH	7.1	0.1	6.0	1.0
C <sub>5</sub> H <sub>8</sub>	510.0	23.2	441.9	45.0
C <sub>10</sub> H <sub>16</sub>	85.4	2.3	70.2	12.9

1148  
 1149

1150  
1151  
1152  
1153  
1154  
1155  
1156  
1157  
1158  
1159

Table 4: The tropospheric chemical budget terms and burden for O<sub>3</sub> during 2006 for the 1° x 1° simulation, with all quantities being given in Tg O<sub>3</sub> yr<sup>-1</sup>. The associated percentage changes are given when comparing against the 3° x 2° simulation (1° x 1°/3° x 2°). The definition of the chemical tropopause and the calculation of the STE are calculated using the methodology outlined in Stevenson et al. (2006). The stratospheric nudging term refers to total change in the mass of O<sub>3</sub> in the stratospheric column when constraining zonal distributions towards observational values from the MSR (Huijnen et al., 2010). The contribution to each term from the SH extra-tropics/tropics/NH extra-tropics regions (defined as 90-30°S/30°S-30°N/30-90°N) are provided.

Term	Global	%	SH	%	Tropics	%	NH	%
Net STE	579	-6.7	166	3.9	396	-7.5	16	240
Strat. Nudging	1440	-0.7	-224	2.8	1615	-	49	5.8
Trop.Chem.Prod	5532	-1.9	389	-2.2	3938	-3.5	1206	-2.2
Trop.Chem.Loss	5162	-2.4	440	-1.0	3869	-2.5	853	-2.8
BO <sub>3</sub>	378	-2.0	72	1.7	203	-2.3	104	-3.4
Strat BO <sub>3</sub>	80	-2.0	23	9.1	38	-6.5	24	-2.0
Deposition	949	0.8	115	0.6	465	-	369	1.9
O <sub>3</sub> S Deposition	97	5.0	19	7.5	37	-1.2	42	10.0

1160  
1161  
1162  
1163  
1164  
1165  
1166  
1167

Table 5: The annual NO to NO<sub>2</sub> re-cycling terms involving peroxy-radicals given in Tg N yr<sup>-1</sup> for 2006 at 1° x 1° resolution. In mCB05v2 XO<sub>2</sub> represents lumped alkyl-peroxy radicals (Yarwood et al, 2005). The NO + RO<sub>2</sub> term is an aggregate of numerous specific peroxy-radical conversion terms in the modified CB05 mechanism (Williams et al., 2013; Tables 1 and 2). Also provided are the approximate percentage differences when comparing with 3° x 2° (1° x 1°/3° x 2°). The chemical tropopause is defined using the methodology outlined in Stevenson et al. (2006).

Reaction	Global	%	SH	%	Tropics	%	NH	%
NO + HO <sub>2</sub>	1058	-1.2	79	-1.2	740	-1.9	239	1168
NO + CH <sub>3</sub> O <sub>2</sub>	407	-2.2	31	-2.6	294	-2.8	82	1169
NO + XO <sub>2</sub>	147	-2.1	7	-3.6	111	-2.6	29	1170
NO + RO <sub>2</sub>	9.4	-4.4	0.4	-2.6	6.3	-4.4	2.7	1171
NO + O <sub>3</sub>	5403	0.1	518	7.5	2933	-3.9	1953	1172

1176  
1177

1178 Table 6: The seasonal mean absolute biases as calculated using weekly [NO] values ( $\mu\text{g m}^{-3}$ ). The weekly  
 1179 means are composed from daily measurements taken at 13:00 for DJF and JJA (given as the difference in the  
 1180 measurements-model). Values are shown for both the  $3^\circ \times 2^\circ$  and  $1^\circ \times 1^\circ$  simulations for all stations with  
 1181 available data. Those with differences  $< 5\%$  are considered to exhibit no discernible change in the bias.  
 1182

EMEP Station	Lat	Lon	DJF $3^\circ \times 2^\circ$	DJF $1^\circ \times 1^\circ$	JJA $3^\circ \times 2^\circ$	JJA $1^\circ \times 1^\circ$
CH01	46.32	7.59	-0.01	-0.01	0.00	-0.01
CZ03	49.35	15.50	-4.05	-3.30	-1.61	-1.35
DE43	47.48	11.10	-2.37	-2.36	-0.47	-0.48
DK05	54.44	10.44	-2.51	-2.61	-1.29	-1.51
ES07	58.23	21.49	-3.80	-3.84	-1.45	-1.48
ES08	43.26	-4.51	-2.08	-2.09	-1.00	-1.01
ES09	41.16	-3.80	-0.93	-0.93	-1.07	-1.07
ES10	38.28	3.19	-1.14	-1.24	-0.75	-0.88
ES11	39.50	-6.55	-1.07	-1.07	-0.44	-0.45
ES12	41.17	-1.60	-1.34	-1.34	-0.95	-0.95
ES13	41.24	-5.52	-2.50	-1.90	-0.74	-0.62
ES14	39.31	0.43	-2.21	-2.20	-1.27	-1.27
ES15	43.13	-4.21	-1.62	-1.61	-0.99	-1.00
ES16	43.37	-7.41	-2.39	-2.39	-1.11	-1.11
FR13	46.39	0.11	-1.90	-1.94	-0.52	-0.52
FR15	55.18	0.45	-3.09	-3.04	-1.51	-1.58
GB02	50.35	-3.12	-1.23	-1.23	-0.93	-0.92
GB13	54.20	-3.42	-1.28	-1.32	-0.58	-0.55
GB14	52.30	-0.48	-3.03	-3.04	-0.98	-0.98
GB31	53.23	-3.11	-1.74	-1.74	-0.90	-0.91
GB37	50.47	-1.45	-3.09	-3.08	-1.22	-1.21
GB38	51.13	0.10	-2.87	-2.78	-1.92	-1.72
GB44	51.17	-3.20	-1.65	-1.45	-0.27	-0.67
GB45	52.17	0.17	-1.80	0.11	0.20	0.19
GB51	52.33	0.46	-3.68	-3.42	-1.29	-1.17
NL91	52.18	4.30	-4.47	-3.51	-1.98	-1.86

1183  
 1184  
 1185

1186 Table 7: As for Table 5 except for NO<sub>2</sub>.  
 1187

EMEP Station	Lat	Lon	DJF 3° x 2°	DJF 1° x 1°	JJA 3° x 2°	JJA 1° x 1°
BE32	50.30	4.59	10.56	1.27	1.69	-2.13
CH01	46.32	7.59	-0.04	-0.03	-0.02	-0.01
CZ03	49.35	15.50	-4.04	0.03	-1.62	0.34
DE43	47.48	11.10	-2.37	-2.36	-0.49	-0.48
DK05	54.44	10.44	6.07	5.56	1.04	-0.02
ES07	58.23	21.49	-1.13	-1.79	-0.96	-1.15
ES08	43.26	-4.51	-2.01	-2.10	-0.93	-1.01
ES09	41.16	-3.80	-0.95	-0.94	-1.07	-1.07
ES10	42.19	3.19	2.18	1.46	0.92	-0.01
ES11	38.28	-6.55	-1.08	-1.08	-0.44	-0.44
ES12	39.50	-1.60	-1.36	-1.35	-0.95	-0.95
ES13	41.17	-5.52	-2.51	-0.29	-0.74	0.19
ES14	41.24	0.43	-2.22	-2.21	-1.27	-1.26
ES15	39.31	-4.21	-1.64	-1.63	-0.99	-0.99
ES16	43.13	-7.41	-2.40	-2.39	-1.11	-1.11
FI09	59.46	21.22	0.79	-0.91	-0.10	-0.53
FI37	60.31	27.41	10.04	9.60	1.70	0.92
FI96	62.35	24.11	0.40	0.34	0.31	0.17
FR13	68.00	24.09	-1.96	-1.95	-0.54	-0.54
FR15	43.37	0.11	-3.84	-3.91	-1.78	-1.81
GB02	46.39	0.45	3.12	3.42	0.82	0.54
GB13	55.18	-3.12	-2.17	-2.13	-1.00	-0.98
GB14	50.35	-3.42	5.02	3.93	1.17	1.50
GB31	54.20	-0.48	-1.71	-1.71	-0.90	-0.90
GB37	52.30	-3.11	-3.10	-3.08	-1.25	-1.25
GB38	53.23	-1.45	-4.05	-4.03	-2.20	-2.19
GB44	50.47	0.10	6.21	6.69	0.61	1.42
GB45	51.13	-3.20	6.28	6.00	3.48	1.94
GB51	52.17	-0.17	12.56	16.60	4.11	4.50
GR01	41.45	42.49	0.50	2.07	0.40	1.05
NL09	53.2	6.16	-3.21	-1.63	-1.18	-0.19
NL10	51.32	5.51	3.48	3.52	0.92	-0.29
NL91	52.18	4.30	11.81	6.42	1.48	-0.81

1188  
 1189

1190

1191 Table 8: The tropospheric chemical budget for the CH<sub>2</sub>O given in Tg CH<sub>2</sub>O yr<sup>-1</sup> during 2006 for the 1°  
 1192 x 1° simulation. Percentage differences are shown against the corresponding 3° x 2° simulation.  
 1193

Budget Term	Global	%	SH	%	Tropics	%	NH	%
CH <sub>2</sub> O CP	1919	-1.1	147	-0.3	1491	-1.0	281	-2.0
CH <sub>2</sub> O CD	1739	-1.6	134	-0.5	1349	-1.1	256	-2.3
CH <sub>2</sub> O Dep.	193	3.1	15	2.0	149	3.9	29	-

1194

1195 Table 9: The seasonal mean biases of daily [SO<sub>2</sub>] (µg m<sup>-3</sup>) at 13:00 for DJF and JJA, when taking the  
 1196 difference between measurements-model values. Values are shown for both the 3° x 2° and 1° x 1°  
 1197 simulations. Those with differences < 5% are considered to exhibit no discernible change in the bias.  
 1198

EMEP Station	Lat	Lon	DJF 3° x 2°	DJF 1° x 1°	JJA 3° x 2°	JJA 1° x 1°
AT02	47.46	16.46	-3.34	-3.15	-0.89	-0.53
AT05	46.40	12.58	-0.42	-0.41	-0.14	-0.14
AT48	47.50	14.26	-0.64	-0.63	-0.14	-0.15
CZ03	49.35	15.50	-3.52	3.65	-0.69	0.64
ES07	58.23	21.49	1.22	0.73	0.38	0.31
ES08	43.26	-4.51	-2.98	-3.21	-1.19	-1.58
ES09	41.16	-3.80	-0.62	-0.61	-0.42	-0.42
ES10	42.19	3.19	2.37	2.45	1.93	1.53
ES11	38.28	-6.55	-0.63	-0.61	-0.70	-0.70
ES12	39.50	-1.60	-0.47	-0.45	-0.32	-0.32
ES13	41.17	-5.52	-0.81	2.71	-0.78	0.55
ES14	41.24	0.43	-0.70	-0.67	-0.47	-0.47
ES15	39.31	-4.21	-0.40	-0.37	-0.45	-0.46
ES16	43.13	-7.41	-3.84	-3.82	-1.66	-1.66
GB37	52.30	-3.11	-2.92	-2.91	-1.72	-1.72
GB38	53.23	-1.45	2.93	2.75	0.39	1.33
GB43	51.14	-4.42	-1.49	4.77	-2.03	-0.63
GB45	52.17	-0.17	3.87	7.20	1.01	1.77
GR01	38.22	23.50	1.70	2.77	0.74	1.50
NL07	52.50	6.34	2.58	-1.67	0.46	-1.03
NL08	52.70	5.12	1.77	1.56	-0.14	-0.30
NL09	53.2	6.16	2.53	2.16	0.47	0.27

1199

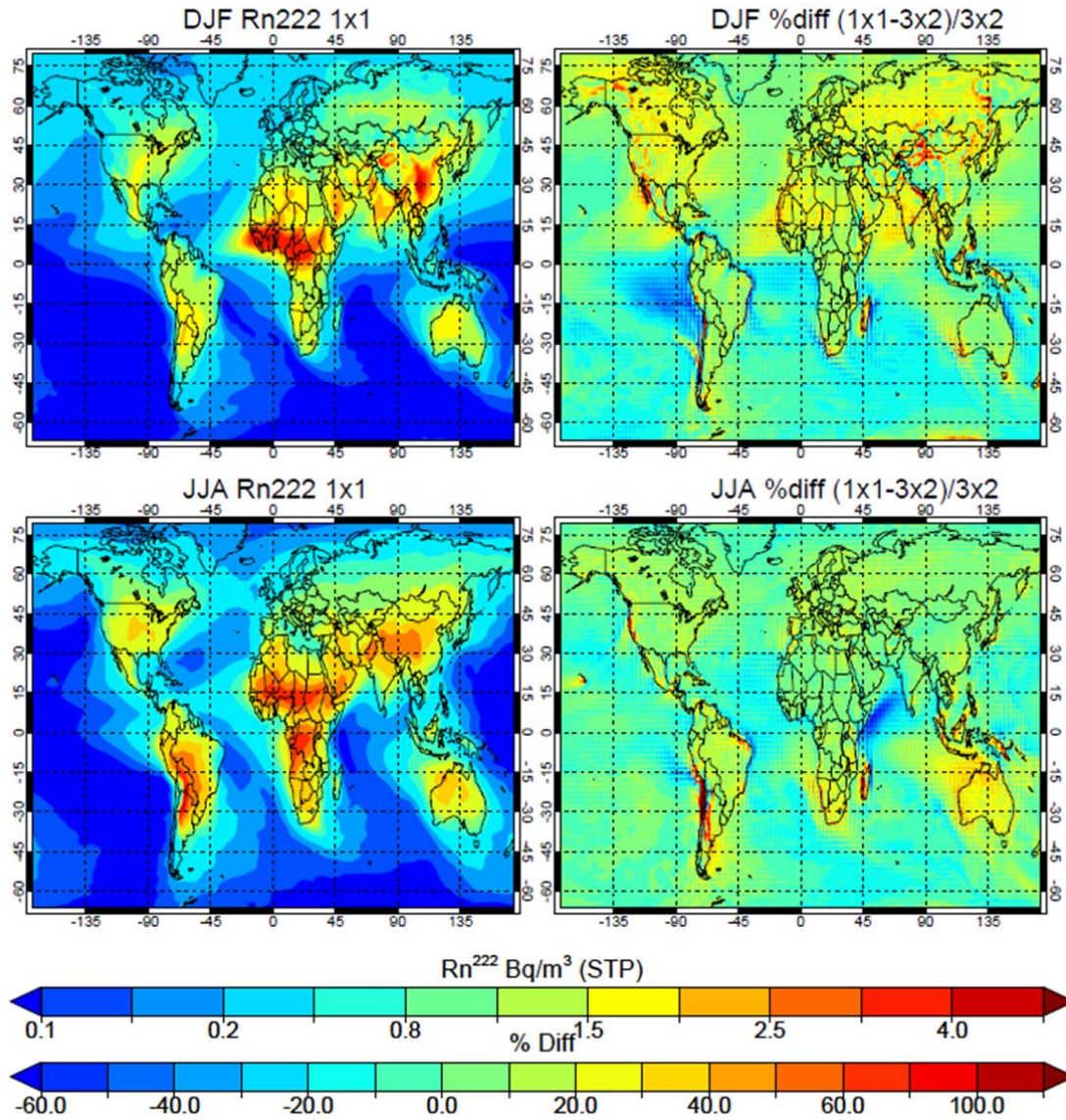
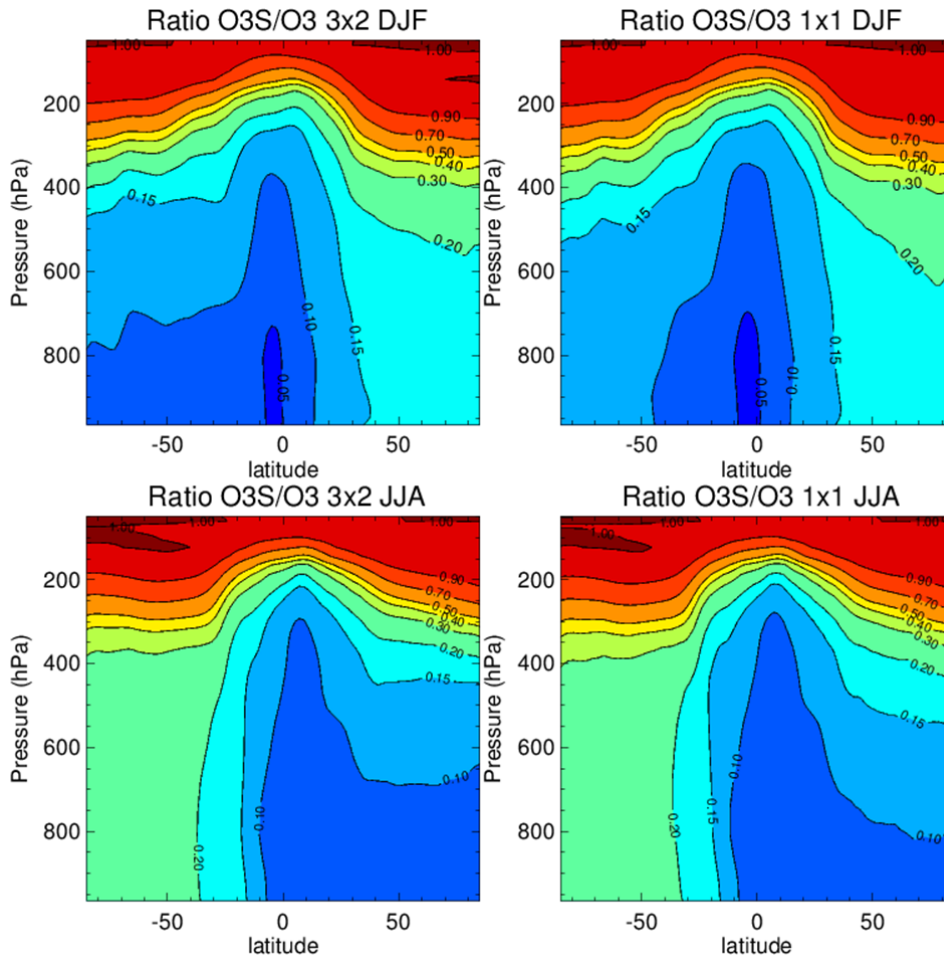


Figure 1: The seasonal distributions of  $Rn^{222}$  averaged between 800 and 900hPa for DJF (top) and JJA (bottom) for the  $3^\circ \times 2^\circ$  (left) and  $1^\circ \times 1^\circ$  (right) simulation, with the associated percentage differences when compared against the  $3^\circ \times 2^\circ$  simulation.

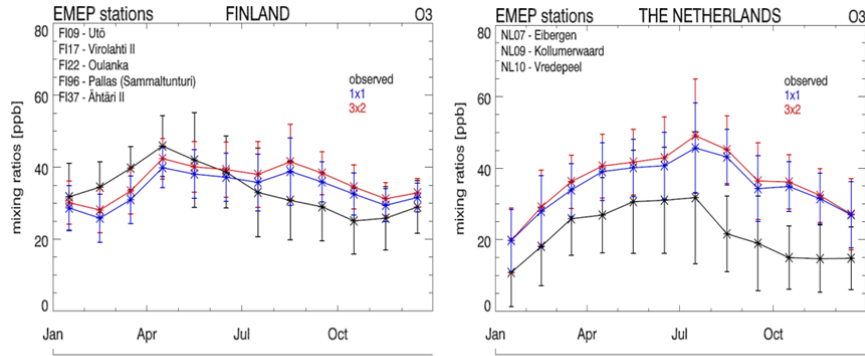
1200  
1201  
1202  
1203  
1204  
1205  
1206  
1207



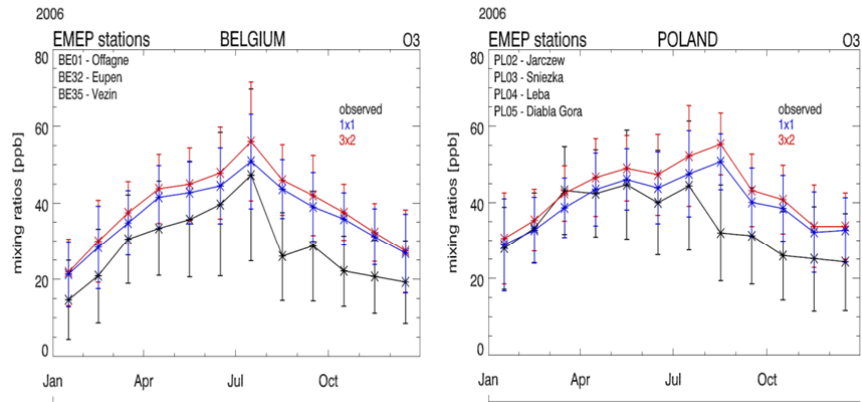
1208  
 1209  
 1210  
 1211

Figure 2: Zonal mean seasonal distribution of the TM5-MP  $O_3S/O_3$  ratio for the 3° x 2° (left) and 1° x 1° (right) simulations.

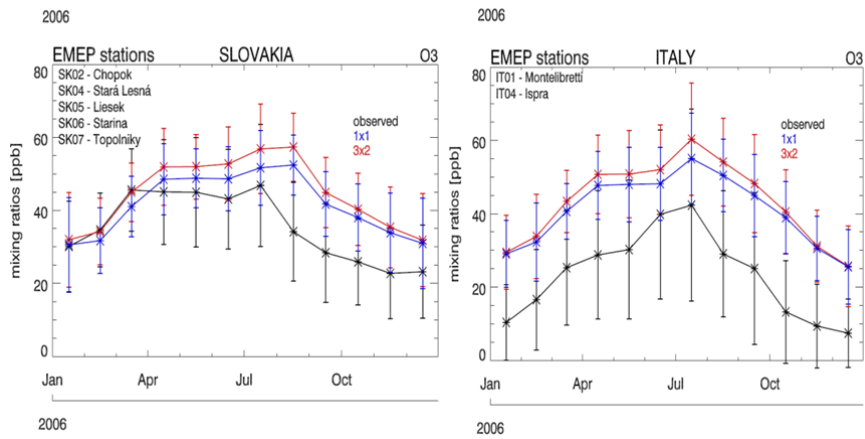
1212



1213



1214



1215

1216

1217

1218

1219

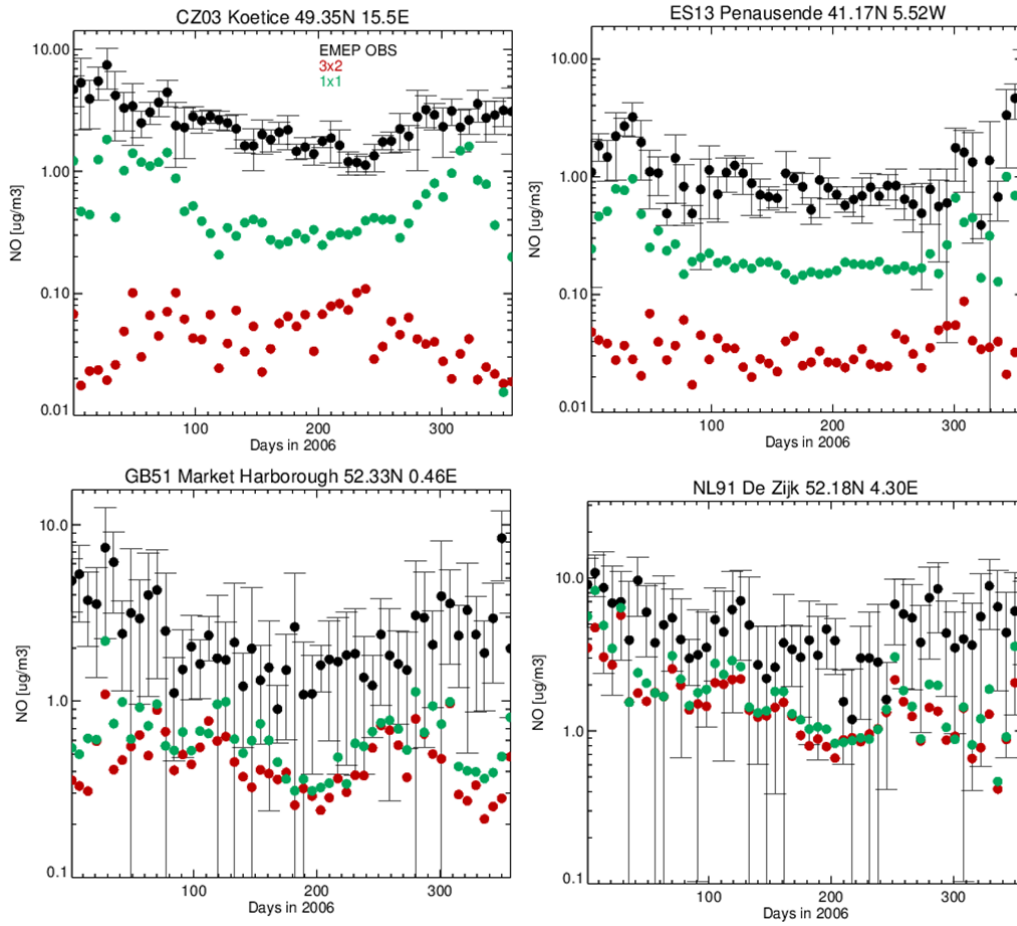
1220

1221

1222

1223

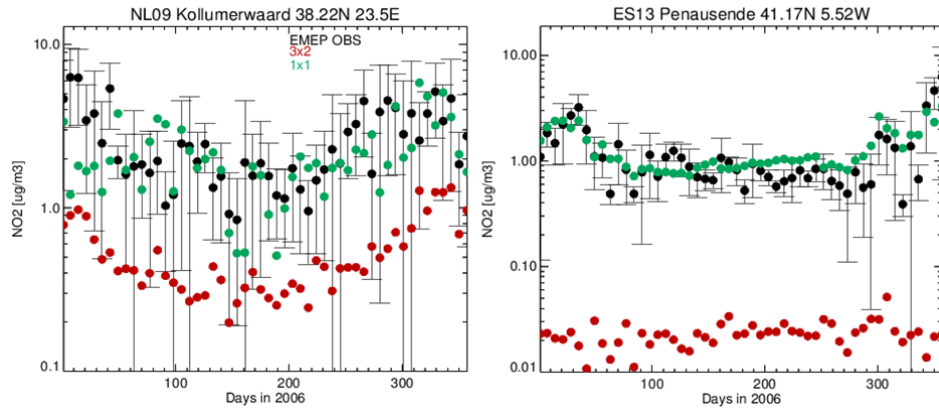
Figure 3: Comparisons of the seasonal variability in TM5-MP mass mixing ratios for surface  $O_3$  against composites of measurements taken across the EMEP monitoring network for 2006. Both the co-located TM5-MP  $3^\circ \times 2^\circ$  and  $1^\circ \times 1^\circ$  monthly mean values are shown, along with the  $1-\sigma$  variability for Finland, The Netherlands, Belgium, Poland, Slovakia and Italy. Individual stations that are aggregated are given in the panels.

1224  
1225

1226

1227  
1228  
1229  
1230  
1231  
1232  
1233  
1234  
1235  
1236  
1237  
1238

Figure 4: Comparison of TM5-MP weekly [NO] sampled at 13:00 UT each day during 2006 with observed [NO] ( $\mu\text{g m}^{-3}$ ). The selected sites shown are in the Czech Republic (top left), Spain (top right), Great Britain (bottom left) and The Netherlands (bottom right).



1239  
 1240  
 1241  
 1242  
 1243  
 1244  
 1245  
 1246

Figure 5: Comparison of weekly TM5-MP [NO<sub>2</sub>] sampled at 13:00 UT each day during 2006 with observed [NO<sub>2</sub>] (μg m<sup>-3</sup>). The selected sites shown are in The Netherlands (left) and Spain (right).

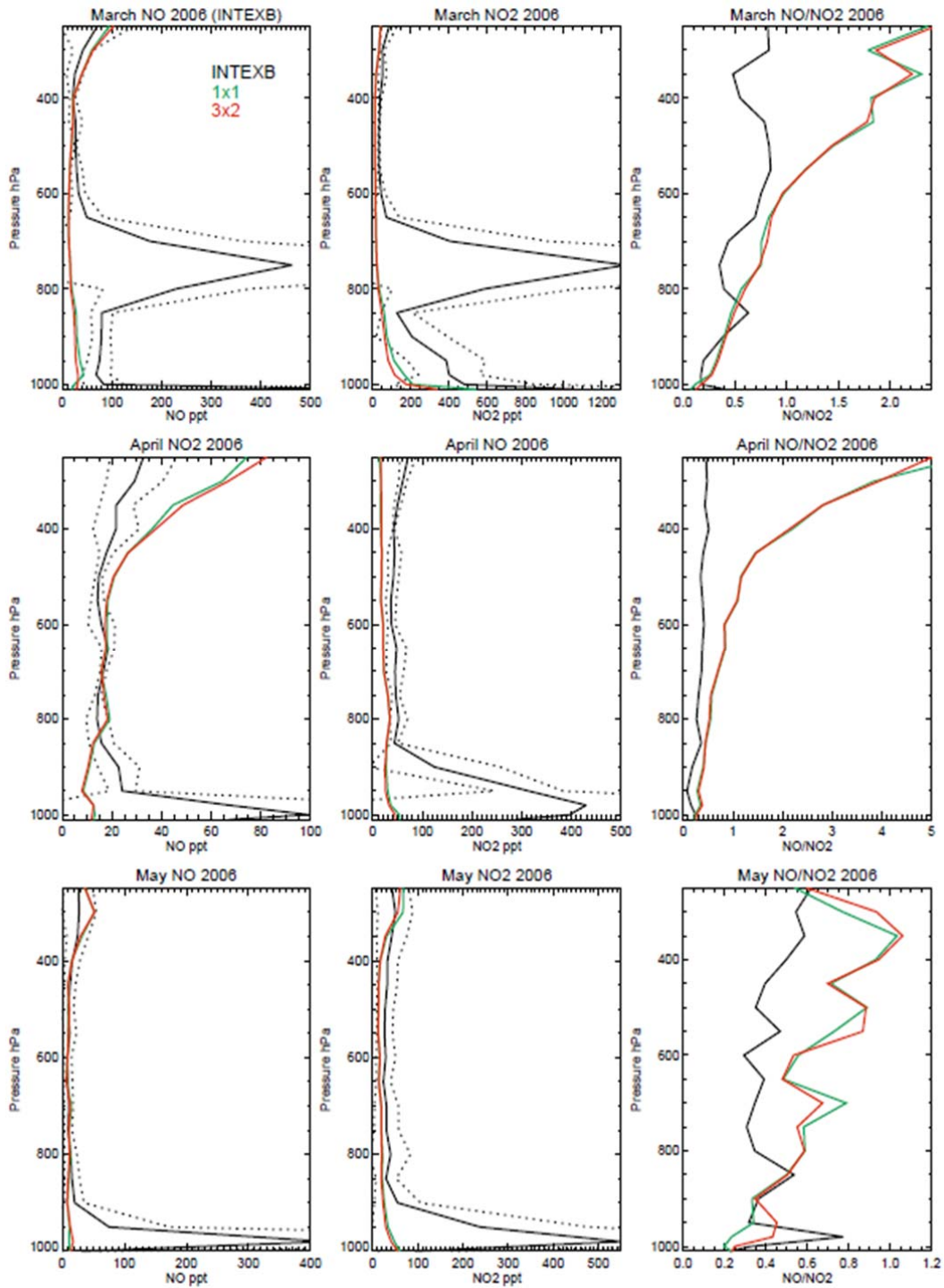
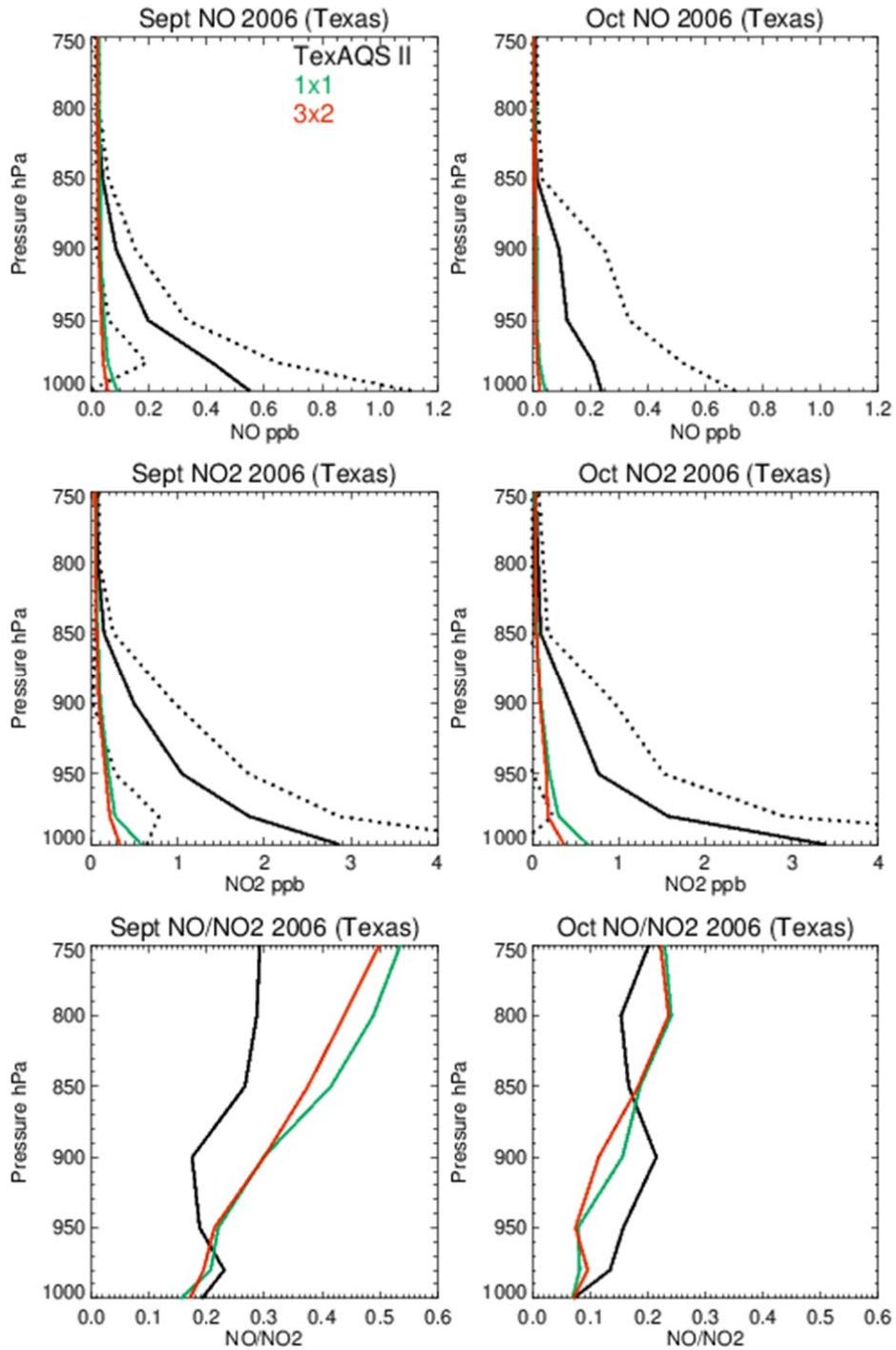


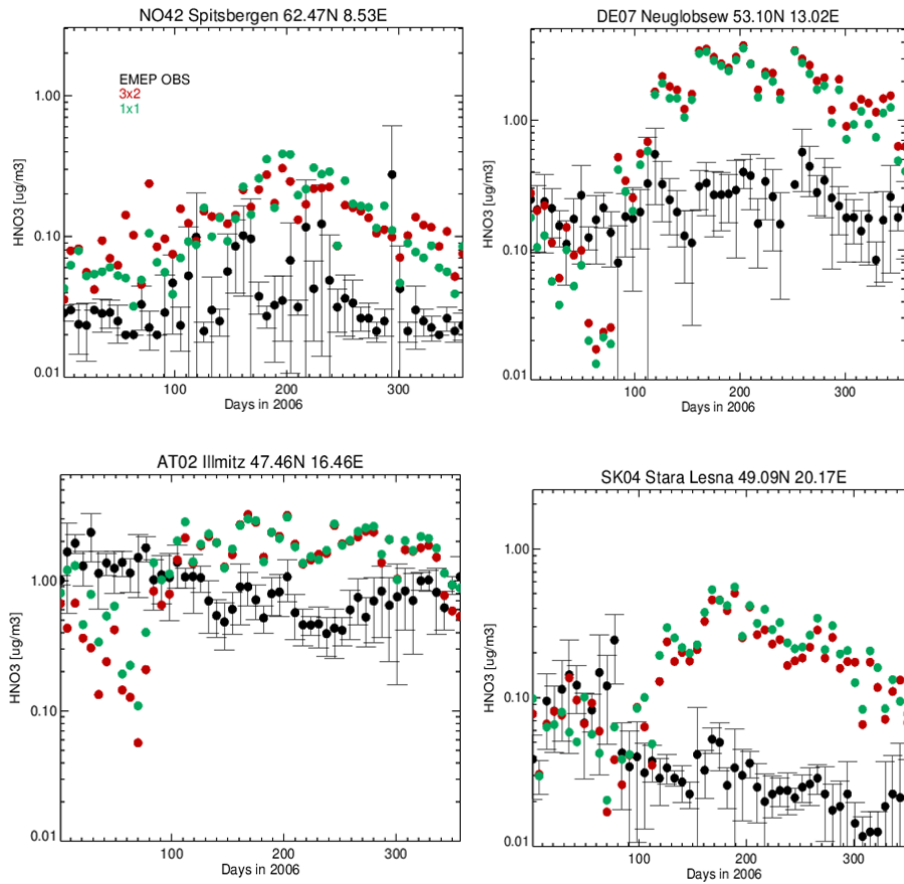
Figure 6: Monthly mean comparisons of NO (left), NO<sub>2</sub> (middle) and the resulting NO/NO<sub>2</sub> ratio (right) from INTEX-B measurements and TM5-MP simulations. The dotted line represents the 1- $\sigma$  deviation in the mean of the measurements. For details of the locations for each month the reader is referred to Singh et al. (2009).

1247  
 1248  
 1249  
 1250  
 1251  
 1252  
 1253  
 1254



1255  
 1256  
 1257  
 1258  
 1259  
 1260  
 1261  
 1262  
 1263

Figure 7: Monthly mean comparisons of NO (left), NO<sub>2</sub> (middle) and the resulting NO/NO<sub>2</sub> ratio (right) from the TexAQSI campaign during September and October 2006 and TM5-MP simulations. The dotted line represents the 1-σ deviation in the mean of the measurements. For details of the locations for each month the reader is referred to Parrish et al. (2009).



1264

1265

1266

1267

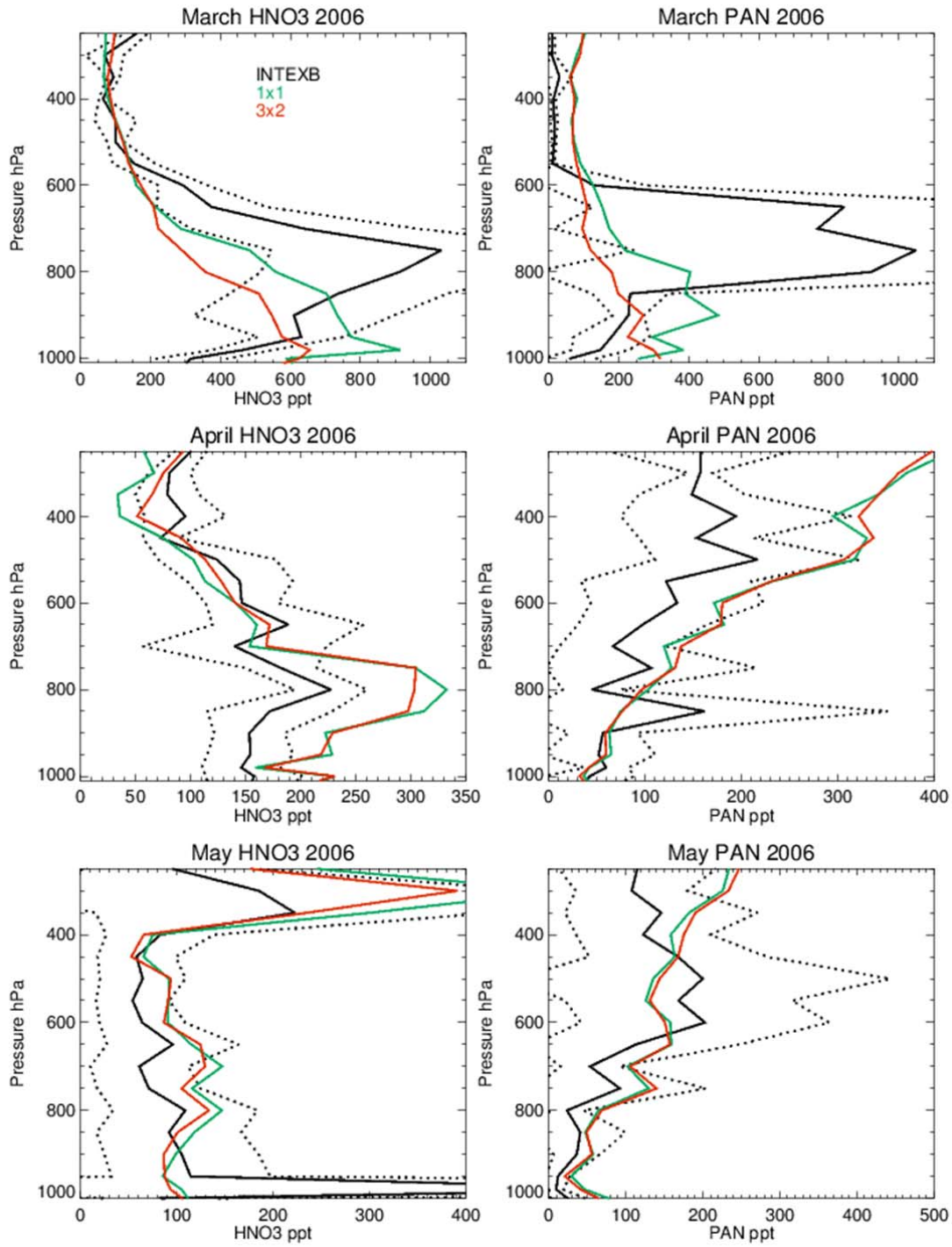
1268

1269

1270

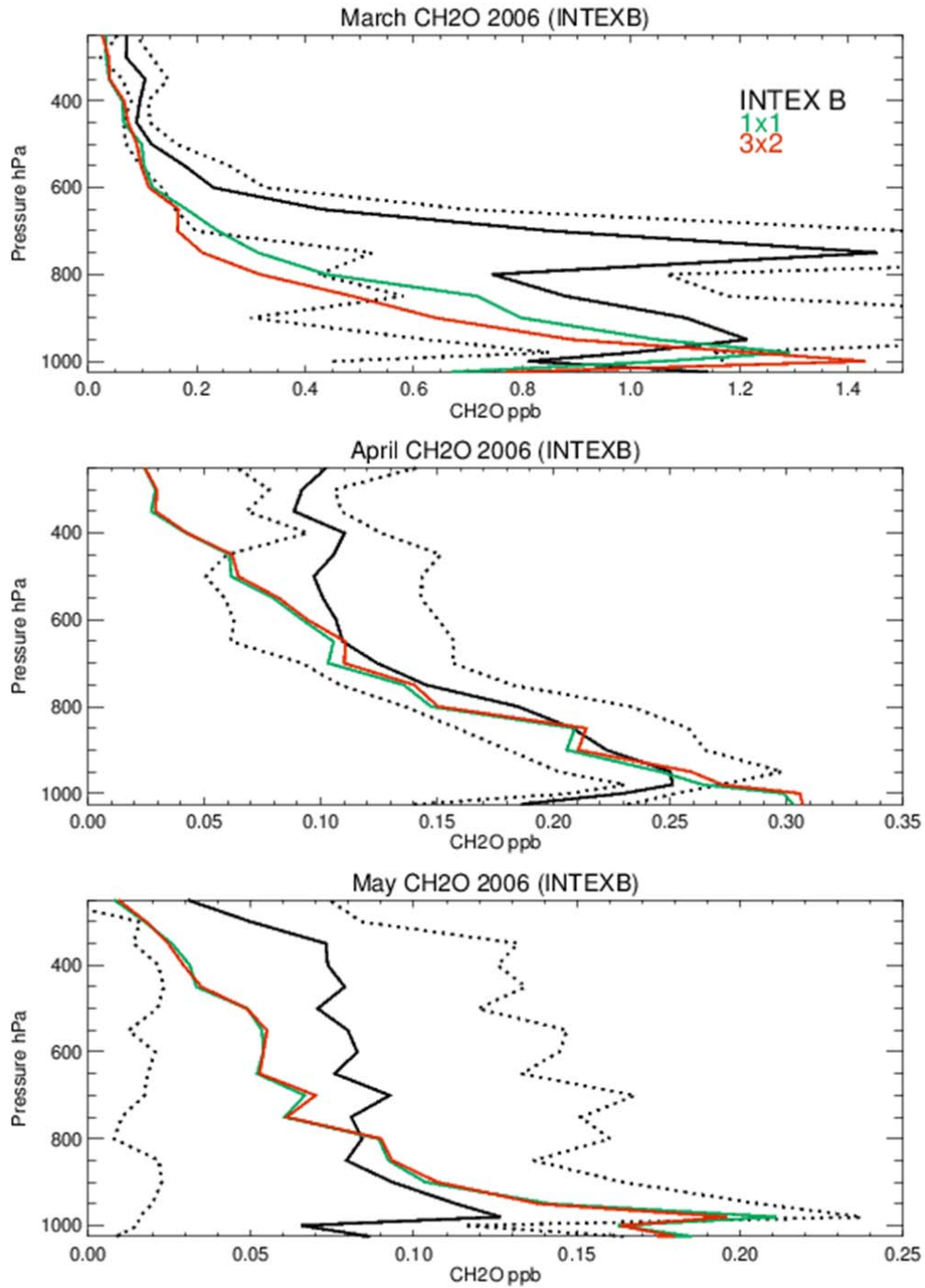
1271

Figure 8: Comparison of weekly  $[\text{HNO}_3]$  ( $\mu\text{g m}^{-3}$ ) from both  $3^\circ \times 2^\circ$  and  $1^\circ \times 1^\circ$  simulations at 4 selected EMEP sites for 2006. The  $1\text{-}\sigma$  deviation in the weekly observations are shown as error bars. The selected sites shown are in Norway (top left), Germany (top right), Austria (bottom left) and Slovakia (bottom right).



1272  
 1273  
 1274  
 1275  
 1276  
 1277  
 1278

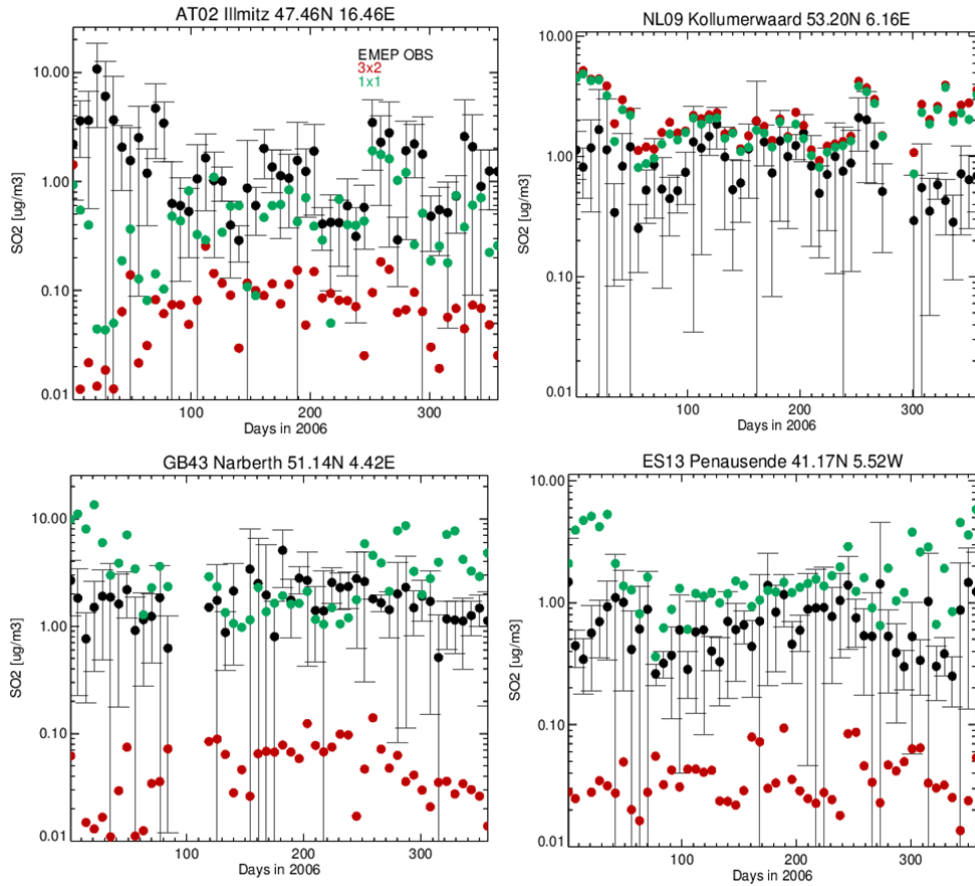
Figure 9: Monthly mean comparisons of HNO<sub>3</sub> (left) and PAN (right) from the INTEX-B measurements and TM5-MP simulations. The dotted line represents the 1- $\sigma$  deviation in the mean of the measurements. For details of the locations for each month the reader is referred to Singh et al. (2009).



1279  
1280  
1281  
1282  
1283  
1284  
1285  
1286

Figure 10: Comparisons of the vertical distribution of CH<sub>2</sub>O from both 3° x 2° and 1° x 1° simulations against measurements made as part of the INTEX-B during 2006. The dotted line represents the 1- $\sigma$  deviation in the mean of the measurements. For details on the exact location of the flights the reader is referred to Parrish et al. (2009).

1287  
1288  
1289

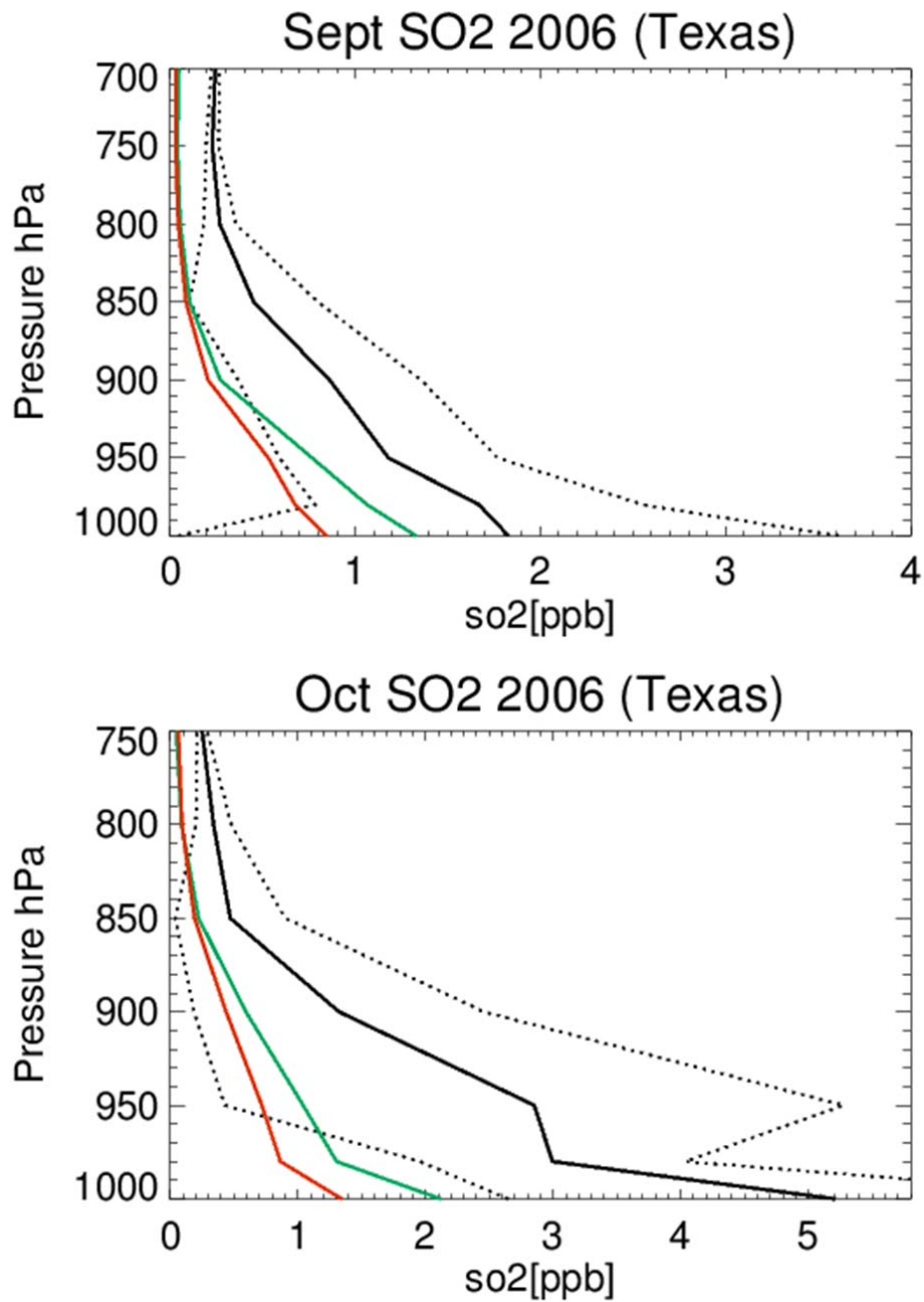


1290

1291  
1292  
1293  
1294  
1295  
1296  
1297

Figure 11: Comparison of weekly  $[SO_2]$  ( $\mu\text{g m}^{-3}$ ) at 13:00 from both the  $3^\circ \times 2^\circ$  and  $1^\circ \times 1^\circ$  simulations at 4 selected EMEP sites for 2006. The selected sites shown are in Austria (top left), the Netherlands (top right), Great Britain (bottom left) and Spain (bottom right).

1298



1299  
 1300  
 1301  
 1302  
 1303  
 1304  
 1305

Figure 12: Comparisons of the monthly tropospheric SO<sub>2</sub> profile assembled from data taken during September and October 2006 as part of TexAQS II. The 1- $\sigma$  deviation of the mean derived from the measurements is shown as the dotted line. For details of the flight paths the reader is referred to Parrish et al. (2009).

1306 **References**

- 1307 Aan de Brugh, J. M. J., Schaap, M., Vignati, E., Dentener, F., Kahnert, M., Sofiev, M., Huijnen, V., and Krol,  
1308 M. C.: The European aerosol budget in 2006, *Atms. Phys. Chem.*, 11, 1117-1139, doi:10.5194/acp-11-1117-  
1309 2011, 2011.
- 1310 Aas, W., Hjellbrekke, A.-G., Schaug, J., and Solberg, S.: Data quality 1999, quality assurance and field  
1311 comparisons, Kjeller, Norwegian Institute for Air Research, EMEP/CCC Report 6/2001, 2001.
- 1312 Abbatt, J. P. D., Lee, A. K. Y., and Thornton, J. A.: quantifying trace gas uptake to tropospheric aerosol: recent  
1313 advances and remaining challenges, *Chem. Soc. Rev.*, 41, 6555–6581, doi:10.1039/c2cs35052a, 2012.
- 1314 Alonza Gray, B., Wang, Y., Gu, D., Bandy, A., Mauldin, L., Clarke, A., Alexander, B., and Davis, D. D.:  
1315 Sources, transport, and sinks of SO<sub>2</sub> over the equatorial Pacific during the Pacific Atmospheric Sulfur  
1316 Experiment, *J. Atmos. Chem.*, 68, 27-53, doi: 10.1007/s10874-010-9177-7, 2011.
- 1317 Atkinson, R., Baulch, D. L., Cox, R. A., Crowley, J. N., Hampson, R. F., Hynes, R. G., Jenkin, M. E., Rossi,  
1318 M. J., and Tore, J., Evaluated kinetic and photochemical data for atmospheric chemistry: Volume I –gas phase  
1319 reactions of O<sub>x</sub>, HO<sub>x</sub>, NO<sub>x</sub> and SO<sub>x</sub> species, *Atmos. Chem. Phys.*, 4, 1461-1738, 2004.
- 1320 Atkinson, R., Baulch, D. L., Cox, R. A., Crowley, J. N., Hampson, R. F., Hynes, R. G., Jenkin, M. E., Rossi,  
1321 M. J., and Tore, J., Evaluated kinetic and photochemical data for atmospheric chemistry: Volume II –gas phase  
1322 reactions of organic species, *Atmos. Chem. Phys.*, 6, 3625-4055, 2006.
- 1323 Bândă, N., Krol, M., van Noije, T., van Weele, M., Williams J. E., Le Sager, P., Niemeier, U., Thomason, L.  
1324 and Röckmann, T.: The effect of stratospheric sulfur from Mount Pinatubo on tropospheric oxidizing capacity  
1325 and methane, *J. Geophys. Res. Atmos.*, 120, doi:10.1002/2014JDO22137, 2015.
- 1326 Boersma, K. F., Jacob, D. J., Eskes, H. J., Pinder, R. W., Wang, J. and van der A, R. J.: Intercomparison of  
1327 SCIAMACHY and OMI tropospheric NO<sub>2</sub> columns: observing the diurnal evolution of chemistry and  
1328 emissions from space, *J. Geophys. Res.*, 2, 113, 1-14, doi:10.1029/2007JD008816, 2008.
- 1329 Boersma, K. F., Eskes, H. J., Dirksen, R. J., van der A, R. J., Veefkind, J. P., Stammes, P., Huijnen, V.,  
1330 Kleipool, Q. L., Sneep, M., Claas, J., Leitao, J., Richter, A., Zhou, Y. and Brunner, D.: An improved  
1331 tropospheric NO<sub>2</sub> column retrieval algorithm for the Ozone Monitoring Instrument, *Atmos. Meas. Tech.*, 4,  
1332 1905-1928, 2011.
- 1333 Bregman, B., Segers, A., Krol, M., Meijer, E., and van Velthoven, P.: On the use of mass-conserving wind  
1334 fields in chemistry-transport models, *Atmos. Chem. Phys.*, 3, 447–457, doi:10.5194/acp-3-447-2003, 2003.
- 1335 Browne, E. C., Perring, A. E., Wooldridge, P. J., Apel, E., Hall, S. R., Huey, L. G., Mao, J., Spencer, K. M., St.  
1336 Clair, J. M., Weinheimer, A. J., Wisthaler, A., and Cohen, R. C.: Global and regional effects of the  
1337 photochemistry of CH<sub>3</sub>ONO<sub>2</sub>: evidence from ARCTAS, *Atmos. Chem. Phys.*, 11, 4209-4219, 2011.
- 1338 Carslaw, D. C. and Beevers, S. D.: Estimations of road vehicle primary NO<sub>2</sub> exhaust emission frctions using  
1339 monitoring data in London, *Atmos. Environ.*, 39(1), 167-177, 2005.

- 1340 De Smedt, I., Muller, J.-F., Stavrou, T., van der A., R., Eskes, H. and Van Roozendael, M.: Twelve years of  
1341 global observations of formaldehyde in the troposphere using GOME and SCIAMACHY sensors, *Atmos.*  
1342 *Chem. Phys.*, 8, 4947-4963, 2008.
- 1343 Dee, D. P., Uppala, S. M., Simmons, A. J., Berrisford, P., Poli, P., Kobayashi, S., Andrae, U., Balmaseda, M.  
1344 A., Balsamo, G., Bauer, P., Bechtold, P., Beljaars, A. C. M., van de Berg, L., Bidlot, J., Bormann, N., Delsol,  
1345 C., Dragani, R., Fuentes, M., Geer, A. J., Haimberger, L., Healy, S. B., Hersbach, H., Hólm, E. V., Isaksen, L.,  
1346 Kållberg, P., Köhler, M., Matricardi, M., McNally, A. P., Monge-Sanz, B. M., Morcrette, J.-J., Park, B.-K.,  
1347 Peubey, C., de Rosnay, P., Tavolato, C., Thépaut, J.-N. and Vitart, F.: The ERA-Interim reanalysis:  
1348 configuration and performance of the data assimilation system, *Q. J. Royal Met. Soc.*, 137, 656, 553-597, 2011.
- 1349 Dunlea, E. J., Herndon, S. C., Nelson, D. D., Volkamer, R. M., San Martini, F., Sheehy, P. M., Zahniser,  
1350 M. S., Shorter, J. H., Wormhoudt, J. C., Lamb, B. K., Allwine, E. J., Gaffney, J. S., Marley, N. A., Grutter, M.,  
1351 Marquez, C., Blanco, S., Cardenas, B., Retama, A., Ramos Villegas, C. R., Kolb, C. E., Molina, L. T., and  
1352 Molina, M. J.: Evaluation of nitrogen dioxide chemiluminescence monitors in a polluted urban environment,  
1353 *Atmos. Chem. Phys.*, 7, 2691–2704, 2007, <http://www.atmos-chem-phys.net/7/2691/2007/>
- 1354 Dupuy, E., Urban, J., Ricaud, P., Le Flochmoën, E., Lautié, N., Murtagh, D., De La Noë, J., El Amraoui, L.,  
1355 Eriksson, P., Forkman, P., Frisk, U., Jégou, F., Jiménez, C. and Olberg, M.: Starto-mesospheric measurements  
1356 of carbon monoxide with the Odin Sub-Millimetre Radiometer: Retrieval and first results, *Geophys. Res.*  
1357 *Letts.*, 31, L20101, doi:10.1029/2004GL020558, 2004.
- 1358 Emmons, L. K., Walters, S., Hess, P. G., Lamarque, J.-F., Pfister, G. G., Fillmore, D., Granier, C., Guenther,  
1359 A., Kinnison, D., Laepple, T., Orlando, J., Tie, X., Tyndall, G., Wiedinmyer, C., Baughcum, S. L., and Kloster,  
1360 S.: Description and evaluation of the Model for Ozone and Related chemical Tracers, version 4 (MOZART-4),  
1361 *Geosci. Model Dev.*, 3, 43–67, doi: 10.5194/gmd-3-43-2010, 2010.
- 1362 Evans, M. J. and Jacob, D. J.: Impact of new laboratory studies of N<sub>2</sub>O<sub>5</sub> hydrolysis on global model budgets of  
1363 tropospheric nitrogen oxides, ozone and OH, *Geophys. Res. Letts.*, 32, doi:10.1029/2005GL022469, 2005.
- 1364 Fortuin, J. P. F. and Kelder, H.: An ozone climatology based on ozonesonde and satellite measurements. *J.*  
1365 *Geophys. Res.*, 103, 31709–31734, 1998.
- 1366 Gonçalves, M., Dabdub, D., Chang, W. L., Jorba, O. and Baldasano, J. M.: Impact of HONO sources on the  
1367 performance of mesoscale air quality models, *Atmos. Environ.*, 54, Pages 168–176,  
1368 doi:10.1016/j.atmosenv.2012.02.079, 2012.
- 1369 Gonzi, S., Palmer, P. I., Barkley, M., De Smedt, I. and Roozendael, M. V.: Biomass burning emission  
1370 estimates inferred from satellite column measurements of HCHO: Sensitivity to co-emitted aerosol and  
1371 injection height, *Geophys. Res. Letts.*, 38, L14807, 2011.
- 1372 Granier, C., Bessagnet, B., Bond, T., D'Angiola, A., Denier van der Gon, H., Frost, G. J., Heil, A., Kaiser, J.  
1373 W., Kinne, S., Klimont, Z., Kloster, S.-F., Lamarque, J., Liousse, C., Masui, T., Meleux, F., Mieville, A.,  
1374 Ohara, T., Raut, J.-C., Riahi, K., Schultz, M. G., Smith, S. J., Thompson, A., van Aardenne, J., van der Werf,  
1375 G. R., and van Vuuren, D. P.: Evolution of anthropogenic and biomass burning emissions of air pollutants at

- 1376 global and regional scales during the 1980–2010 period, *Climate Change*, 109, 163–190, doi: 10.1007/s10584-  
1377 011-0154-115, 2011.
- 1378 Grooß, J.-U. and Russell III, J. M.: Technical note: A stratospheric climatology for O<sub>3</sub>, H<sub>2</sub>O, CH<sub>4</sub>, NO<sub>x</sub>, HCl  
1379 and HF derived from HALOE measurements, *Atmos. Chem. Phys.*, 5, 2797–2807, doi:10.5194/acp-5-2797-  
1380 2005, 2005.
- 1381 Hardacre, C., Wild, O. and Emberson, L.: An evaluation of ozone dry deposition in global scale chemistry  
1382 climate models, *Atms. Chem. Phys.*, 15, 6419-6436, doi:10.5194/acp-15-6419-2015, 2015.
- 1383 Hauglustaine, D. A., Balkanski, Y. and Schulz, M.: A global model simulation of present and future nitrate  
1384 aerosols and their direct radiative forcing of climate, *Atms. Chem. Phys.*, 14, 11031-11063, doi:10.5194/acp-  
1385 14-11031-2014, 2014.
- 1386 Heckel, A., Kim, S.-W., Frost, G. J., Richter, A., Trainer, M. and Burrows, J. P.: Influence of low spatial  
1387 resolution a priori data on tropospheric NO<sub>2</sub> satellite retrievals, *Atmos. Meas. Tech.*, 4, 1805-1820, 2011.
- 1388 Huijnen, V., Williams, J., van Weele, M., van Noije, T., Krol, M., Dentener, F., Segers, A., Houweling, S.,  
1389 Peters, W., de Laat, J., Boersma, F., Bergamaschi, P., van Velthoven, P., Le Sager, P., Eskes, H., Alkemade,  
1390 F., Scheele, R., Nédelec, P., and Pätz, H.-W., The global chemistry transport model TM5: description and  
1391 evaluation of the tropospheric chemistry version 3.0, *Geosci. Model Dev.*, 3, 445-473, 2010.
- 1392 Holtlag, A. A. and Boville, B. A.: Local versus non-local boundary layer diffusion in a global climate model,  
1393 *J. Climate*, 10, 1825–1842, 1993.
- 1394 Huijnen, V., Williams, J. E., and Flemming, J.: Modeling global impacts of heterogeneous loss of HO<sub>2</sub> on  
1395 cloud droplets, ice particles and aerosols, *Atmos. Chem. Phys. Discuss.*, 14, 8575–8632, doi: 10.5194/acpd-14-  
1396 8575-2014, 2014.
- 1397 Jacob, D. J., Prather, M. J., Rasch, P. J., Shia, R. L., Balkanski, Y. J., Beagley, S. R., Bergmann, D. J.,  
1398 Blackshear, W. T., Brown, M., Chiba, M., Chipperfield, M. P., de Grandpré, J., Dignon, J. E., Feichter, J.,  
1399 Genthon, C., W. L. Grose, W. L., Kasibhatla, P. S., Köhler, I., Kritz, M. A., Law, K., Penner, J. E., Ramonet,  
1400 M., Reeves, C. E., Rotman, D. A., Stockwell, D. Z., Van Velthoven, P. F. J., Verver, G., Wild, O., Yang, H and  
1401 Zimmermann, P.: Evaluation and intercomparison of global atmospheric transport models using <sup>222</sup>Rn and  
1402 other short-lived tracers, *J. Geophys. Res.*, 102(D5), 5953-5970, doi:10.1029/96JD02955, 1997.
- 1403 Jacob, J. D.: Heterogeneous chemistry and tropospheric ozone, *Atmos. Environ.*, 34, 2131–2159, 2000.
- 1404 Jégou, F., Urban, J., de La Noë, J., Ricaud, P., Le Flochmoën, E., Murtagh, D. P., Eriksson, P., Jones, A.,  
1405 Petelina, S., Llewellyn, E. J., Lloyd, N. D., Haley, C., Lumpe, J., Randall, C., Bevilacqua, R. M., Catoire, V.,  
1406 Huret, N., Berthet, G., Renard, J. B., Strong, K., Davies, J., Mc Elroy, C. T., Goutail, F., and Pommereau, J. P.:  
1407 Technical Note: Validation of Odin/SMR limb observations of ozone, comparisons with OSIRIS, POAM III,  
1408 ground-based and balloon-borne instruments, *Atmos. Chem. Phys.*, 8, 3385–3409, doi:10.5194/acp-8-3385-  
1409 2008, 2008.
- 1410 Kim, S.-W., McKeen, S. A., Frost, G. J., S.-H. Lee, S.-H., M. Trainer, M., Richter, A., Angevine, W. M.,  
1411 Atlas, E., Bianco, L., Boersma, K. F., Brioude, J., Burrows, J. P., de Gouw, J., Fried, A., Gleason, J., Hilboll,

- 1412 A., Mellqvist, J., Peischl, J., Richter, D., Rivera, C., Ryerson, T., te Lintel Hekkert, S., Walega, J., Warneke,  
1413 C., Weibring, P., and Williams, E.: Evaluations of NO<sub>x</sub> and highly reactive VOC emission inventories in Texas  
1414 and their implications for ozone plume simulations during the Texas Air Quality Study 2006, *Atmos. Chem.*  
1415 *Phys.*, 11, 11361–11386, doi:10.5194/acp-11-11361-2011, 2011.
- 1416 Krol, M., Houweling, S., Bregman, B., van den Broek, M., Segers, A., van Velthoven, P., Peters, W., Dentener,  
1417 F., and Bergamaschi, P.: The two-way nested global chemistry-transport zoom model TM5: algorithm and  
1418 applications, *Atmos. Chem. Phys.*, 5, 417–432, doi:10.5194/acp-5-417-2005, 2005.
- 1419 Lawrence, M. G. and Crutzen, P. J.: The impact of cloud particle gravitational settling on soluble trace gas  
1420 distributions, *Tellus*, 50B, 263–289, 1998.
- 1421 Lee, C., Martin, R. V., van Donkelaar, A., Lee, H., Dickerson, R. R., Hains, J. C., Krotkov, N., Richter, A.,  
1422 Vinnikov, K. and Schwab, J. J.: SO<sub>2</sub> emissions and lifetimes: Estimates from inverse modeling using in situ  
1423 and global, space-based (SCIAMACHY and OMI) observations, *J. Geophys. Res.*, 116, D06304,  
1424 doi:10.1029/2010JD014758, 2011.
- 1425 Lelieveld, J., Peters, W., Dentener, F. J., and Krol, M. C.: Stability of tropospheric hydroxyl chemistry, *J.*  
1426 *Geophys. Res.*, 107(D23), 4715, doi:10.1029/2002JD002272, 2002.
- 1427 Lin, J. T., Martin, R. V., Boersma, K. F., Sneep, M., Stammes, P., Spurr, R., Wang, P., Van Roozendaal, M.,  
1428 Clémer, K., and Irie, H.: Retrieving tropospheric nitrogen dioxide from the Ozone Monitoring Instrument:  
1429 effects of aerosols, surface reflectance anisotropy, and vertical profile of nitrogen dioxide, *Atmos. Chem.*  
1430 *Phys.*, 14, 1441–1461, doi:10.5194/acp-14-1441-2014, 2014.
- 1431 Lee, C., Martin, R. V., van Donkelaar, A., Lee, H., Dickerson, R. R., Hains, J. C., Krotkov, N., Richter, A.,  
1432 Vinnikov, K. and Schwab, J. J.: SO<sub>2</sub> emissions and lifetimes: Estimates from inverse modeling using in situ  
1433 and global, space-based (SCIAMACHY and OMI) observations, *J. Geophys. Res.*, 116, D06304,  
1434 doi:10.1029/2010JD014758, 2011.
- 1435 Louis, J. F.: A parametric model of vertical eddy fluxes in the atmosphere, *Bound.-Layer Meteor.*, 17, 187–  
1436 202, 1979.
- 1437 Marais, E. A., Jacob, D. J., Kurosu, T. P., Chance, K., Murphy, J. C., Reeves, C., Mills, G., Casadio, S., D. B.  
1438 Millet, D. B., Barkley, M. P., Paulot, F., and Mao, J.: Isoprene emissions in Africa inferred from OMI  
1439 observations of formaldehyde columns, *Atms. Chem. Phys.*, 12, 6219–6235, doi:10.5194/acp-12p6219-2012,  
1440 2012.
- 1441 Martin, G. M., Johnson, D. W., and Spice, A.: The measurement and parameterization of effective radius of  
1442 droplets in warm stratocumulus clouds, *J. Atmos. Sci.*, 51, 1823–1842, 1994.
- 1443 Meijer, E. W., van Velthoven, P. F. J., Brunner, D. W., Huntrieser, H., and Kelder, H.: Improvement and  
1444 evaluation of the parameterisation of nitrogen oxide production by lightning, *Phys. Chem. Earth*, 26, 557–583,  
1445 2001.
- 1446 Meloan, J., Siegmund, P., van Velthoven, P., Kelder, H., Sprenger, M., Wernli, H., Kentarchos, A., Roelofs,  
1447 G., Feichter, J., Land, C., Forster, C., James, P., Stohl, A., Collins, W., and Cristofanelli, P.: Stratosphere-

- 1448 troposphere exchange: A model and method intercomparison, *J. Geophys. Res.*, 108(D12), 8256,  
1449 doi:10.29/2002JD002274, 2002.
- 1450 Möllner, A. K., Valluvadasan, S., Feng, L., Sprague, M. K., Okumura, M., Milligan, D. B., Bloss, W.J., Sander,  
1451 S. P., Martien, P. T., Harley, R. A.,
- 1452 Olsen, S. C., McLinden, C. A., and Prather, M. J.: Stratospheric N<sub>2</sub>O–NO<sub>y</sub> system: Testing uncertainties in a  
1453 three-dimensional framework, *J. Geophys. Res.*, 106, 28771–28784, 2001.
- 1454 Olszyna, K. J., Bailey, E. M., Simonaitis, R. and Meagher, J. F.: O<sub>3</sub> and NO<sub>y</sub> relationships at a rural site,  
1455 99(D7), 14557–14563, doi:10.1029/94JD00739, 1994.
- 1456 Palmer, P. I., Abbot, D. S., Fu, T.-M., Jacob, D. J., Chance, K., Kurosu, P., Guenther, A., Wiedinmyer, C.,  
1457 Stanton, J. C., Pilling, M. J., Pressley, S. N., Lamb, B. and Sumner, A. L.: Quantifying the seasonal and  
1458 interannual variability of North American isoprene emissions using satellite observations of the formaldehyde  
1459 column, *J. Geophys. Res.*, 111, D12315, doi:10.1029/2005JD006689, 2006.
- 1460 Parrish, D. D., Allen, D. T., Bates, T. S., Estes, M., Fehsenfeld, F. C., Feingold, G., Ferrare, R., Hardesty, R.  
1461 M., Meagher, J. F., Nielsen-Gammon, J. W., Pierce, R. B., Ryerson, T. B., Seinfeld, J. H. and Williams, E. J.:  
1462 Overview of the Second Texas Air Quality Study (TexAQS II) and the Gulf of Mexico Atmospheric  
1463 Composition and Climate study (GoMACCS), *J. Geophys. Res.*, 114 (D00F13), doi: 10.1029/2009JD011842,  
1464 2009.
- 1465 Phillips, G. J., Makkonen, U., Schuster, G., Sobanski, N., Hakola, H. and Crowley, J. N.: The detection of  
1466 nocturnal N<sub>2</sub>O<sub>5</sub> as HNO<sub>3</sub> by alkali- and aqueous-denuder techniques, *Atmos. Meas. Tech.*, 6, 231-237,  
1467 doi:10.51094/amt-6-231-2013, 2013.
- 1468 Pope, R. J., Chipperfield, M. P., Savage, N. H., Ordóñez, C., Neal, L.S., Lee, L.A., Dhomse1, S. S., Richards,  
1469 N. A. D. and Kestlake, T. D.: Evaluation of a regional air quality model using satellite column NO<sub>2</sub>: treatment  
1470 of observation errors and model boundary conditions and emissions, *Atmos. Chem. Phys.*, 15, 5611–5626,  
1471 doi:10.5194/acp-15-5611-2015, 2015
- 1472 Russell, A. R., Perring, A. E., Valin, L. C., Bucse1a, E. J., Browne, E. C., Wooldridge, P. J. and Cohen, R. C.:  
1473 A high spatial resolution retrieval of NO<sub>2</sub> column densities from OMI: method and evaluation, *Atmos. Chem.*  
1474 *Phys.*, 11, 8543-8554, doi:10.5194/acp-11-8543-2011, 2011.
- 1475 Schery, S. D.: Progress on Global Rn<sup>222</sup> Flux Maps and Recommendations for Future Research, in: 1st  
1476 International Expert Meeting on Sources and Measurements of Natural Radionuclides Applied to Climate and  
1477 Air Quality Studies (Gif-sur-Yvette, France, June 2003), edited by: Barrie, L. A. and Lee, H. N., WMO TD  
1478 1201, Gif-sur-Yvette, France, 43–47, 2004.
- 1479 Schwartz, S. E.: Mass-transport considerations pertinent to aqueous-phase reactions of gases in liquid-water  
1480 clouds, in: *Chemistry of Multiphase Atmospheric Systems*, edited by: Jaechske, W., Springer, Heidelberg,  
1481 415–471, 1986.
- 1482 Seltzer, K. M., Vizuetes, W. and Henderson, B. H.: Evaluation of updated nitric acid chemistry on ozone  
1483 precursors and radiative effects, *Atmos. Chem. Phys. Discuss.*, 15, 3219–3255, 2015.

- 1484 Shettle, E. P. and Fenn, R. W.: Models for the aerosols of the lower atmosphere and the effects of the humidity  
1485 variations on their optical properties, *Environ. Res. Paper*, 676, AFGL-TR-79-0114, 91 pp, 1979.
- 1486 Sindelarova, K., Granier, C., Bouarar, I., Guenther, A., Tilmes, S., Stavrou, T., Müller, J.-F., Kuhn, U.,  
1487 Stefani, P. and Knorr, W.: Global dataset of biogenic VOC emissions calculated by the MEGAN model over  
1488 the last 30 years, *Atmos. Phys. Chem.*, 14, 9317–9341, doi:10.5194/acp-14-9317-2014, 2014.
- 1489 Singh, H. B., Brune, W. H., Crawford, J. H., et al.: Chemistry and transport of pollution over the Gulf of  
1490 Mexico and the Pacific: spring 2006 INTEX-B campaign overview and first results, *Atmos. Chem. Phys.*, 9,  
1491 2301-2318, doi:10.5194/acp-9-2301-2009, 2009.
- 1492 Stavrou, T., Müller, J.-F., De Smedt, I., Van Roozendaal, M., van der Werf, G. R., Giglio, L., and Guenther,  
1493 A.: Global emissions of non-methane hydrocarbons deduced from SCIAMACHY formaldehyde columns  
1494 through 2003-2006, *Atms. Chem. Phys.*, 9, 3663-3679, 2009.
- 1495 Steinbacher, M., Zellweger, C., Schwarzenbach, B., Bugmann, S., Buchmann, B., Ordóñez, C., Prevot, A. S.  
1496 H., and Hueglin, C.: Nitrogen oxides measurements at rural sites in Switzerland: bias of conventional  
1497 measurement techniques, *J. Geophys. Res.*, 112, D11307, doi:10.1029/2006JD007971, 2007.
- 1498 Stevenson, D. S., Dentener, F. J., Schultz, M. G., Ellingsen, K., van Noije, T. P. C., Wild, O., Zeng, G.,  
1499 Amann, M., Atherton, M., Bell, N., Bergmann, D. J., Bey, I., Bulter, T., Cofala, J., Collins, W. J., Derwent, R.  
1500 G., Doherty, R. M., Drevet, J., Eskes, H. J., Fiore, A. M., Gauss, M., Hauglustaine, D. A., Horowitz, L. W.,  
1501 Isaksen, I. S. A., Krol, M. C., Lamarque, J.-F., Lawrence, M. G., Montanaro, V., Müller, J. F., Pitari, G.,  
1502 Prather, M. J., Pyle, J. A., Rast, S., Rodriguez, J. M., Sanderson, M. G., Savage, N. H., Shindell, D. T.,  
1503 Strahan, S. E., Sudo, K., and Szopa, S.: Multimodel ensemble simulations of present-day and near future  
1504 tropospheric ozone, *J. Geophys. Res.*, 111, D08301, doi: 10.1029/2005JD006338, 2006.
- 1505 Sutton, R. T., Dong, B. and Gregory, J. M.: Land/sea warming ratio in response to climate change: IPCC AR4  
1506 model results and comparison with observations, *Geophys. Res. Letts.*, 34(2), 10.1029/2006GL028164, 2007.
- 1507 Tang, Q., Prather, M. J. and Hsu, J.: Stratosphere-troposphere exchange ozone flux related to deep convection,  
1508 *Geophys. Res. Letts.*, 38, L03806, doi:10.1029/2010GL046039, 2011.
- 1509 Thouret, V., Marenco, A., Logan, J. A., Nédélec, P., and Grouhel, C.: Comparisons of ozone measurements  
1510 from the MOZAIC airborne program and the ozone sounding network at eight locations, *J. Geophys. Res.*, 103,  
1511 25695–25720, 1998.
- 1512 Tiedtke, M.: A comprehensive mass flux scheme for cumulus parameterization in large-scale models, *Mon.*  
1513 *Weather. Rev.*, 117(8), 1779–1800, 1989.
- 1514 Tørseth, K., Aas, W., Breivik, K., Fjaeraa, A. M., Fiebig, M., Hjellbrekke, A. G., Lund-Myrhe, C., Solberg, S.  
1515 and Yttri, K. E.: Introduction to the European Monitoring and Evaluation Programme (EMEP) and observed  
1516 atmospheric composition change during 1972-2009, *Atmospheric Chemistry and Physics*, 12, 5447-5481,  
1517 2012.

- 1518 Urban, J., Pommier, M., Murtagh, D. P., Santee, M. L., and Orsolini, Y. J.: Nitric acid in the stratosphere based  
1519 on Odin observations from 2001 to 2009 – Part 1: A global climatology, *Atmos. Chem. Phys.*, 9, 7031–7044,  
1520 doi:10.5194/acp-9-7031-2009, 2009.
- 1521 Valks, P., Pinardi, G., Richter, A., Lambert, J.-C., Hao, N., Loyola, D., Van Roozendaal, M., and Emmadi, S.:  
1522 Operational total and tropospheric NO<sub>2</sub> column retrieval for GOME-2, *Atmos. Meas. Tech.*, 4, 1491–1514,  
1523 doi:10.5194/amt-4-1491-2011, 2011.
- 1524 van Geffen, J.H.G.M., Boersma, K. F., Eskes, H. J., Maasackers J. D. and Veefkind, J. P., TROPOMI  
1525 Algorithm Theoretical Basis Document (ATBD) tropospheric and total NO<sub>2</sub>, S5P-KNMI-L2-0005-RP, 56pp,  
1526 2016.
- 1527 van der A, R. J., Allaart, M. A. F., and Eskes, H. J.: Multi sensor reanalysis of total ozone, *Atmos. Chem. Phys.*  
1528 *Discuss.*, 10, 11401–11448, doi: 10.5194/acpd-10-11401-2010, 2010.
- 1529 van der Werf, G. R., Randerson, J. T., Giglio, L., Collatz, G. J., Mu, M., Kasibhatla, P. S., Morton, D. C.,  
1530 DeFries, R. S., Jin, Y., and van Leeuwen, T. T.: Global fire emissions and the contribution of deforestation,  
1531 savanna, forest, agriculture, and peat fires (1997–2009) *Atmos. Chem. Phys.*, 10, 11707–11735, 2010,  
1532 <http://www.atmos-chem-phys.net/10/11707/2010/>.
- 1533 Veefkind, J.P., Aben, I., McMullan, K., Förster, H., de Vries, J., Otter, G., Claas, J., Eskes, H. J., de Haan, J.  
1534 F., Kleipool, Q., van Weele, M., Hasekamp, O., Hoogeveen, R., Landgraf, J., Snel, R., Tol, P., Ingmann, P.,  
1535 Voors, R., Kruizinga, B., Vink, R., Visser, H. and Levelt, P. F.: TROPOMI on the ESA Sentinel-5 Precursor:  
1536 A GMES mission for global observations of the atmospheric composition for climate, air quality and ozone  
1537 layer applications, *Remote. Sens. Environ.*, 120, 70–83, doi:10.1016/j.rse.2011.09.027, 2012.
- 1538 Verstraeten, W. V., Neu, J. L., Williams, J. E., Bowman, K. W. and Worden, J. R.: Rapid increases in  
1539 tropospheric ozone production and export from China, *Nature Geosci.*, 8, 690–695, doi: 10.1038/ngeo2493,  
1540 2015.
- 1541 Vinken, G. C. M., Boersma, K. F., Jacob, D.J. and Meijer, E. W.: Accounting for non-linear chemistry of ship  
1542 plumes in the GEOS-Chem global chemistry transport model, *Atms. Chem. Phys.*, 11, *Atmos. Chem. Phys.*,  
1543 11707–11722, doi:10.5194/acp-11-11707-2011, 2011.
- 1544 Vinken, G. C. M., Boersma, K. F., Maasackers, J. D., Adon, M. and Martin, R. V.: Worldwide biogenic soil  
1545 NO<sub>x</sub> emissions inferred from OMI NO<sub>2</sub> observations, *Atmos. Chem. Phys.*, 14, doi:10.5194/acp-14-10363-  
1546 2014, 10363–10381, 2014.
- 1547 Vogelegang, D. H. P. and Holtslag, A. A. M.: Evaluation and model impacts of alternative boundary-layer  
1548 height formulations, *Bound.-Layer Meteor.*, 81, 245–269, 1996.
- 1549 Von Kuhlmann, R. and Lawrence, M. G.: The impact of ice uptake of nitric acid on atmospheric chemistry,  
1550 *Atms. Chem. Phys.*, 6, 225–235, 2006.
- 1551 Wild, O. and Prather, M. J.: Global tropospheric ozone modeling: Quantifying errors due to grid resolution, *J.*  
1552 *Geophys. Res.*, 111, D11305, doi:10.1029/2005JD006605, 2006.

- 1553 Williams, J. E., Strunk, A., Huijnen, V. and van Weele, M.: The application of the Modified Band Approach  
1554 for the calculation of on-line photodissociation rate constants in TM5: implications for oxidative capacity,  
1555 *Geosci. Model Dev.*, 5, 15-35, doi:10.5194/gmd-5-15-2012,2012.
- 1556 Williams, J. E., van Velthoven, P. F. J., and Brenninkmeijer, C. A. M.: Quantifying the uncertainty in  
1557 simulating global tropospheric composition due to the variability in global emission estimates of Biogenic  
1558 Volatile Organic Compounds, *Atmos. Chem. Phys.*, 13, 2857–2891, doi: 10.5194/acp-13-2857-2013, 2013.
- 1559 Williams, J. E., Le Bras, G., Kukai, A., Ziereis, H., and Brenninkmeijer, C. A. M.: The impact of the chemical  
1560 production of methyl nitrate from the  $\text{NO} + \text{CH}_3\text{O}_2$  reaction on the global distribution of alkyl nitrates, nitrogen  
1561 oxides and tropospheric ozone: a global modeling study, *Atmos. Chem. Phys.*, 14, 2363-2382, 2014.
- 1562 Worden, J., Liu, X., Bowman, K., Chance, K., Beer, R., Eldering, A., Gunson, M. and Worden, H., Improved  
1563 tropospheric ozone profile retrievals using OMI and TES radiances, *Geophys. Res. Lett.*, 34, L01809,  
1564 doi:10.1029/2006GL027806, 2007.
- 1565 Yamaji, K., Ikeda, K., Irie, H., Kurokawa, J. and Ohara, T.: Influence of model grid resolution on  $\text{NO}_2$  vertical  
1566 column densities over East Asia, *J. Air. Waste Manage. Assoc.*, 64(4), 436-444, 2014.
- 1567 Yarwood, G., Rao, S., Yocke, M., and Whitten, G.: Updates to the carbon bond chemical mechanism: CB05,  
1568 Final report to the US EPA, EPA Report Number: RT-0400675, available at: [www.camx.com](http://www.camx.com) (last access: 15  
1569 January 2014), 2005.
- 1570 Zhang, K., Feichter, J., Kazil, J., Wan, H., Zhuo, W., Griffiths, A. D., Sartorius, H., Zahorowski, W., Ramonet,  
1571 M., Schmidt, M., Yver, C., Neubert, R. E. M. and E.-G. Brunke, E.-G.: Radon activity in the lower troposphere  
1572 and its impact on ionization rate: a global estimate using different radon emissions, *Atmos. Chem. Phys.*, 11,  
1573 7817–7838, doi:10.5194/acp-11-7817-2011, 2011.
- 1574 Zeng, G., Williams, J. E., Fisher, J.A., Emmons, L. K., Jones, N. B., Morgenstern, O., Robinson, J., Smale, D.,  
1575 Paton-Walsh, C. and Griffith, D. W. T.: Multi-model simulation of CO and HCHO in the Southern  
1576 Hemisphere: comparison with observations and impact of biogenic emissions, *Atmos. Chem. Phys.*, 15, 7217-  
1577 7245, doi:10.5194/acp-15-7217-2015, 2015.
- 1578 Zdunkowski, W. G., Welsch, R. M., and Kord, G. J.: An investigation of the structure of typical 2-stream  
1579 methods for the calculation of solar fluxes and heating rates in clouds, *Contrib. Atmos. Phys.*, 53, 215-238,  
1580 1980.
- 1581 Zhou, Y., Brunner, D., Hueglin, C., Henne, S., and Staehelin, J.: Changes in OMI tropospheric  $\text{NO}_2$  columns  
1582 over Europe from 2004 to 2009 and the influence of meteorological variability. *Atmos Environ*, 46, 482-495,  
1583 2012.
- 1584 Zyrichidou, I., Koukouli, M. E., Balis, D., Markakis, K., Poupkou, A., Katragkou, E., Kioutsioukis, I., Melas,  
1585 D., Boersma, K. F. and van Roozendael, M.: Identification of surface  $\text{NO}_x$  emission sources on a regional  
1586 scale using OMI  $\text{NO}_2$ , *Atms. Environ.*, 101, 82-93, 2015.